UNIMOLECULAR REACTION DYNAMICS IN HELIUM NANODROPLETS

by

Daniil Stolyarov

A Dissertation Presented to the

FACULTY OF THE GRADUATE SCHOOL

UNIVERSITY OF SOUTHERN CALIFORNIA

In Partial Fulfillment of the

Requirements for the Degree

DOCTOR OF PHILOSOPHY

(CHEMISTRY)

May 2005

Contents

List of Figures

Abstract

Helium nanodroplet isolation technique provide an unique opportunity to study elementary chemical reactions in the ultracold liquid helium environment. The main question addressed in this work is how does the liquid helium environment affect chemical reaction dynamics. The discussion is limited to the case of unimolecular reactions.

First, it is shown how the spectrum of elementary excitation of helium droplets can be obtained. This spectrum is then used for evaluation of microcanonical thermodynamic functions of helium droplets at low temperature, as well as description of the process known as evaporative cooling.

Second, Feynman's microscopic theory of liquid helium is exctended to the case of helium droplets and other systems of liquid helium in confined geometries. Possible effects due to the finite size of helium droplets are also discussed. The extention of the microscopic theory allows for the prediction of the dynamic properties of helium droplets. The model of unimolecular reactions in conditions of collisional energy transfer, is adapted for the case of unimolecular reactions in the liquid helium environment. The energy transfer rate function in this case is evaluated based on the dynamic properties of liquid helium and helium droplets.

Finally, the experiments on mass depletion spectroscopy of the NO_2 molecule in the regions below and above its gas phase dissociation threshold are described. In the first experiment a mass depletion spectrum in the region 17700-18300 cm^{-1} is recorded.

Gas phase NO_2 is believed to be vibronically chaotic at these energies. Transitions are broadened and blue-shifted relative to those of the gas phase by 7 cm^{-1}. Modest dispersion (i.e. 90% lie within 2 cm^{-1} of the central values) are consistent with quantum chaos in NO_2. It is shown that the relaxation is dominated by interactions of NO_2 with its non-superfluid helium nearest neighbors.

In the second experiment, the guest-host dynamics of NO_2 embedded in He_n droplets have been examined by recording depletion spectra of mass spectrometer signals at m/z values of 8 (He_2^+), 30 (NO^+), and 46 (NO_2+), throughout the wavelength range 340-402 nm. Above the gas-phase dissociation threshold (D_0), it is shown that there is no net unimolecular decomposition all the way up to D_0 + 4300 cm^{-1}. At the upper end of this range, gas-phase NO_2 decomposes with rate coefficients whose values are $\sim 5\times10^{12}$ s^{-1}, which is expected to be larger than the deactivation rates in liquid helium. To within the experimental uncertainty, it is found that reaction products do not leave the droplets. This is attributed to efficient relaxation and (at the highest energies examined) recombination within the droplets. On the basis of these results, it is concluded that small polyatomics embedded in He_n droplets that have $\langle n\rangle$ values of $\sim 10^4$ or larger will not undergo net unimolecular reaction if the gas-phase pathway is barrierless, with two possible exceptions:(i) if one or both of the products has a positive chemical potential and (ii) if the scattering cross section of the product(s) with helium is small.

Preface

Reactions proceeding at low temperatures have attained great interest over the past decades. These kinds of reactions can be considered as a versatile means of preparing new types of compounds. Liquid helium is a perfect environment for this kind of reaction. However, the study of a chemical reactions in bulk liquid helium is complicated due to the coalescence of reacting species that entangles the reaction mechanism.

Discovery of helium nanodroplets, i.e. clusters containing $10^3 - 10^6$ helium atoms signified a new era in experimental cryochemistry. It has been found that the helium nanodroplets not only inherit unique properties of liquid helium such as superfluidity but also can be easily doped with foreign atoms or molecules. Thus the coalescence problem can be avoided. It provides an unique opportunity to observe and study elementary chemical reactions.

The interaction between embedded species and liquid helium environment is rather weak. Neither the interaction changes the chemical identities of reactants nor does it restrict their mutual motion during the reaction. However, liquid helium acts as an efficient coolant. The major influence of the liquid helium environment on the chemical reaction is that liquid helium drains the energy of the reacting molecules. Thus, dynamic properties of liquid helium are of primary concern. The dynamic properties of bulk liquid helium differ from the dynamic properties of liquid helium in confined geometries

and hence the influence of liquid helium on a chemical reaction is different in these two cases.

This thesis is organized in the following way: chapter 1 will use the normal mode approach to find the elementary excitation spectrum of helium droplets at low temperatures. There are two types of elementary excitations of helium nanodroplets:surface and compression modes. Then the microcanonical thermodynamic functions based on the spectrum obtained will be evaluated and the rate of evaporative cooling of helium droplets will be calculated. The latter process allows droplets to maintain the temperature of $\sim$0.37 K.

In chapter 2, the microscopic theory of bulk liquid helium introduced by R. Feynman will be extended to the case of helium droplets and other systems of liquid helium in confined geometries, taking into account the possible finite size effects. This approach generalizes the consideration of the bulk liquid helium and the liquid helium in confined geometries, and hence helps to find differences and similarities of these systems. Later this chapter will develop the model of unimolecular reactions in the liquid helium environment. It is based on the model of an unimolecular reaction that proceeds in conditions of collisional energy transfer. The energy transfer rate function of this model is evaluated based on dynamical properties of liquid helium and helium nanodroplets given by the microscopic theory.

Spectroscopy is a reliable tool to explore molecular dynamics. Thus, comparing a spectrum of a free molecule with a spectrum of the molecule in liquid helium environment, the influence of the liquid helium environment on the molecular dynamics is revealed. Results of the experiment on measuring absorption spectra of NO_2 molecule below and above its gas phase dissociation threshold are also discussed in chapters 3, 4 and 5. The NO_2 molecule was chosen as the candidate for this study because it exhibits

a rich absorption spectrum along entire visible region. This molecule has been thoroughly studied and the great wealth of knowledge about its spectroscopic properties and dynamics is available.

The chapter 3 contains the description of the mass spetrometric technique used in these experiments. This technique allows the absorption spectra of molecules embedded in helium droplets to be obtained. It also can be used to study unimolecular reaction in helium nanodroplets. This chapter also contains a brief description of the experimental setup procedure used in the experiments described in the last two chapters.

In chapter 4 the experiment on mass depletion spectroscopy of NO_2 below its gas phase dissociation threshold, in the region of excitation energies where NO_2 is believed to be vibronically chaotic is discussed. The obtained spectrum has essentially the same pattern as the absorption spectrum of the free molecule. This suggests that the molecular identity is not destroyed by the interaction of the molecule with liquid helium environment. The line shifts have a modest dispersion, which is attributed quantum chaos of NO_2. The broadening of spectral lines are attributed to the fast deactivation of the molecule by liquid helium. The model developed in the chapter 2 is employed to describe the modest dispersion of the line widths.

In the experiment described in the chapter 5, NO_2 molecule trapped inside helium droplet is excited above its gas phase dissociation threshold. It was found that the liquid helium environment completely supresses the unimolecular reaction. The conclusion is made that no photoexcited polyatomic molecule will undergo barrierless unimolecular decomposition in He_n droplets of sizes similar to the ones used here, with two possible exceptions. First, a product with a positive chemical potential inside the droplet will be expelled, as with alkali atoms. Second, a small cross section for collision of a product with a helium atom, as with atomic hydrogen, enhances the escape probability.

Chapter 1

Elementary excitations of a helium nanodroplet (Discrete spectrum)

1.1 Surface excitation

The excitations with the lowest energy of a helium droplet are *surface modes*, i.e. oscillations involving deformation of the helium droplet while the helium density remains unperturbed. Surface tension acts as the restoring force.

The approach which is applied to find the vibrational normal modes of a polyatomic molecule can be adapted to the case of the helium droplet. Lets follow the procedure used in this approach. The first step is to assign a symmetry point group. A helium droplet has the spherical shape. Thus, it belongs to the totally symmetric point group of three-dimensional rotations $\mathbb{K}_h$. It is known that spherical harmonics $Y_{l,m}(\theta, \phi)$ form full basis set in this symmetry point group [3]. This group has irreducible representations with dimensions of $r = 1, 3, 5, \ldots, (2l + 1); l = 1, 2, 3, \ldots$ Therefore, the shape of the droplet can be expressed in terms of normal mode coordinates in the following way:

$$R(\theta, \phi) = R_0\Big(1 + \sum_{l,m} \alpha_{l,m} Y_{l,m}(\theta, \phi)\Big) \tag{1.1}$$

where $\{\alpha_{l,m}\}$ is the set of normal mode coordinates. It is noteworthy that the mode with $l = 0$ corresponds to "breathing", i.e. compression-dilution motion of the droplet and the mode with $l = 1$ to the motion of the whole droplet.

As long as $\alpha_{l,m}$ are normal coordinates, The potential and kinetic energies can be introduced as quadratic forms:

$$T = \frac{1}{2}\sum_{l,m}\mu_l|\dot{\alpha_{l,m}}|^2 \tag{1.2a}$$

$$V = \frac{1}{2}\sum_{l,m}\kappa_l|\alpha_{l,m}|^2 \tag{1.2b}$$

where μ_l and κ_l are the effective mass and the force constant of the normal mode oscillator, respectively. Obviously, the equations of motion expressed in the normal coordinates are:

$$\ddot{\alpha_{l.m}} + \omega_l\alpha_{l.m} = 0 \tag{1.3}$$

where the oscillator frequency is given by standard expression:

$$\omega_l = \sqrt{\frac{\kappa_l}{\mu_l}} \tag{1.4}$$

To proceed further it is necessary to express the effective mass and force constant of the normal mode oscillators through properties of liquid bulk helium such as surface tension and density.

1.1.1 Force constant

To beging, consider the force constant κ_l. By definition, the surface tension plays the role of the restoring force for the surface modes. The increase of the surface energy associated with a deformation of the droplet is equal to $\Delta E = \sigma\Delta S$, where ΔS is increment of the free surface area due to the deformation and σ is the surface tension of liquid helium. The macroscopic value of the surface tension $\sigma = 0.37$ mJ/m^2 [5] can be

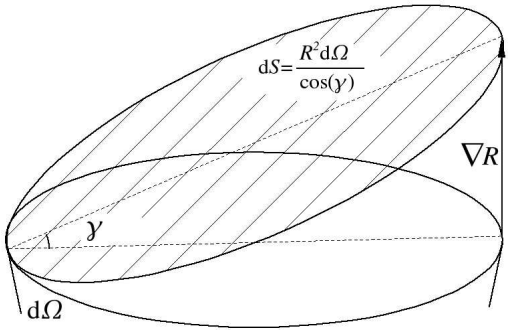

Figure 1.1: Calculation of the elementary surface

employed as a good approximation to be used in consideration of the processes even on the microscopic scale.

Consider a surface element of the deformed droplet seen in the direction (θ, ϕ) at elementary solid angle $d\Omega$ from the center of the droplet. As it can be seen in figure 1.1, the area of this surface element is:

$$dS = \frac{R^2 d\Omega}{\cos\gamma}$$

where γ is approximately equal to $|\nabla R|$. Expanding to the second order of the deformation parameter, one can obtain:

$$dS \approx \frac{d\Omega R^2}{1 - \frac{1}{2}|\nabla R|^2} \approx d\Omega \left(R^2 + \frac{1}{2} R_0^2 |\nabla R|^2 \right);$$

In order to obtain the increment of the surface area of the deformed droplet, this must be integrated over the entire solid angle:

$$\Delta S = \int d\Omega \left(R^2 + \frac{1}{2} R_0^2 |\nabla R|^2 \right) \tag{1.5}$$

Taking into account the following equalities:

$$\int \nabla \left(R\nabla R \right) d\Omega = \int \left(\nabla R \cdot \nabla R \right) d\Omega + \int R\nabla^2 R d\Omega = 0;$$
$$R^2 - R_0^2 = 2R_0 \left(R - R_0 \right) + \left(R - R_0 \right)^2;$$

one obtains:

$$\Delta S = \int 2R_0(R - R_0)d\Omega + \int (R - R_0)^2 d\Omega - \int \frac{1}{2} R\nabla^2 R d\Omega; \tag{1.6}$$

Substituting the expression for $R(\theta, \phi)$ given by equation (1.1) and taking into account the properties of spherical harmonics

$$\int Y_{l,m} Y^*_{l',m'} d\Omega = \delta_{l,l'} \delta_{m,m'};$$
$$\nabla^2 Y_{l,m} = -l(l+1) Y_{l,m};$$
$$Y_{00} = \frac{1}{\sqrt{4\pi}};$$

Integrating the above expression gives:

$$\Delta S = R_0^2 \left(2\sqrt{4\pi}\alpha_0 + \sum_{l,m} \alpha_{l,m}^2 + \frac{1}{2} \sum_{l,m} l(l+1)\alpha_{l,m}^2 \right) \tag{1.7}$$

Taking into account the assumption of the incompressibility of the fluid made in the beginning of the previous section, one finds the relationship between α_0 and coefficient,s $\alpha_{l,m}$. The density function can be defined in the following way:

$$\rho(r, \theta, \phi) = \rho_0 \chi(r - R(\theta, \phi)) \tag{1.8}$$

where $\eta(x)$ is the Heaviside function. Assuming that the deformation of the droplet $|R - R_0| \ll R_0$ is small, the density function can be expanded as a series of $(R - R_0)$:

$$\begin{aligned}\rho(r,\theta,\phi) = \rho_0(\eta(r - R(\theta,\phi)) + (R - R_0)\delta(r - R_0) \\ - \frac{1}{2}(R - R_0)^2\delta'(r - R_0) + \cdots)\end{aligned} \tag{1.9}$$

Integrating the last expression over entire space, one must obtain the mass of the droplet $M = 4\pi R_0^3\rho_0/3$. Integrals of these terms are given by

$$\begin{aligned}\int \rho_0(\eta(r - R(\theta,\phi))r^2 dr d\Omega &= \rho_0\frac{4\pi R_0^3}{3} \\ \int \rho_0(R - R_0)\delta(r - R_0)r^2 dr d\Omega &= \rho_0 R_0^2 \int (R - R_0)d\Omega = \rho_0 R_0^2\alpha_0\sqrt{4\pi} \\ \frac{1}{2}\int \rho_0(R - R_0)^2\delta'(r - R_0)r^2 dr d\Omega &= -\rho_0 R_0^2 \sum_{l,m} \alpha_{l,m}^2\end{aligned}$$

The first integral gives the entire mass of the droplet. Thus, the contribution of the second and the third integrals must cancel each other out, giving the desired relationship between α_0 and $\alpha_{l,m}$:

$$\alpha_0 = -\frac{1}{\sqrt{4\pi}} \sum_{l,m} \alpha_{l,m}^2 \tag{1.10}$$

Substituting equation (1.10) into the equation (1.7) gives:

$$\Delta S = \frac{1}{2} R_0^2 \sum_{l,m} (l - 1)(l + 2)\alpha_{l,m}^2 \tag{1.11}$$

The potential energy is given by the expression

$$V = \sigma\Delta S = \sigma R_0^2 \frac{1}{2} \sum_{l,m} (l - 1)(l + 2)\alpha_{l,m}^2 \tag{1.12}$$

Combining the equation (1.12) with the equation (1.2b) gives the expression for the force constant κ_l:

$$\kappa_l = \sigma R_0^2 (l-1)(l+2) \tag{1.13}$$

1.1.2 Mass parameter

The mass parameter appears in the expression for the kinetic energy of the droplet (1.2a). On the other hand, the kinetic energy of the oscillating droplet can be expressed as:

$$T = \int_V \frac{\rho_{\text{He}} \mathbf{v}^2}{2} dV \tag{1.14}$$

where ρ_{He} is the density of helium in the droplet. The velocity field $\mathbf{v}$ can be obtained by solving the hydrodynamic equations for the motion of the liquid in the oscillating droplet

$$\nabla^2 \chi = 0 \tag{1.15}$$

where χ is the velocity potential. It relates to the velocity field as:

$$\mathbf{v} = -\nabla \chi \tag{1.16}$$

The solution of the equation (1.15) for the case of oscillating liquid helium droplet is given by:

$$\chi(r, \theta, \phi) = \sum_{l,m} c_{l,m} r^l Y_{l,m}(\theta, \phi) \tag{1.17}$$

The relationship between coefficients $c_{l,m}$ and $\dot{\alpha_{l,m}}$ can be found from the boundary conditions. At the droplet boundary $v_r = \dot{R}$, and hence:

$$\begin{aligned}
\dot{R} &= R_0 \sum_{l,m} \dot{\alpha}_{l,m} Y_{l,m}(\theta, \phi) \\
v_r &= \frac{\partial \chi}{\partial r}|_{r=R_0} = \sum_{l,m} c_{l,m} l R_0^{l-1} Y_{l,m}(\theta, \phi) \\
c_{l,m} &= l R_0^{l-2} \dot{\alpha}_{l,m}
\end{aligned} \tag{1.18}$$

The kinetic energy is then given by:

$$T = \frac{1}{2}\rho_{\mathrm{He}} R_0^2 \int \left(\chi \frac{\partial \chi}{\partial r}\right)_{r=R_0} d\Omega = \frac{1}{2}\rho_{\mathrm{He}} R_0^2 \sum_{l,m} c_{l,m}^2 l r^{2l-1}|_{r=R_0} \tag{1.19}$$

Combining the above equation with equations (1.2a) and (1.18) gives the expression for the mass parameter, μ_l:

$$\mu_l = \frac{1}{l}\rho_{\mathrm{He}} R_0^5 = \frac{3}{4\pi}\frac{1}{l} N m_{\mathrm{He}} R_0^2 \tag{1.20}$$

where N is the number of atoms in a helium droplet and m_{He} is the mass of a helium atom. Significantly, the mass parameter is proportional to the mass of the droplet, thereby indicating that the entire droplet rather than only surface region participates in the motion.

Substituting the force constant (1.13) and the mass parameter (1.20) into the frequency equation (1.4), gives the final expression for the frequencies of the surface modes:

$$\omega_l = \sqrt{\frac{4\pi}{3} l(l-1)(l+2)\frac{\sigma}{m_{\mathrm{He}} N}} \tag{1.21}$$

The frequencies calculated from the expression (1.21) for the droplet having $N = 10^4$ atoms are $\hbar\omega_l$ =0.10, 0.21, 0.32, 0.44, 0.58, 0.72, 0.88 K for l =2, 3, 4, 5, 6 and 7 respectively.

1.2 Compression modes

Beside the surface excitations discussed in the previous section, helium droplets possess another type of excitation originating from the oscillations involving fluctuations of helium density. The bulk helium counterparts of these excitations are sound waves. To calculate energy spectrum corresponded to these types of excitations, consider the density of the helium in the droplet:

$$\rho(\mathbf{r}) = \rho_0 + \delta\rho(\mathbf{r}) \tag{1.22}$$

where ρ_0 is the equilibrium density and $\delta\rho(\mathbf{r})$ represents the density fluctuations. The relationship of the density fluctuation $\delta\rho$ and excess pressure δp is given by:

$$\frac{\delta p}{\delta\rho} = m_{\mathrm{He}}c^2 \tag{1.23}$$

where c is the speed of sound in liquid helium. The hydrodynamics equations that govern the motion of the fluid expanded to the first order of $\delta\rho$ and δp can be written as:

$$\frac{\partial}{\partial t}\delta\rho(\mathbf{r},t) + \rho_0\nabla\cdot\mathbf{v}(\mathbf{r},t) = 0 \tag{1.24a}$$

$$\frac{d\mathbf{v}}{dt} = \frac{\partial}{\partial t}\mathbf{v}(\mathbf{r},t) = -\frac{1}{\rho_0}\delta p(\mathbf{r},t) \tag{1.24b}$$

Taking into account equation (1.23), the above equations can be recast into the wave equation:

$$\nabla^2 \delta\rho(\mathbf{r}, t) - \frac{1}{c^2}\frac{\partial^2}{\partial t^2}\delta\rho(\mathbf{r}, t) = 0 \tag{1.25}$$

The solution of the above equation for the helium droplet is given by:

$$\delta\rho = \rho_0 j_l(k_{nl} r) Y^*_{l,m}(\theta, \phi)\alpha_{nlm}(t) \tag{1.26a}$$

$$\mathbf{v} = \frac{1}{k^2_{nl}}\nabla(j_l(k_{nl} r) Y^*_{l,m}(\theta, \phi))\dot{\alpha}_{nlm}(t) \tag{1.26b}$$

where j_l is spherical Bessel function defined as:

$$j_l(x) = (-1)^l x^l \left(\frac{d}{xdx}\right)^l \frac{\sin(x)}{x} \tag{1.27}$$

The first few functions are

$$\begin{aligned} j_0(x) &= \frac{\sin(x)}{x}; \\ j_1(x) &= \frac{\sin(x)}{x^2} - \frac{\cos(x)}{x}; \\ j_2(x) &= \left(\frac{3}{x^3} - \frac{1}{x}\right)\sin(x) - \frac{3}{x^2}\cos(x); \end{aligned}$$

The eigenvalues are determined by the boundary condition

$$j_l(k_{nl} R_0) = 0 \tag{1.28}$$

meaning that there is no excess pressure at the surface of the droplet.

The few lowest compression mode frequencies are given by the following expression

$$\omega_{nl} = \frac{c}{R_0} \begin{cases} 3.14 & l = 0,\ n = 1 \\ 4.49 & l = 1,\ n = 1 \\ 5.76 & l = 2,\ n = 1 \end{cases} \tag{1.29}$$

The energy of the lowest compression monopole excitation can be calculated from this equation [1]:

$$\omega_M = 26 N^{-\frac{1}{3}}\,\mathrm{K} \tag{1.30}$$

1.3 Density of states and microcanonical thermodynamic functions of helium droplets

Helium droplets contain $10^3 - 10^6$ atoms, suggesting that the system is large enough to be described statistically. The statistical approach assumes that the system is described with a set of thermodynamic functions such as temperature, entropy, specific heat, etc. The standard procedure for calculating the thermodynamic functions begins with evaluating the *partition function* of the system under consideration. Assuming that excitations of helium droplet obey Bose statistic, the expression for the partition functioncan be written as [1]:

$$\ln Z(\beta) = -\sum_i \ln(1 - e^{\epsilon_i \beta}) \tag{1.31}$$

where $\beta = (kT)^{-1}$, i enumerates all the states of helium droplet.

As discussed above, helium droplets posses two type of excitations: deformation and compression modes. It was found experimentally that the stationary temperature

of helium droplets is equal to 0.37 K. [6], which will be discussed in more detail in the next section. Using the equation (1.30), the lowest compression mode of a helium droplet containing 10^3 atoms is calculated to be ~ 2.6 K. Thus it can be assumed that the compression modes have relatively high energies and remain mostly unpopulated. Therefore they can be excluded from our consideration and focus will be placed on surface excitations.

The expression for the partition function for the surface excitations is given by:

$$\ln Z(\beta) = -\sum_l l(l+1)\ln(1-e^{\epsilon_l \beta}) \tag{1.32}$$

where $\epsilon_l = \hbar\omega_l$, which are the energies of surface excitations, and ω_l is given by equation (1.21). The next step is to replace the sum in the expression above with an integral. If $\lambda = l + \frac{1}{2}$ is put in the expression for the frequencies of the surface excitations then it becomes:

$$\begin{aligned}\omega_\lambda &= \sqrt{\frac{4\pi}{3}\frac{\sigma}{m_{\mathrm{He}}N}\left(\lambda-\frac{3}{2}\right)\left(\lambda-\frac{1}{2}\right)\left(\lambda+\frac{3}{2}\right)} \\ &\backsimeq \left(\frac{4\pi}{3}\frac{\sigma}{m_{\mathrm{He}}N}\right)^{\frac{1}{2}}\lambda^{2/3}\end{aligned}$$

Equation (1.32) then becomes:

$$\ln Z(\beta) = -2\int_0^\infty \lambda\left(1-e^{-\beta\hbar\omega_l}\right)d\lambda \tag{1.33}$$

Evaluation of the integral in this expression gives

$$\ln Z(\beta) = -4\pi\beta^{-\frac{4}{3}}N^{\frac{2}{3}}\xi\left(\frac{3}{4\pi}\frac{m_{\mathrm{He}}}{\sigma}\right)^{\frac{2}{3}} \tag{1.34}$$

where ξ is given by

$$\xi = \frac{1}{3\pi}\int_0^\infty x^{\frac{1}{3}}\ln(1-e^{-x})dx = -0.134$$

Evaluation of the thermodynamic functions usually proceeds as follows. First, the free energy function given by [4]

$$F(\beta) = -\frac{1}{\beta}\ln Z(\beta) \tag{1.35}$$

is calculated. Substituting the expression for $\ln Z(\beta)$ calculated above, giving:

$$F(\beta) = -a\beta^{-\frac{7}{3}}N^{\frac{2}{3}} \tag{1.36}$$

where we denote

$$a = 4\pi\xi\left(\frac{3}{4\pi}\frac{m_{\mathrm{He}}}{\sigma}\right)^{\frac{2}{3}} \tag{1.37}$$

Then, the relationship between functions is used to evaluate other functions of the system. For example, the relationship between energy of the system and the free energy is given by the following expression:

$$E = F + \beta\frac{\partial F}{\partial\beta} = \frac{4}{3}a\beta^{-\frac{7}{3}}N^{\frac{2}{3}} \tag{1.38}$$

Entropy of the helium droplet is equal to:

$$S = \beta(E-F) = \frac{7}{3}a\beta^{-\frac{4}{3}}N^{\frac{2}{3}} = bE^{\frac{4}{7}}N^{\frac{2}{7}} \tag{1.39}$$

with

$$b = \frac{7}{4}\left(\frac{4}{3}a\right)^{\frac{3}{7}}$$

Knowing the partition function, an analytical expression for the density of states can be obtained [1]. The relationship between the density of states, $\rho(E)$, and the partition function is given by:

$$Z(\beta) = \int_0^\infty \rho(E) e^{-E\beta} dE \tag{1.40}$$

The equation above coincides with the definition of the Laplace transform of the density of states function:

$$Z(\beta) = \mathscr{L}[\rho(E)] \tag{1.41}$$

Thus, the density of states is given by the inverse Laplace transform of the partition function

$$\rho(E) = \mathscr{L}^{-1}[Z(\beta)] \tag{1.42}$$

The inverse Laplace transform is given by the Bromvich integral [2]:

$$\rho(E) = \frac{1}{2\pi i} \int_{\gamma - i\infty}^{\gamma + i\infty} d\beta' e^{\beta' E} Z(\beta') = \frac{1}{2\pi i} \int_{\gamma - i\infty}^{\gamma + i\infty} d\beta' e^{\beta'(E - F(\beta'))} \tag{1.43}$$

The contour of integration is chosen so that γ is greater than the real part of all the singularities of $Z(\beta')$. The integral can be calculated expanding the exponent up to the second order in $(\beta - \beta')$ and evaluating the Gaussian integral [1]. The result is:

$$\begin{aligned} \rho(E) &= \frac{1}{\sqrt{-2\pi \frac{\partial E}{\partial \beta}}} e^{S(E)} \\ &= c E^{-\frac{5}{7}} N^{\frac{1}{7}} \exp(S(E)) \end{aligned} \tag{1.44}$$

with

$$c = \sqrt{\frac{3}{14\pi}} \left(\frac{4}{3} a\right)^{\frac{3}{14}}$$

1.4 Evaporative cooling

As already mentioned, experiments show that the temperature of helium droplet is $\sim$0.37 K. [6]. The droplet maintains low temperature by evaporating helium atoms from its surface. This process results in dumping of the elementary excitations described above. It causes the broadening of the corresponding resonanses and the spectrum of the droplet becomes congested.

Liquid helium environment's major influence on chemical reactions is draining the energy from reacting molecules, which will be discussed in detail later. Thus, it is a problem of primary importance to describe quantitatively the process of evaporative cooling.

The approach described below at first was developed by Weisskopf to calculate rates of nuclear reactions [7], and later it was used by D.M. Brink and S. Stringary [1] to calculate the rate of evaporative cooling.

Consider a helium droplet as a big molecule. Then, evaporation of a helium atom can then be considered as a chemical reaction:

$$\mathrm{He}_N \leftrightarrows \mathrm{He}_{N-1} + \mathrm{He}$$

k_u and k_b are the rates of direct and reverse reactions respectively. The energy conservation law is given by:

$$E_N = E_{N-1} + E_0 + \epsilon \tag{1.45}$$

where E_N and E_{N-1} are the energies of He_N and He_{N-1} clusters, ϵ is the kinetic energy of the He atom, and E_0 is the binding energy. The binding energy can be estimated as a sum of zero point energy and surface energy per atom in the cluster:

$$E_0 = E_{\text{z.p.}} - \frac{2}{3} 4\pi\sigma N^{-1/3} = 7.15\ K - \frac{2}{3} 6.95\ K \tag{1.46}$$

From the microscopic reversibility of the reaction, it follows

$$k_u = k_b \frac{[\mathrm{He}_{N-1}] \cdot [\mathrm{He}]}{\mathrm{He}_N} \tag{1.47}$$

Assume that the cluster and the atom are enclosed in a box of volume V. The bimolecular reaction rate constant is given by:

$$k_b = \frac{su}{V} \tag{1.48}$$

where u is the speed of the helium atom and s is collision cross section that can be safely replaced with geometrical cross section of the helium cluster. The equilibrium constant can be replaced with densities of states

$$k_u = k_b \frac{[\mathrm{He}_{N-1}] \cdot [\mathrm{He}]}{\mathrm{He}_N} = k_b \frac{w_t(\epsilon) w_{\mathrm{He}_{N-1}}(E_{N-1})}{w_{\mathrm{He}_N}(E_N)} \tag{1.49}$$

The translational density of states is given by:

$$w_t(\epsilon) = \frac{4}{\pi^2 \hbar^3} m_{\mathrm{He}}^{3/2} \sqrt{2E} V \tag{1.50}$$

Substituting it into the equation (1.49) for the equilibrium constant we obtain:

$$k_u(E, \epsilon) = \frac{8\epsilon s m_{\mathrm{He}}}{\pi^2 \hbar^3} \frac{w_{N-1}(E - E_0 - \epsilon)}{w_N(E)} \tag{1.51}$$

The density of ripplon states calculated in the previous section is given by the equation (1.44). Substituting it into the equation (1.51) gives:

$$k_u(E,\epsilon) = \frac{8\epsilon s m_{\mathrm{He}}}{\pi^2\hbar^3}\left(\frac{N-1}{N}\right)^{1/7}\left(\frac{E}{E-E_0-e}\right)^{5/7}\times$$
$$\exp\left(\frac{4}{7}\left(\frac{3}{4}\right)^{\frac{3}{7}}\left(E^{\frac{4}{7}}N^{\frac{5}{7}}-(E-E_0-\epsilon)^{\frac{4}{7}}(N-1)^{\frac{5}{7}}\right)\right) \tag{1.52}$$

Evaporative rate is then given by the integral:

$$\Gamma \equiv \frac{dN}{dt} = \int_0^{E-E_0} k_u(E,\epsilon)d\epsilon \tag{1.53}$$

and the energy dissipation rate is given by:

$$\frac{dE}{dt} = \int_0^{E-E_0} (E_0+\epsilon)E,\epsilon)d\epsilon \tag{1.54}$$

Reference List

[1] D.M. Brink and S. Stringary. Density of states and evaporation rate of helium cluster. *Z. Phys. D.*, 15:257–263, 1990.

[2] Arfken G. *Mathematical Methods for Physicists*, chapter 15.12. Academic Press, 1985.

[3] Granino A. Korn and Theresa M. Korn. *Mathematical handbook for scientists and engineers*. McGraw-Hill, 1961.

[4] L.D. Landau and E. M. Lifshitz. *Statistical Physics, Part 1*, volume 5 of *Course of Theoretical Physics*. Pergamon Press, Oxford, 3rd edition, 1978.

[5] Steven W. Van Sciver. *Helium Cryogenics*. International Cryogenics Monograph Series. Plenum Press, 1986.

[6] Vilesov Andrei F. Toennies J. Peter. Spectroscopy of atoms and molecules in liquid helium. *Annual Review of Physical Chemistry*, 49(1):1–41, 1998.

[7] V. Weisskopf. Statistics and nuclear reactions. *Physical Review*, 52:295–303, 1937.

Chapter 2

Dynamic properties of liquid ^{4}He and ^{4}He clusters and their influence on the unimolecular reaction rate

In the previous chapter the liquid drop theory of the helium droplet was discussed. In frames of this theory The helium droplet was treated as a big molecule and found the droplet excitation spectrum using the normal mode approximation. Based on this theory, one can calculate the thermodynamic properties of the droplet, explain the phenomenon of evaporative cooling and describe the shape of the spectral lines.

This theory predicts that the droplet would have a discrete excitation spectrum. However, the spectrum is congested. Evaporative cooling limits the lifetime of the droplet excitation leading to the broadening of the corresponded resonances, resulting in congestion of the spectrum. Beside that, the energy of the droplet excitation depends on the size of the droplet. The droplet beam that experimentalists are usually dealing with have a rather broad log-normal distribution of sizes of the droplets [32]. There is no convenient way of producinge a helium droplet beam that consists of the droplets having a narrow size distribution. Thus, the spectrum of the droplet should be averaged over this distribution and this averaging make it to look “bulk-like” rather than having isolated resonances.

This reasoning suggests another perspective for which to consider helium droplets. It is not unreasonable to assume that the droplet, being made of liquid helium would

inherit some of its microscopic properties. Thus, one can start with microscopic theory of liquid helium and then introduce corrections to take into account finite size effects. These effects include suppression of the excitations having wavelengths exceeding characteristic size of the droplets and appearance of new types of excitations originated from surface phenomena. This approach is expected to provide an adequate description of the high energy part of the excitation spectra because the wavelength of the corresponding excitations is smaller than the droplet size.

Another advantage of this approach is that it may help to reveal the relationship between phenomena observed in bulk and confined quantum fluid systems. Beside the case of helium nanodroplets these confined systems include but are not limited to, helium films and helium confined in a porous media such as helium filled aerogel.

Early experiments led to discovery of superfluidity [22], $\lambda-$transition [19] and other unusual properties of liquid helium. Originally, these effects were attributed to the phenomenon of Bose-Einstein condensation [29, 30]. Later, L. D. Landau opposed this idea arguing that Bose-Einstein condensation phenomenon was derived for an ideal gas while interaction between helium atoms in liquid helium is rather strong [25]. Instead, he suggested considering liquid helium from another perspective. He introduced the concept of quasiparticle that represents some sort of collective motion of helium atoms and proposed that a system consisting of these quasiparticles is equivalent (i.e. possesses the same properties) to liquid helium [26]. Landau also derived the excitation spectrum of liquid helium from an analysis of its thermodynamic properties [25]. The shape of the spectrum suggested by Landau was later conformed by neutron scattering measurements [11]. Based on this theory, Landau explained the unusual properties of liquid helium.

It is noteworthing, that Landau's theory was based on quantization of hydrodynamic equations rather than being derived from the microscopic consideration of liquid

helium. The first consistent microscopic theory was originally introduced by Feynman in 1954 [15]. This theory allows the derivation of the Landau spectrum from the microscopic perspective. In addition, it provides the description of the dynamic properties of liquid helium.

The results of the neutron scattering experiments will be considered later in this chapter. These experiments are interesting not only because they allow for exploration of the microscopic properties of liquid helium but also because they explain how energy dissipation occurs in helium on a molecular scale. The energy dissipation processes impose dramatic influence on the chemical reactions in liquid helium, as will be discussed later. Unfortunately there is no data are currently available on the neutron scattering on helium droplets. However, the finite size of the helium droplets facilitate computer simulations that can be a source of the information about microscopic structure and dynamics. The results of these computer simulations will be discussed later.

Finally unimolecular chemical reaction proceeding in liquid helium environment will be considered. The major influence of the liquid helium environment on the impurity molecule that undergoes an unimolecular reaction is that the energy of the molecule can be transfered to the liquid helium. In other words, helium acts as an efficient coolant. The unimolecular reaction rate in conditions of collisional energy transfer using Lindermann mechanism based on detailed balance equations will be derived. In frames of this consideration the environment is characterized by energy transfer rate. The energy transfer rate for the liquid helium environment will be derived in the last section.

2.1 Developement of conceptual framework of the theory of liquid helium

2.1.1 Early experiments on liquid helium

The first time liquid helium was obtained was in 1908 by Kammerling Onnes. Early experiments revealed that liquid helium possesses a set of unusual properties. Keesom and Wolfke discovered two phases of liquid helium: He I and He II observing a sharp maximum and a discontinuity of the density temperature function $\rho(T)$ at the temperature around T =2.2 K [18]. It was found later that the transition between these two phases is accompanied by the divergence of the specific heat function C_v at the temperature of 2.17 K [19]. This transition was denoted as λ-transition.

The fact that the viscosity of the liquid helium flowing through capillaries vanishes at temperatures below the temperature of λ-transition was simultaneously reported by Kapitza [22] and Allen and Misener [3]. This remarkable property of liquid helium was later called *superfluidity*. The first attempts to measure the thermal conductivity of the He II phase showed that it is very high and even infinite for the small heat currents. These observations could not be explained by the "classical" fluid theory. F. London was the first who proposed that unususal properties possessed by liquid helium might have quantum origin [29, 30]. He noticed that the dependence of the specific heat function of liquid helium on temperature was somewhat similar to the calculated behavior of the specific heat of an ideal Bose gas (refer to Fig. 2.1).

Bose gas is an ensemble of non-interacting particles having zero or integer spin. Many-particle wavefunctions of such a system are symmetrical with respect to particle permutations. Therefore, occupation numbers of the quantum states of the system can

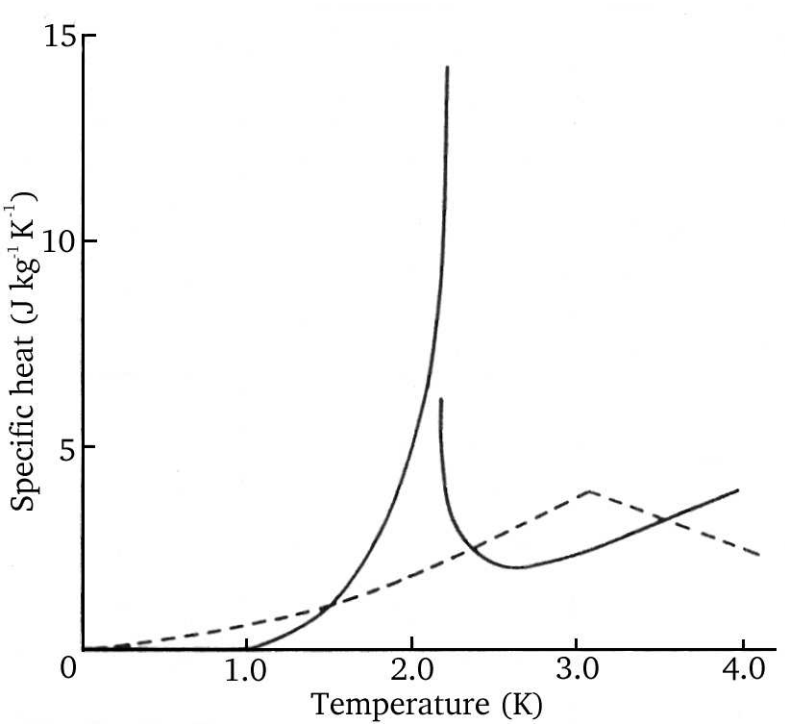

Figure 2.1: Specific heat of liquid ^{4}He. The broken line shows the calculated specific heat of an ideal Bose gas having the same density as liquid ^{4}He.

exceed unity in contrast to the situation with an ensemble of fermions, i.e. the particles having half-integer spin. The theory shows that there is a critical temperature, which is:

$$T_c = \frac{3.31\hbar^2}{m}\rho_N^{2/3} \tag{2.1}$$

where m is the mass of the particles and ρ_N is the number density of the gas [30]. For the temperatures below T_c, a macroscopic number of the particles of the gas occupies the lowest quantum state. These particles have zero momentum and form so-called Bose condensate. The critical temperature T_c calculated from equation (2.1) with the mass and number density of the liquid helium is equal to 3.1 K, which is fairly close to the temperature of λ-transition T_λ. In the framework of this theory, London explained many other properties of the liquid helium.

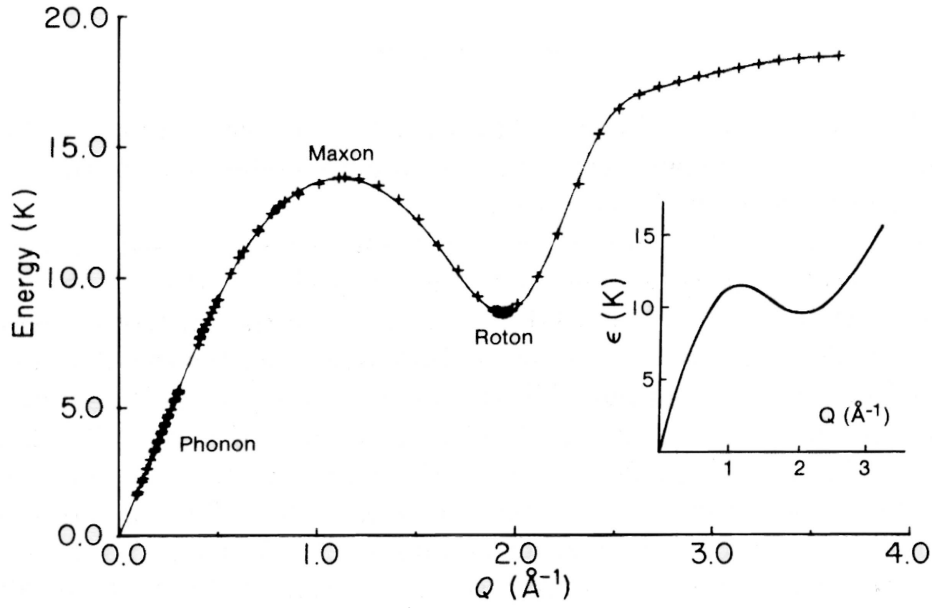

Figure 2.2: Liquid ^{4}He elementary excitation energy spectrum measured by neutron scattering. [11] The insert shows the energy spectrum predicted by Landau. [25]

Inspired by the ideas of London, Tisza introduced macroscopic phenomenological two-fluid theory [40]. In frames of this theory, liquid helium is considered as a "mixture" of two fractions: "normal" having density ρ_n and "superfluid" with density ρ_s. These fractions can interpenetrate each other and have independent velocity fields $\mathbf{v}_n$ and $\mathbf{v}_s$. According to Tisza, the superfluid fraction corresponded to the Bose condensate does not participate in dissipation processes. At $T = 0$ K the fluid consists of only a superfluid component $\rho = \rho_s$. As the temperature grows, some of the helium atoms leave condensate and form normal component. The equations for the density and mass flow become:

$$\rho = \rho_n + \rho_s \tag{2.2a}$$

$$\mathbf{j} = \rho_n \mathbf{v}_n + \rho_s \mathbf{v}_s \tag{2.2b}$$

It was successy used to describe the results of the experiments on helium II. The major succsess of this theory was a prediction of the existence of thermal waves, which were later called “second sound” [41].

2.1.2 Concepts of quasiparticle and elementary excitation energy spectrum

L.D. Landau opposed the idea that Bose condensate represents the superfluid fraction of liquid helium [25]. He argued that the interaction between atoms in liquid helium is quite strong in contrast to the situation with ideal Bose gas for which the phenomenon of the condensation was predicted. Moreover, nothing prevents helium atoms from momentum exchange through collisions. The last consideration contradicts the main assumption of the two-fluid theory in Tisza’s interpretation.

Landau developed the two fluid model from quite different physical perspective [24, 25, 28]. He introduced the concept of elementary excitation or “quasiparticle”. It is postulated in Landau’s theory that the excitation of any many-particle quantum system to its low lying quantum state that corresponds to some sort of collective motion can be described as an appearance of a quasiparticle with momentum $\hbar\mathbf{q}$ and energy $\mathcal{E}(\mathbf{q})$. These quasiparticles move in the space occupied by the original quantum system. The ensemble of quasiparticles mimic the statistical properties of the quantum system. Formulas of statistical theory can be applied to the ensemble of quasiparticles and the thermodynamic functions obtained are those of the original quantum system. [26]

The quasiparticle approach is similar to the normal mode approximation used to describe the vibrations of symmetric polyatomic molecules. The approximation was successfully employed in the previous chapter to describe vibrations of the helium droplet. In frame of this approximation, collective motion of several atoms in the molecule are replaced by an imaginary oscillator having an effective mass and a force

constant. Normal modes of a molecule with harmonic bonding are independent. Anharmonicity of the molecule in the first order approximation can be described as an interaction between the normal modes.

Thus, the dependence of the energy of elementary excitations on their momentum $\mathcal{E}(\mathbf{p})$, that is frequently called "energy spectrum" or dispersion relation, plays an important role in Landau's theory [26]. The energy spectrum of liquid helium proposed by Landau [25] is shown in figure 2.2. It is in the remarkable correspondence with experimental data on neutron scattering available nowdays [11, 1].

The only excitations available at low energies are *phonons*. The energy of a phonon is proportional to its mometum:

$$\mathcal{E}(p) = cp \tag{2.3}$$

where c is the speed of sound in liquid helium. At the energies higher than the energy of attraction between atoms, liquid helium would behave as an ideal gas and the energy spectrum should correspond to the one of a free particle: [1]

$$\mathcal{E}(p) = \frac{p^2}{2m} \tag{2.4}$$

Landau also proposed the exsistence of quasiparticles corresponding to vortex motion of liquid helium called *rotons* [24]. Originally he suggested the following form of the dispersion relation for the rotons:

$$\mathcal{E}(p) = \Delta + \frac{p^2}{2\mu}$$

[1] Comparing the spectra shown in figure 2.2 one can easily see that the energy spectrum of liquid helium obtained in the neutron scattering experiment [11] does not follow the free particle part at high q. That is because at high momenta the excitations tend to decay to pair of rotons [37]. This issue will be discussed in details on the page 41 later in this chapter.

where μ is an effective mass of a roton. Later, analyzing the data on the velocity of the second sound [36], he corrected the roton dispersion relation and it became [25]:

$$\mathcal{E}(p) = \Delta + \frac{(p - p_0)^2}{2\mu} \tag{2.5}$$

where $\Delta = 8.7\mathrm{K}$, $\mu = 0.16 m_{\mathrm{He}}$ and $p_0/\hbar = 1.9\mathrm{cm}^{-1}$.

Landau explained the phenomenon of supefluidity based on the shape of the excitation energy spectrum [24]. He showed that the necessary condition for the superfluidity to occur at $T = 0$ is:

$$\frac{d\mathcal{E}(p)}{p}\Big|_{p=0} \neq 0 \tag{2.6}$$

A macroscopic body moving through liquid helium can create elementary excitations only if its velocity exceeds the critical velocity $E(p)/p$. For the phonons, this critical velocity corresponds to the speed of sound $c = 250$ m/s, while for the rotons it is equal to $\sqrt{\Delta/2\mu} \approx 57$ m/s. The dissipation only occurs if any of these excitations can be created or, in other words, the velocity of the body exceeds the value of $\min(\mathcal{E}(p)/p)$, which is the roton critical velocity. However, the above arguments are made for a macroscopic body, with kinetic energy and momentum infinite compared to the energy and momentum of the elementary excitations. In the most interesting case of microscopic objects, such as atoms or molecules, the criteria for the superfluidity and even the meaning of superfluidity itself must be reformulated.

It must be underlined that the Landau's theory is essentialy based upon quantization of the hydrodynamic equations. It does not address microscopic properties of liquid helium. However, as discussed above, this theory correctly describes thermodynamic properties of liquid helium and explains the phenomenon of superfluidity. In other words the energy spectrum, at first predicted by Landau and then confirmed experimentally, is a fundamental property of liquid helium. Any theory persuing the objective to explain

behavior of liquid helium should also be able to reconstruct the elementary excitation energy spectrum.

The first attempt to build such a theory was made by Bogolubov [35]. He considered an almost ideal Bose gas with weak interaction between particles. By diagonalizing the hamiltonian of such a system, he obtained a diagonal hamiltonian corresponding to "a perfect Bose gas of certain "quasiparticles" representing the elementary excitations, which cannot be identified as individual molecules [35]. The eigenvalues of the hamiltonian give the energy spectrum of the "quasiparticles":

$$\mathcal{E}(q) = \sqrt{\frac{q^2\nu(q)}{mv} + \frac{q^4}{4m^2}} \tag{2.7}$$

where $q = p/\hbar$ is wavevector of the "quasiparticles," the $\nu(q)$ is the Fourier component of the potential of interaction between helium atoms, and v is the volume per helium atom.

It can be seen from the equation (2.7) that the Bogolubov's energy spectrum qualitatively follows the spectrum suggested by Landau: (i) at $q \to 0$, the energy is proportional to momentum; (ii) at the region of high momenta, $\mathcal{E}(p) = p^2/2m$; (iii) for the intermediate momenta the shape of the $\nu(q)$ function can be chosen so that $d\mathcal{E}(p)/dp = 0$, which corresponds to the roton part of the spectrum. Another important conclusion of the Bogolubov's theory is that the interaction between particles of a Bose gas does not preclude Bose-Einstein condensation to occur. However, in the non-perfect Bose gas some of the particles remain out of the condensate even at $T = 0$.

Although the interaction between atoms of liquid helium is weak, liquid helium cannot be regarded as "almost ideal Bose gas." Thus, the question of microscopic justification of Landau theory remains open. The first successful attempt to make such a justification and build a consistent microscopic theory of liquid helium was made by

Feynman [15]. This theory is important for our further discussion and we will consider it in details in the next section.

2.2 Feynman's microscopic theory of liquid helium

In this theory liquid helium is considered as a system of N interacting Bose particles. Feynman proposed the following form for the wavefunction of an excited state:

$$\psi(\mathbf{r}_1 \dots \mathbf{r}_N) = \sum_{i=1}^{N} f(r_i)\phi(\mathbf{r}_1 \dots \mathbf{r}_N) \tag{2.8}$$

where $\mathbf{r}_1 \dots \mathbf{r}_N$ are the coordinates of the helium atoms and $\phi(\mathbf{r}_1 \dots \mathbf{r}_N)$ is the wavefunction of the ground state of the liquid helium. The wavefunction (2.8) is not normalized.

The Hamiltonian of the system can be written as:

$$\hat{H} = -\frac{\hbar^2}{2m}\sum_{i=1}^{N}\nabla_i^2 + U - E_0 \tag{2.9}$$

Here U is the potential energy of the system and E_0 is the energy of the ground state. So that

$$\hat{H}\phi = 0 \tag{2.10}$$

Lets calculate the result of the action if the Hamiltonian (2.9) on the excited wavefunction

$$\psi = F\phi \tag{2.11}$$

with

$$F = \sum_{i=1}^{N} f(r_i) \tag{2.12}$$

taking into account the expression (2.10):

$$\hat{H}\psi = \hat{H}(F\phi) = -\frac{\hbar^2}{2m}\sum_{i=1}^{N}\left(\phi\nabla_i^2 F + 2\nabla_i\phi\nabla_i F\right) = \\ -\frac{1}{\phi}\frac{\hbar^2}{2m}\sum_{i=1}^{N}\nabla_i(\rho_N\nabla_i F) \tag{2.13}$$

In this equation, $\rho_N = \phi^2$ is the probability density for the ground state (the ground state wavefunction does not have nodes and can be chosen to be real).

The energy of the system is given by the following expression:

$$\mathfrak{E} = E\cdot\mathfrak{I} = \int \psi^*\hat{H}\psi\, d\mathbf{r}_1\ldots d\mathbf{r}_N = \\ \frac{\hbar^2}{2m}\sum_{i=1}^{N}\int(\nabla_i F^*\cdot\nabla_i F)\rho_N d\mathbf{r}_1\ldots d\mathbf{r}_N \tag{2.14}$$

where $\mathfrak{I}$ is the normalization integral:

$$\mathfrak{I} = \int \psi^*\psi\, d\mathbf{r}_1\ldots d\mathbf{r}_N = \int F^*F\rho_N d\mathbf{r}_1\ldots d\mathbf{r}_N \tag{2.15}$$

Substituting (2.12) into (2.15) we get:

$$\mathfrak{I} = \sum_{i=1}^{N}\sum_{j=1}^{N}\int f^*(\mathbf{r}_i)f(\mathbf{r}_j)\rho_N d\mathbf{r}_1\ldots d\mathbf{r}_N \tag{2.16}$$

The density functions are defined as:

$$\rho_k(\mathbf{r}'_1,\mathbf{r}'_2,\ldots,\mathbf{r}'_k) = \sum_{i=1}^{N}\sum_{j=1}^{N}\cdots\sum_{n=1}^{N}\int\delta(\mathbf{r}_i-\mathbf{r}'_1) \\ \times\delta(\mathbf{r}_j-\mathbf{r}'_2)\cdots\delta(\mathbf{r}_k-\mathbf{r}'_n)\rho_N(\mathbf{r}_1\ldots\mathbf{r}_N)d\mathbf{r}_1\ldots d\mathbf{r}_N \tag{2.17}$$

These functions have the following physical meaning: $\rho_1(\mathbf{r})$ is simply a probability to

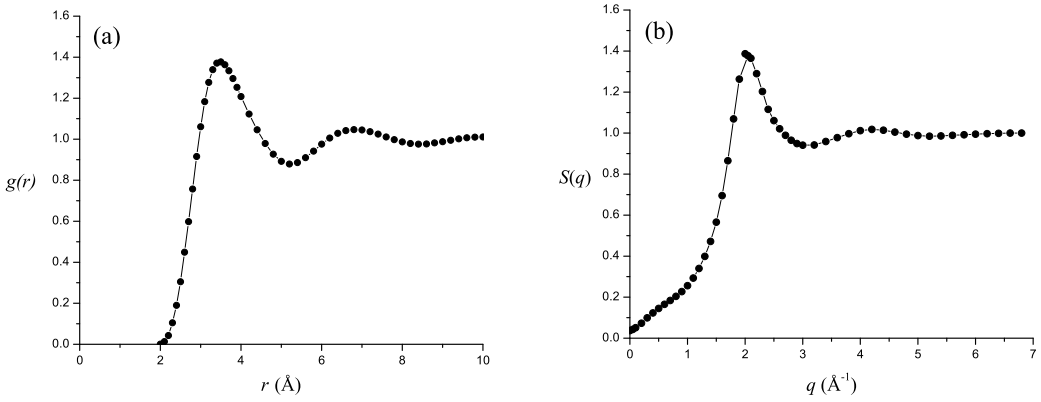

Figure 2.3: Pair correlation function (a) and static structure function (b) of liquid heliumobtained in neutron scattering experiments [38].

find an atom at the position $\mathbf{r}$ in the liquid in its ground state. It does not depend on the coordinate and is equal to the number density ρ_0. The function $\rho_2(\mathbf{r}_1, \mathbf{r}_2)$ is equal to $\rho_0 p(\mathbf{r}_1 - \mathbf{r}_2)$, where p is the probability of finding an atom at the position $\mathbf{r}_2$ when another atom is known to be located at $\mathbf{r}_1$. This function is called *correlation function*.

Keeping in mind these definitions and integrating (2.16) over all coordinates except $\mathbf{r}_1$ and $\mathbf{r}_2$, the normalization integral can be rewritten in the following way:

$$\begin{aligned} \mathfrak{I} &= \int f^*(\mathbf{r}_1) f(\mathbf{r}_2) \rho_2(\mathbf{r}_1, \mathbf{r}_2) d\mathbf{r}_1 d\mathbf{r}_2 = \\ &= \rho_0 \int f^*(\mathbf{r}_1) f(\mathbf{r}_2) p(\mathbf{r}_1 - \mathbf{r}_2) d\mathbf{r}_1 d\mathbf{r}_2 \end{aligned} \tag{2.18}$$

The energy integral (2.14) after the substitution (2.12) becomes:

$$\mathfrak{E} = \frac{\hbar^2}{2m} \sum_{i=1}^{N} \int \nabla_i f^*(\mathbf{r}_i) \nabla_i f(\mathbf{r}_i) \rho_N d\mathbf{r}_1 \ldots d\mathbf{r}_N \tag{2.19}$$

Integrating the last expression over all coordinates except one gives:

$$\mathfrak{E} = \frac{\hbar^2}{2m} \int \nabla f^*(\mathbf{r}) \nabla f(\mathbf{r}) d\mathbf{r} \tag{2.20}$$

The variation of the ratio (2.20) to (2.18) results in the equation:

$$E \int p(\mathbf{r}_1 - \mathbf{r}_2) f(\mathbf{r}_2) d\mathbf{r}_2 = -\frac{\hbar^2}{2m} \nabla^2 f(\mathbf{r}_1) \tag{2.21}$$

where E is equal to $\mathfrak{E}/\mathfrak{I}$. The solution of this equation is:

$$f(\mathbf{r}) = e^{i(\mathbf{qr})} \tag{2.22}$$

The energy of the system is given by the expression:

$$E(\mathbf{q}) = \frac{\hbar^2 q^2}{2mS(\mathbf{q})} \tag{2.23}$$

where $S(\mathbf{q})$ is a Fourier transform of the pair correlation function,

$$S(\mathbf{q}) = \int p(\mathbf{r}) e^{i(\mathbf{q}\cdot\mathbf{r})} d\mathbf{r} \tag{2.24}$$

$S(\mathbf{q})$ is known as *static structure function*. The main achievement of the Feynman theory is that the relationship between the excitation spectrum and microscopic properties of liquid helium was established and given by equations (2.23) and (2.24). The structure function can be obtained experimentally from results of X-ray or neutron scattering. These experiments will be discussed later in detail.

A simple analysis may help to predict the behavior of the structure function. First, it must be noticed that the pair correlation function contains a delta-function: $p(\mathbf{r}_1 - \mathbf{r}_2) = \rho_N \left(\delta(\mathbf{r}_1 - \mathbf{r}_2) + \ldots\right)$ as long as there is an atom at the position $\mathbf{r}_1$. Therefore, at large q

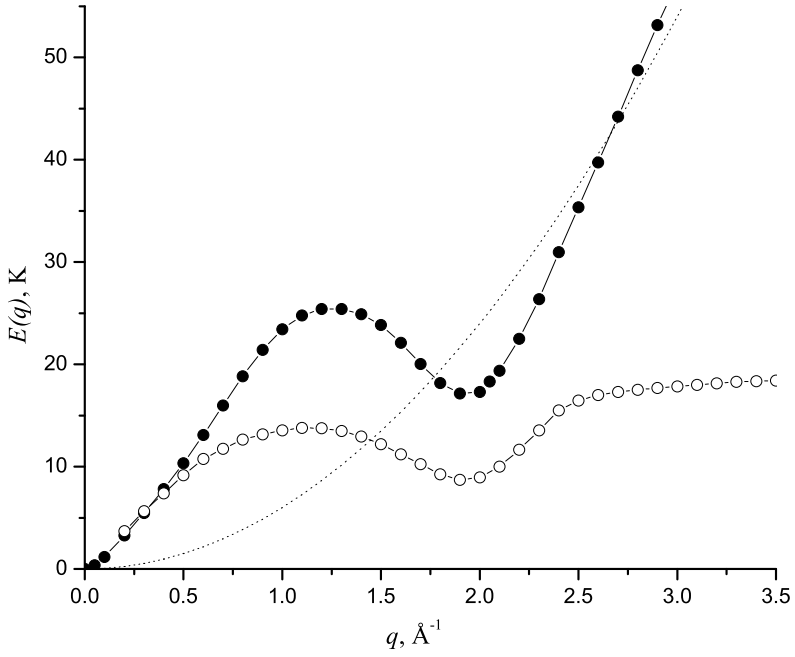

Figure 2.4: Comparison of the energy spectrum predicted by Feynman's theory with one obtained experimentally. The energy spectrum calculated from the equation (2.23) using the structure factor values obtained in neutron scattering experiment [38] is marked by solid circles. The energy spectrum measured experimentally by neutron scattering [1] is marked with open circles. The free particle energy spectrum: $\hbar^2 q^2/2m$ is shown by the dashed line.

the structure function $S(q) \to 1$ and the energy $E(q) \to \hbar^2 q^2/2m$, which corresponds to the energy of a free particle. It has been shown that the only excitations in liquid helium having low momenum are phonons. The energy spectrum of the phonons is $E(q) = \hbar qc$, where c is the speed of sound in liquid helium. According to equation (2.24), the structure factor is equal to $S(q) = \hbar q/2mc$. The pair correlation function goes over a maximum at $r = 2\pi/a$, where a is mean interatomic distance. Accordingly, the structure function has a maximum at $q = 1.9\text{Å}^{-1}$, and the energy function has a minimum that corresponds to the roton minimum.

The problem with definition of the structure function given by the expression (2.24) is that both $p(\mathbf{r})$ and $S(\mathbf{q})$ contain a delta function. To avoid this problem sometimes $S(\mathbf{q})$ is defined in differently [17, 13]:

$$S(\mathbf{q}) = 1 + \rho \int e^{i\mathbf{qr}}[g(\mathbf{r}) - 1]d\mathbf{r} \tag{2.25}$$

The function $g(\mathbf{r})$ is called the *static correlation function*, and it gives a probability of finding an atom at the position $\mathbf{r}$ while another atom is known to be located at the origin. And ρ is the fluid density.

By pluging the solution (2.22) into the expression for the normalization integral $\mathfrak{I}$ from the equation (2.18), one can obtain:

$$\begin{aligned}
\mathfrak{I} &= \int \psi^* \psi d\mathbf{r}_1 \dots d\mathbf{r}_N = \sum_{a=1}^{N}\sum_{b=1}^{N} \int e^{-i\mathbf{qr}_a} e^{i\mathbf{qr}_b} \psi_0^* \psi_0 d\mathbf{r}_1 \dots d\mathbf{r}_N = \\
&= \rho_0 \int e^{-i\mathbf{qr}_1} e^{i\mathbf{qr}_2} p(\mathbf{r}_1 - \mathbf{r}_2) d\mathbf{r}_1 d\mathbf{r}_2 \Big|_{\mathbf{r}=\mathbf{r}_2-\mathbf{r}_1} = \\
&= \rho_0 V \int e^{i\mathbf{qr}} p(\mathbf{r}) d\mathbf{r} = NS(\mathbf{q})
\end{aligned} \tag{2.26}$$

Thus, the normalized wavefunction of an excited state of liquid helium would be:

$$\psi_{\mathbf{q}}(\mathbf{r}_1 \dots \mathbf{r}_N) = \frac{1}{\sqrt{NS(q)}} \sum_{a=1}^{N} e^{i\mathbf{qr}_a} \phi_0(\mathbf{r}_1 \dots \mathbf{r}_N) \tag{2.27}$$

where $\phi_0(\mathbf{r}_1 \dots \mathbf{r}_N)$ is the ground state wavefunction.

From the equation (2.26), it follows that the static structure function can be written as:

$$S(\mathbf{q}) = \frac{1}{N} \int \psi_{\mathbf{q}}^* \psi_{\mathbf{q}} \, d\mathbf{r}_1 \dots d\mathbf{r}_N \tag{2.28}$$

2.2.1 Inelastic neutron scattering in frames of Feynman's theory

Neutron scattering experiments are the source of information about the microscopic structure of liquid helium. In addition, these experiments are interesting because inelastic scattering of a neutron represents an elementary dissipation process in liquid helium in which a microscopic object (a neutron) is involved. The results of this experiment will be discussed in the next section.

Here, lets see how neutron scattering in liquid helium can be described in frames of Feynman's microscopic theory [10]. While a neutron moving through liquid helium, dissipation of the neutron energy may occur under certain conditions. In an elementary act of this dissipation, the neutron loses its kinetic energy, while liquid is promoted from its initial to one of its excited states. In terms of the quasiparticle representation, one can say that neutron energy goes on creation of a quasiparticle with momentum $\hbar\mathbf{q}$ and the energy $\mathcal{E}(q)$. This process is governed by momentum and energy conservation laws:

$$\mathbf{k}_i = \mathbf{k}_f + \mathbf{q} \tag{2.29a}$$

$$\frac{\hbar^2 k_i^2}{2m_n} = \frac{\hbar^2 k_f^2}{2m_n} + \mathcal{E}(q) \tag{2.29b}$$

where $\mathbf{k}_i$ and $\mathbf{k}_f$ are the wavevectors of the initial and final states of the scattered neutron, and m_n is the mass of the neutron.

This event is essentially a transition between two continuum states. Thus, the probability of this event occuring in unit time is given by *Fermi Golden Rule* formula:

$$dw_{fi} = \frac{2\pi}{\hbar}|U_{fi}|^2 \cdot \delta\left(E_i - E_f\right) d\nu_f \tag{2.30}$$

In this formula, $d\nu_f$ denote the interval of the continuum of the final states. The Born approximation will be used to calculate the scattering cross section. In this approximation, the initial and the final states of the scattered particle are states with certain momentum, i.e. plane waves. Thus, in our case $d\nu_f$ denotes an elementary volume in the phase space of the final states of the neutron:[2]

$$d\nu_f = \frac{d^3\mathbf{k}_f}{(2\pi)^3}$$

Taking into account the last consideration together with equation (2.29b), the equation (2.30) can be rewritten:

$$dw_{fi} = \frac{2\pi}{\hbar}|U_{fi}|^2 \cdot \delta\left(\frac{\hbar^2 k_i^2}{2m_n} - \frac{\hbar^2 k_f^2}{2m_n} - \mathcal{E}(q)\right)\frac{d^3\mathbf{k}_f}{(2\pi)^3} \tag{2.31}$$

The scattering of neutron occurs when it collides with nuclei of helium atoms. Electrons do not participate in the scattering. The interaction between nuclei and neutrons is strong and short-ranged. To model this interaction, the *pseudo-potential* introduced by E. Fermi [14] will be used:

$$U_F(\mathbf{r}) = \frac{2\pi\hbar^2}{m}\sum_{l=1}^{N} b\delta(\mathbf{r} - \mathbf{r}_l) \tag{2.32}$$

where $\mathbf{r}_l$ denotes position of the atom l of the fluid. The value b, called *scattering length*, is chosen such that the total scattering cross-section given by $\sigma = 4\pi b^2$ corresponds to the total cross section of the neutron.

[2]Here assume a unitary volume of liquid helium ($V = 1$)

The matrix element U_{fi} must be taken between the initial and the final states of the system consisting of the fluid and the neutron. The wavefunction of such a system is a direct product of the fluid and neutron wavefunctions :

$$\Psi(\mathbf{r}_n, \mathbf{r}_1 \dots \mathbf{r}_N) = \psi(\mathbf{r}_n) \cdot \phi(\mathbf{r}_1 \dots \mathbf{r}_N) \tag{2.33}$$

where $\psi(\mathbf{r}_n)$ is the neutron wavefunction, $\phi(\mathbf{r}_1 \dots \mathbf{r}_N)$ is a wavefunction of the liquid helium and $\mathbf{r}_1 \dots \mathbf{r}_N$ are the coordinates of all the He atoms. In frames of Born approximation, the wavefunctions of the initial and the final states of the neutron are plane waves: $\psi_i(\mathbf{r}) = e^{i\mathbf{k}_i\mathbf{r}}, \psi_f(\mathbf{r}) = e^{i\mathbf{k}_f\mathbf{r}}$. The wavefunctions of liquid helium are defined by the expression (2.27). Thus, the matrix element U_{fi} is:

$$\begin{aligned} U_{fi} &= \int \Psi_f^* U_F \Psi_i d\mathbf{r}_n d\mathbf{r}_1 \dots d\mathbf{r}_N = \\ &= \int e^{i(\mathbf{k}_i - \mathbf{k}_f)\mathbf{r}_n} \phi_f^*(\mathbf{r}_1 \dots \mathbf{r}_N) U_F \phi_i(\mathbf{r}_1 \dots \mathbf{r}_N) d\mathbf{r}_n d\mathbf{r}_1 \dots d\mathbf{r}_N \end{aligned}$$

Taking into account the momentum consevation law we can substitute $\mathbf{k}_i - \mathbf{k}_f = \mathbf{q}$ and rewrite the last expression:

$$\begin{aligned} U_{fi} &= \int e^{i\mathbf{q}\mathbf{r}} \langle \phi_f | U_F | \phi_i \rangle d\mathbf{r} = \\ &= \frac{2\pi\hbar^2}{m} b \sum_{a=1}^{N} \int e^{i\mathbf{q}\mathbf{r}} \langle \phi_f | \delta(\mathbf{r} - \mathbf{r}_a) | \phi_i \rangle d\mathbf{r} = \\ &= \frac{2\pi\hbar^2}{m} b \sum_{a=1}^{N} \langle \phi_f | e^{i\mathbf{q}\mathbf{r}_a} | \phi_i \rangle \end{aligned}$$

Assume that before scattering the liquid helium was in its ground state: $\phi_i = \phi_0$. After the scattering, its wavefunction will be described by the expression (2.27). Keeping this in mind, the last expression can be rewritten in the following way:

$$U_{f0} = \frac{2\pi\hbar^2 b}{m} \frac{1}{\sqrt{NS(q)}} \sum_{a=1}^{N} \sum_{b=1}^{N} \int e^{-i\mathbf{q}\mathbf{r}_a} e^{i\mathbf{q}\mathbf{r}_b} \phi_0^* \phi_0 d\mathbf{r}_1 \dots d\mathbf{r}_N \tag{2.34}$$

Except the coefficient, the last expression coincides with the expression (2.26) for the normalization integral $\mathfrak{I}$, which is equal to $NS(q)$. Finally, obtained in the expression:

$$|U_{f0}|^2 = \left(\frac{2\pi\hbar^2 b}{m}\right)^2 NS(q); \tag{2.35}$$

Consider a possibility of an elastic scattering. In the case of an elastic scattering, the initial state of the liquid remains unchanged. Hence, the matrix element for elastic cross section is given by:

$$U_{00} = \frac{2\pi\hbar^2 b}{m} \sum_{a=1}^{N} \int e^{i\mathbf{q}\mathbf{r}_a} \phi_0^* \phi_0 \, d\mathbf{r}_1 \dots d\mathbf{r}_N = \frac{2\pi\hbar^2 b}{m} \int e^{i\mathbf{q}\mathbf{r}} \rho_1(\mathbf{r}) d\mathbf{r} \tag{2.36}$$

Only particles close to the surface of the liquid give a contribution to the integral in the expression above. Thus, the matrix element vanishes in the case of bulk liquid, meaning that the elastic scattering does not take place. However, for a finite system this surface contribution is noticable, which will be discussed later.

Returning to the equation (2.31). It defines the transition probability between the initial and the final states of the system. To calculate the scattering cross section, it is necessary to normalize this probability on the flux of the incoming neutrons. By definition, the flux is given by the following expression [27]:

$$\langle \hat{\mathbf{j}} \rangle = \frac{1}{2m_n} \left(\psi_i \hat{\mathbf{p}}^* \psi^* + \psi^* \hat{\mathbf{p}} \psi\right) = \frac{\hbar \mathbf{k}_i}{m_n} = \mathbf{v}_i \tag{2.37}$$

where $\mathbf{v}_i$ is the initial velocity of the neutron. Thus:

$$d\sigma = \frac{m_n}{\hbar k_i} dw_{fi}$$

Substituting this into the equation (2.31), gives:

$$d\sigma = \frac{m_n}{(2\pi\hbar)^2 k_i} |U_{fi}(q)|^2 \delta \left(\frac{\hbar^2 k_i^2}{2m_n} - \frac{\hbar^2 k_f^2}{2m_n} - \mathcal{E}(q) \right) d^3\mathbf{k}_f$$

One can replace $d^3\mathbf{k}_f = k_f^2 dk_f d\Omega = (1/2) k_f d(k_f^2)$, where $d\Omega$ is an element of solid angle, substitute the expression for the matrix element from the equation (2.35), and integrate the last expression over dk_f:

$$\frac{d\sigma}{d\Omega} = \frac{m_n}{(2\pi\hbar)^2 k_i} \int |U_{fi}(q)|^2 \delta \left(\frac{\hbar^2 k_i^2}{2m_n} - \frac{\hbar^2 k_f^2}{2m_n} - \mathcal{E}(q) \right) \frac{1}{2} k_f d(k_f^2) =$$
$$= \frac{k_f}{k_i} \frac{m_n}{(2\pi\hbar)^2} \frac{2m_n}{\hbar^2} \frac{(2\pi\hbar^2)^2}{m_n^2} \frac{1}{2} b^2 NS(q) = b^2 \frac{k_f}{k_i} NS(q)$$

The final expression for the neutron scattering cross section obtained in frames of Feynman's microscopic theory is:

$$\frac{d\sigma}{d\Omega} = b^2 \frac{k_f}{k_i} NS(q) \tag{2.38}$$

The value of k_f is given by the solution of the equation (2.29b). Importantly, the set of equations (2.29) do not always has a solution. As discussed above, if the initial speed fo the neutron is less critical speed, this set of equations can not be satisfied at any scattering angle. It is a manifistation of the phenomenon of superfluidity.

The matrix element for scattering to all possible final states is given by the sum rule:

$$\sum_f |U_{f0}|^2 = \langle \phi_0 | U^*(q) U(q) | \phi_0 \rangle = NS(q) \tag{2.39}$$

The result given by the equation (2.39) means that in frames of the scattering theory discussed above, it is assumed that in every scattering event only the quasiparticle is excited. The experiments on neutron scattering from liquid helium that will be discussed in detail in the next section, show that it is true only for low q values. For $q > 0.4$ Å^{-1}, there is evidence of simultaneous excitation of several quasiparticles.

2.3 Dynamic structure factor $S(q, \omega)$ measured in the neutron scattering experiments

It was shown by Van Hove [21] that, in the general case of monoatomic substrate the partial cross section of neutron scattering in the Born approximation with the scattering potential defined by the expression (2.32) is given by:

$$\frac{d\sigma}{d\Omega dE} = \frac{1}{\hbar} N b^2 \frac{k_f}{k_i} S(\mathbf{q}, \omega) \tag{2.40}$$

The function $S(\mathbf{q}, \omega)$ is called *dynamic structure factor*. [3]

The sum rule for the dynamic structure factor $S(q, \omega)$ can be reformulated in the following way [34]:

$$S(q) = \int_0^\infty S(q, \omega) d\omega \tag{2.41}$$

$$\frac{\hbar q^2}{2m} = \int_0^\infty \omega S(q, \omega) d\omega \tag{2.42}$$

As suggested by the equation (2.40), the dynamic structure function is an observable that can be measured directly in the neutron scattring experiment. The dynamic structure

[3] In the case of liquid, the direction of the vector $\mathbf{q}$ is not relevant and $S(\mathbf{q}, \omega) \equiv S(q, \omega)$.

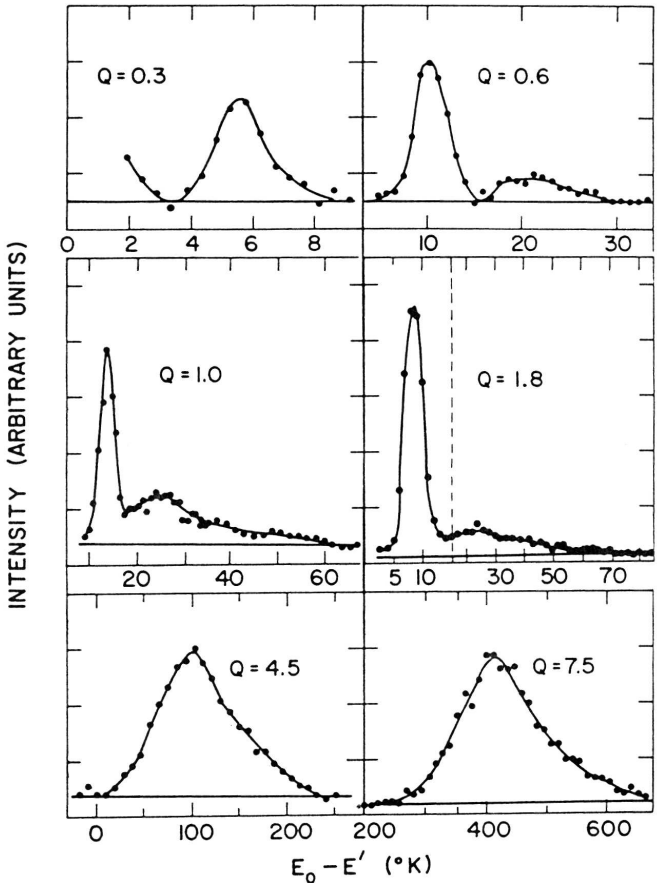

Figure 2.5: Dynamic structure function $S(Q,\omega)$ measured in the neutron scattering experiment [1] at different values of momentum transfer Q. The measurements were made at the temperature $T = 1.1$ K.

factor $S(q,\omega)$ measured at different mometum transfer q at low temperature is shown in figure 2.3.

The theory developed by Feynman and Cohen described in the previous section, assumes that at the momentum transfer q only the single excitation having energy $\mathcal{E}(q)$ appears. Indeed, at low momentum transfer (q <0.4 Å^{-1}),only the sharp peak located at position $\omega_q = \hbar^{-1}\mathcal{E}(q)$ is observed. The width of the peak is defined by the experimental resolution.

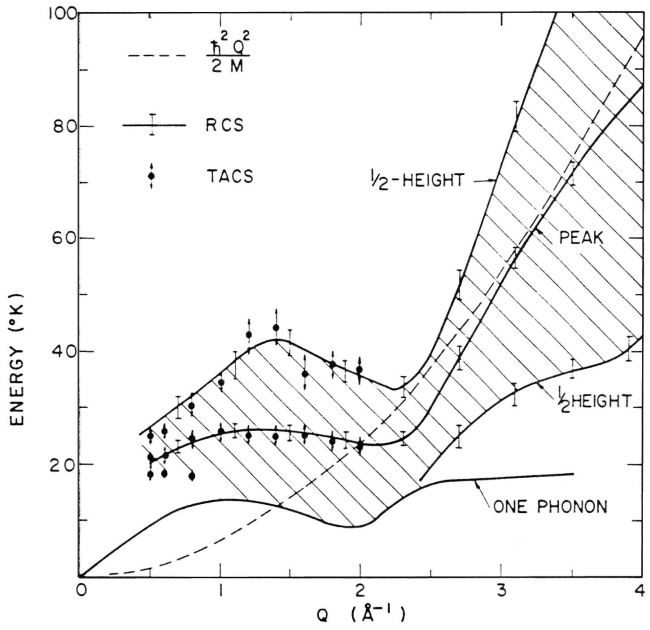

Figure 2.6: Dynamic structure function of the bulk helium measured in the neutron scattering experiment [1] and shown in figure 2.3, mapped on the energy vs. momentum diagram. The hatched area showes the multiphonon scattering region. The upper and lower energy boundaries of the peak corresponding to half the peak intensity are denoted by solid lines. The dashed line represent the free particle dispersion curve $\hbar^2 Q^2/2M$.

However, in the region of intermediate momentum transfer (0.4 $\text{Å}^{-1} < q <$2.5 Å^{-1}), in addition to the sharp peak located at ω_q, another broad peak centered at higher energies start to appear. For example, at q =0.4 Å^{-1}, the broad peak is centered at $\omega = 2.5\omega_q$. The integrated intensity of the broad peak corresponds to 3-5% of the intensity of the sharp peak. The intensity of the broad peak grows linearly with q (up to $q \simeq 1.5\text{Å}^{-1}$) and increases more rapidly thereafter. At $q = 2.5\text{Å}^{-1}$, the intensity of the broad component is about 90% of the intensity of the sharp peak [17]. This broad peak is attributed to the appearance of multiple excitations. The broad component exhibits a noticible structure and a long energy tail [17]. The structure of the broad component can be attributed to the excitation of quasiparticles pairs such as roton-roton, maxon-maxon, and roton-maxon [33].

The intensity of the sharp peak drops rapidly in the region of high momentum transfer ($q >$2.5Å^{-1}). At $q \simeq 3.5$Å^{-1}, it cannot be resolved, buried by the broad component. The explanation of this phenomenon was given by Pitaevskii [37] who suggested that the elementary excitation at this high q tends to decay into a pair of rotons. Indeed, the position of the sharp peak in the region of high momentum transfer where it still can be observed, slowly devates from the energy corresponding to twice of the roton energy $2\Delta_R$ as the momentum transfer grows. This can be seen from the energy spectrum measured in a neutron scattering experiment, shown in figure 2.2.

The broad peak is centered on the energy of free particle $\omega = \hbar q^2/2m$. This region is called the *independent particle region*. The neutron scattering in this region probes the microscopic distribution of the momenta of individual helium atoms in the liquid [33]. The large width of this peak is a manifistation of the fact that even at low temperatures the large portion of helium atoms stays out of the Bose condensate due to the rather strong interatomic interaction.

Miller et. al. [34] suggested that the dynamic structure function can be represented as a sum of two terms:

$$S(q,\omega) = Z(q)\delta(\omega - \omega_q) + S_M(q,\omega) \tag{2.43}$$

where the first term describes the sharp peak and $S_M(q,\omega)$ describes the broad component. The behavior of the functions $Z(q)$ and $S_M(q)$ is shown in figure 2.7. According to the sum rule given by equation (2.41), $Z(q) + S_M(q) = S(q)$ for all q. The static structure factor $S(q)$, measured by X-ray scattering [2], is also shown in figure 2.7 by the dashed line. Clearly, the sum rule (2.41) is obeyed rather precisely.

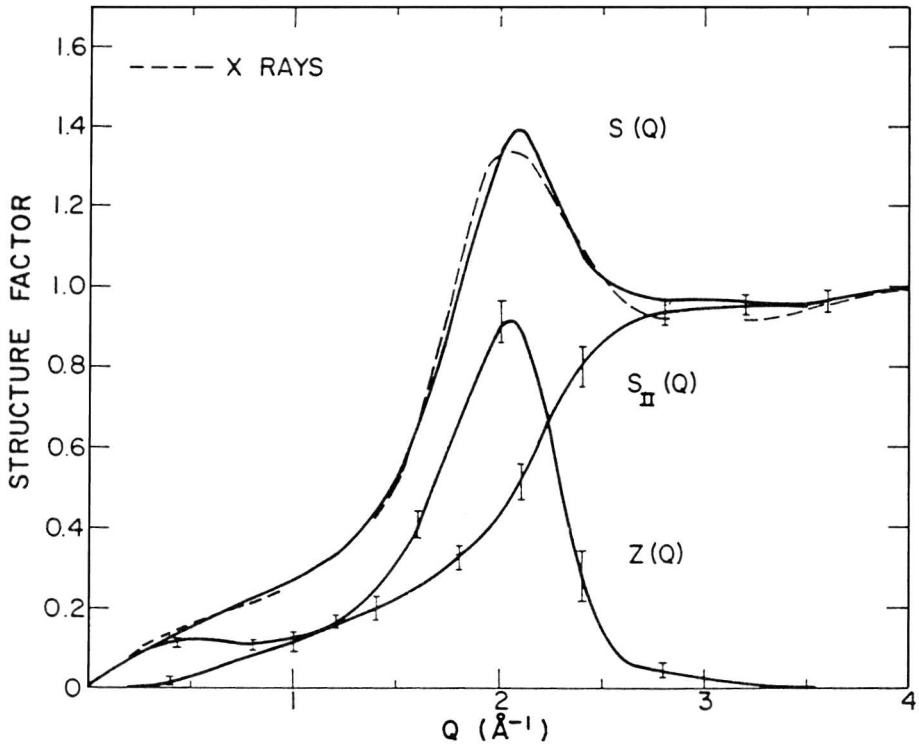

Figure 2.7: Intensity of the one-phonon peak $Z(Q)$, the multiexcitation component $S_M(q,\omega)$, and their sum $S(Q)$ measured in the neutron scattering experiment. [1] The dashed line showes the static structure function measured by X-ray scattering. [2] (The figure is taken from [1])

As discussed above, $Z(q)$ almost completely depleted the sum rule for the $q < 0.4\text{Å}^{-1}$. In the region $q \simeq 1.1\text{Å}^{-1}$, $Z(q)$ and $S_M(q)$ have approximately equal amplitude. $Z(q)$ reaches the maximum approximately in the region of roton minimum and then rapidly decreases. At $q < 3.0\text{Å}^{-1}$ the $S(q)$ completely depletes the sum rule.

The conclusion that can be derived from the discussion above is that the Feynman approximation, assuming only single particle is created in elementary act of inelastic scattering, provides an adequate description of the situation.

2.4 Extention of the microscopic theory of liquid helium on the case of helium nanodroplet

2.4.1 Static structure function $S(\mathbf{q})$

Following the previous discussion, the structure function $S(q)$ plays the central role in Feynman's microscopic theory. Thus, to extend the microscopic theory on the case of finite system such as helium nanodroplet it is necessary to evaluate the structure function $S(q)$ taking into account possible finite size effects.[4] Then, the reconstruction of the excitation energy spectrum (2.23) and the scattering cross section (2.38) will be possible. Also in this section the "*bra-ket*" notation will be used for convinience. In this notation, the Feynman basis set is given by:

$$|\mathbf{q}\rangle = \widehat{\rho_{\mathbf{q}}}|0\rangle \tag{2.44}$$

where $\widehat{\rho_{\mathbf{q}}}$ is Feynman's excitation operator:

$$\widehat{\rho_{\mathbf{q}}} = \sum_{a=1}^{N} e^{i\mathbf{q}\mathbf{r}_a} \tag{2.45}$$

The static structure function $S(\mathbf{q})$ for bulk infinite helium is given by:

$$S(\mathbf{q}) = \frac{1}{N}\langle 0|\widehat{\rho_{\mathbf{q}}}^{+}\widehat{\rho_{\mathbf{q}}}|0\rangle \tag{2.46}$$

which is an analog of the equation (2.28).

It was discussed on the page 37 that elastic scattering does occur in the case of bulk helium because only atoms close to the surface contribute to the elastic scattering and

[4] In this section, the derivation of the static structure function of a finite system given by R. Schiavilla et. al [12] will be followed.

the portion of these atoms is negligible in the case of bulk helium. The situation is different with finite systems such as helium nanodroplets. Thus, it is necessary to subtract the elastic scattering contribution from the overall strength given by $S(\mathbf{q})$. Hence, the expression for the $S(\mathbf{q})$ for helium droplets would be:

$$S_{\mathrm{dr}}(\mathbf{q}) = \frac{1}{N}\langle 0|\widehat{\rho_{\mathbf{q}}}^{+}\widehat{\rho_{\mathbf{q}}}|0\rangle - \frac{1}{N}|\langle 0_R|\widehat{\rho_{\mathbf{q}}}|0\rangle|^2 \tag{2.47}$$

where $|0_R\rangle$ describes the situation when unexcited droplet is moving as a whole.

From (2.45) it directly follows that:

$$\widehat{\rho_{\mathbf{q}}}^{+}\widehat{\rho_{\mathbf{q}}} = N + \sum_{a\neq b} e^{i\mathbf{q}(\mathbf{r}_a - \mathbf{r}_b)} \tag{2.48}$$

Then, the first term of the equation can be rewritten as follows:

$$\begin{aligned}\frac{1}{N}\langle 0|\widehat{\rho_{\mathbf{q}}}^{+}\widehat{\rho_{\mathbf{q}}}|0\rangle &= 1 + \langle 0|\sum_{a\neq b} e^{i\mathbf{q}(\mathbf{r}_a - \mathbf{r}_b)}|0\rangle \\ &= 1 + \frac{1}{N}\int e^{i\mathbf{q}(\mathbf{r}_1 - \mathbf{r}_2)}\rho_2(\mathbf{r}_1, \mathbf{r}_2)d\mathbf{r}_1 d\mathbf{r}_2\end{aligned} \tag{2.49}$$

where $\rho_2(\mathbf{r}_1, \mathbf{r}_2)$ is one of the density functions defined by the equation (2.17). In this notation they can be written as:

$$\begin{aligned}\rho_1(\mathbf{r}_1) &= \sum_{a=1}^{N}\langle 0|\delta(\mathbf{r}_a - \mathbf{r}_1)|0\rangle \\ \rho_2(\mathbf{r}_1, \mathbf{r}_2) &= \sum_{a=1}^{N}\sum_{b=1}^{N}\langle 0|\delta(\mathbf{r}_a - \mathbf{r}_1)\delta(\mathbf{r}_b - \mathbf{r}_2)|0\rangle\end{aligned} \tag{2.50}$$

The $\rho_2(\mathbf{r}_1, \mathbf{r}_2)$ can also be expressed by:

$$\rho_2(\mathbf{r}_1, \mathbf{r}_2) = \rho_1(\mathbf{r}_1)\rho_1(\mathbf{r}_2)g_2(\mathbf{r}_1, \mathbf{r}_2) \tag{2.51}$$

where $g_2(\mathbf{r}_1, \mathbf{r}_2)$ is the pair correlation function. Substituting (2.51) into (2.50) yields:

$$\frac{1}{N}\langle 0|\widehat{\rho_{\mathbf{q}}}^{+}\widehat{\rho_{\mathbf{q}}}|0\rangle = 1 + \frac{1}{N}\left|\int e^{i\mathbf{qr}}\rho_1(\mathbf{r})d\mathbf{r}\right|^2 + \frac{1}{N}\int e^{i\mathbf{q}(\mathbf{r}_1-\mathbf{r}_2)}\rho_1(\mathbf{r}_1)\rho_1(\mathbf{r}_2)[g_2(\mathbf{r}_1,\mathbf{r}_2)-1]d\mathbf{r}_1 d\mathbf{r}_2 \qquad (2.52)$$

The first term in the equation above cancels the elastic contribution. Thus, $S(\mathbf{q})$ becomes:

$$S_{\mathrm{dr}}(\mathbf{q}) = 1 + \frac{1}{N}\int e^{i\mathbf{q}(\mathbf{r}_1-\mathbf{r}_2)}\rho_1(\mathbf{r}_1)\rho_1(\mathbf{r}_2)[g_2(\mathbf{r}_1,\mathbf{r}_2)-1]d\mathbf{r}_1 d\mathbf{r}_2 \qquad (2.53)$$

The equation (2.53) gives an expression of the static structure function for finite systems. For the infinite system, $\rho_1(\mathbf{r}) = \rho_0$ and $g_2(\mathbf{r}_1, \mathbf{r}_2) = g(r)$, where $r = |\mathbf{r}_1 - \mathbf{r}_2|$. Substituting it into the expression above, one can obtain:

$$S_\infty(\mathbf{q}) = 1 + \rho\int e^{i\mathbf{qr}}[g(\mathbf{r})-1]d\mathbf{r}$$

which is coincides with the definition of the structure function in bulk helium given by expression (2.25).

Comparing $S_{\mathrm{dr}}(\mathbf{q})$ with $S_\infty(\mathbf{q})$ one can reach a conclusion that the largest deviation between these two functions are expected to be in the region of small q, namely $q < 2\pi/D$, where D is the diameter of the droplet. Exploring the behavior of the $S_{\mathrm{dr}}(\mathbf{q})$ in this region in a spherical droplet with diameter D, the largest interparticle distance $\mathbf{r}_1 - \mathbf{r}_2$ is bounded. Thus, the exponent $e^{i\mathbf{q}(\mathbf{r}_1-\mathbf{r}_2)}$ can be expanded as series in the region of small $\mathbf{q}$. It is convinient to choose the coordinate system with the origin in the center

of the droplet and the $z-$axis directed along the vector $\mathbf{q}$. In this coordinate system the expansion is given by:

$$e^{i\mathbf{q}(\mathbf{r}_1-\mathbf{r}_2)} = 1 + iq(z_1 - z_2) - \frac{1}{2}q^2(z_1 - z_2)^2 + \cdots \tag{2.54}$$

From the fact that the droplet is spherical and the origin is at the center of the droplet, it can be shown that:

$$\sum_{a=1}^{N} z_a = 0 \tag{2.55}$$

Expanding $S_{\mathrm{dr}}(\mathbf{q})$ given by expression (2.53) up to the first term yields:

$$S_{\mathrm{dr}}(\mathbf{q}) = 1 + \frac{1}{N}\int \rho_2(\mathbf{r}_1, \mathbf{r}_2)d\mathbf{r}_1 d\mathbf{r}_2 - \frac{1}{N}\int \rho_1(\mathbf{r}_1)\rho_1(\mathbf{r}_2)d\mathbf{r}_1 d\mathbf{r}_2 + \cdots \tag{2.56}$$

Both integrals in the equation above can be evaluated:

$$\int \rho_2(\mathbf{r}_1, \mathbf{r}_2)d\mathbf{r}_1 d\mathbf{r}_2 = \sum_{a\neq b} 1 = N(N-1) \tag{2.57a}$$

$$\int \rho_1(\mathbf{r}_1)\rho_1(\mathbf{r}_2)d\mathbf{r}_1 d\mathbf{r}_2 = \sum_{a=1}^{N}\sum_{b=1}^{N} 1 = N^2 \tag{2.57b}$$

By substituting (2.57) into (2.56), one can show that $S_{\mathrm{dr}}(\mathbf{q}) \to 0$ when $q \to 0$.

From symmetry considerations, one can conclude that the terms with odd powers of q do not contribute to $S_{\mathrm{dr}}(\mathbf{q})$. The next term would be the one with q^2. It can be expressed as follows:

$$\begin{aligned} S^{(2)}_{\mathrm{dr}}(\mathbf{q}) = \frac{1}{N}\int (z_1 - z_2)^2 \rho_2(\mathbf{r}_1, \mathbf{r}_2)d\mathbf{r}_1 d\mathbf{r}_2 - \\ - \frac{1}{N}\int (z_1 - z_2)^2 \rho_1(\mathbf{r}_1)\rho_1(\mathbf{r}_2)d\mathbf{r}_1 d\mathbf{r}_2 \end{aligned}$$

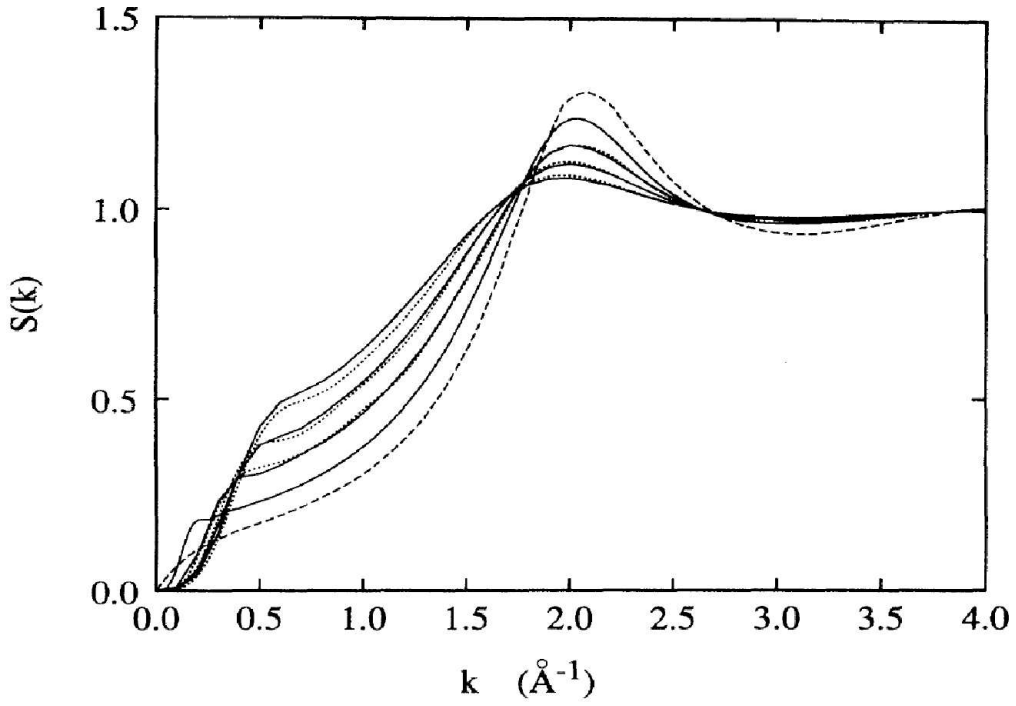

Figure 2.8: The static structure function $S_{\rm dr}(q)$ for the droplets with 20, 40, 112 and 1000 atoms calculated by HNC/EL method (solid lines) [8] and by the DMC method [7](dotted lines). The static structure function for the bulk helium $S_\infty(q)$ [23] is shown by the dashed line.

By using equations (2.50) and (2.55), one can show that $S^{(2)}_{\rm dr}(\mathbf{q})$ is also equal to zero. Thus, the first term that would contribute to the $S^{(2)}_{\rm dr}(\mathbf{q})$ at small $\mathbf{q}$ would be $S^{(4)}_{\rm dr}(\mathbf{q})$, which is proportional to q^4. Thus, $S_{\rm dr}(q) \propto q^4$ when $q \to 0$. This is different from the case of infinite helium, for which $S_\infty(q) \propto q$.

There is currently no available experimental data on neutron scattering on helium nanodroplets. On the other hand, finiteness of the system as well as the relative simplicity of the He-He interaction potential allows computer simulation of microscopic properties of the droplets. The methods include different modification of the Monte Carlo calculations such as Diffusion Monte Carlo (DMC), Variational Monte Carlo (VMC) etc. [42] or Jastrow-Feenberg variational methods such as hypernated chain summation

(HNC) [23]. The latter is not as time consuming as the Monte Carlo methods and allows to calculation for larger clusters. [8].

The static structure functions of helium clusters containing $20, 40, 112$ and 1000 He atoms are shown in Fig. 2.8. These functions were calculated by DMC methods (dotted lines). Indeed, there is a good agreement between these two theories. The structure function of the bulk helium is shown by the dashed line for comparison.

The first conclusion made from the analyzing the results of these calculations is that the shape of the structure function of a very small droplet containing 20 atoms only, is similar to the structure function of bulk helium. Both of these functions reveal the same features:

(i) $S_{\rm dr}(q)$ as well as $S_\infty(q)$ vanishes in the limit of $q \to 0$;

(ii) $S_{\rm dr}(q), S_\infty(q) \to 1$ when $q \to \infty$;

(iii) both of these functions have a maximum at $q \simeq 2\text{Å}^{-1}$. This maximum results in a "roton minimum" on the energy spectrum when the latter is reconstructed with help of Feynman's equation (2.23);

As discussed above, the structure function of a droplet $S_{\rm dr}(q)$ in the region of small q should be proportional to q^4, while the structure function of the bulk helium is proportional to q in this region. Indeed, a "knee" in the region of small q is the most apparent feature of the structure functions of the clusters. This feature is not present on the structure function of the bulk helium and hence should be attributed to the finite size effect. The "knee" region extends from $q = 0$ up to $q = 2\pi/D$. This region shrinks while cluster increases size and completely disappears in the limit of an infinite droplet. However, $D \propto \sqrt[3]{N}$ and the convergence is slow [8].

Another important observation to be made is that the maximum value of $S_{\rm dr}(q)$ is around $q \simeq 2\text{Å}^{-1}$ and is less than the corresponded value of the structure function of the

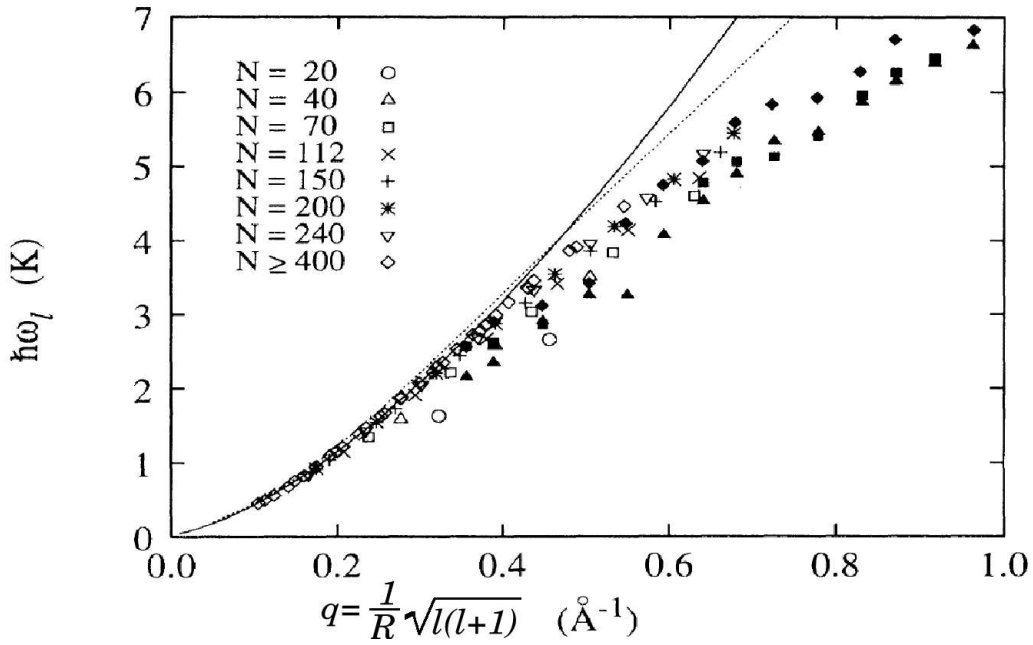

Figure 2.9: Surface excitations energies for the droplets of different sizes. [8]. The lowest excitations with $l \leq 9$ are shown. $R \equiv \sqrt{5/3} r_{rms}$ is a hard sphere radius. Dashed line denotes the lowest excitation energy of a *helium film* adsorbed on graphite surface [9]. The solid line shows fitting curve given by equation (2.59)

bulk helium. It gives much shallower roton minimum when the Feynman's expression for the energy (2.23) is applied. $S_{\rm dr}(q) \to 1$ in the region of high q gives the correct behavior of the energy given by the same equation in the "independent particle" region. It is rather questionable that this equation for the energy spectrum (2.23) can be applied in the region of $q < (2\pi/D)$ because, in this region, the spectrum is discrete and the wavefunction is less likely to be approximated with wavefuntion ofFeynman's type.

2.4.2 Surface excitations

It was discussed in the previous chapter that besides the "breathing" modes that correspond to phonons in bulk helium, helium droplets possesses another type of excitation. In these excitations, oscillations of the droplet are related to its deformation. The surface

tension provide the restoring force for these oscillation. That is why these oscillations called “surface modes” or “ripplons”.

The surface modes are less energetic than the oscillations related to the density fluctuations. Thus, the surface modes provide the major contribution to thermodynamic functions of helium droplet and play an important role in the phenomenon of evaporative cooling.

The wavevector q of the droplet can be defined as $q = \sqrt{l(l+1)/R}$, where R is the hard-sphere radius of the droplet $R = \sqrt{5/3} r_{rms}$. The wavevector is defined so the dispersion relation of the surface modes in the region of the discrete spectrum coincides with the dispersion relation for the “bulk” ripplons, which is given by:

$$\omega_{\mathrm{surf}}(q) = q^{3/2} \sqrt{\frac{\sigma}{mn}} \tag{2.58}$$

The calculated surface excitation energy spectrum [8] for the clusters of different sizes is shown in figure 2.4.2. For comparison the lowest excitations of a helium film absorbed on a graphite surface is also shown in dashed line. It suggests that these excitations are of the same nature.

At small $q < 0.30\text{Å}^{-1}$ the spectrum can be fitted by the following dispersion relation:

$$\hbar\omega_{\mathrm{surf}} = 12.339 q^{3/2} + 0.043 \text{ K} \tag{2.59}$$

The fitting curve given by the equation above is shown in solid line in figure 2.4.2.The surface tension of the helium droplet extracted from the parameters of the fitting expression (2.59) and the equation (2.58) is $\sigma = 0.279\text{K Å}^{-2}$ which is rather close to the value of the bulk helium.

The extention of the microscopic theory to describe surface excitation can be done through assigning the wavefunctions corresponding to surface excitation. To describe

surface excitation, C. Chang and M. Cohen [6] suggested to use the wavefunction proposed by Feynman [15] for the most general case of the motion of Bose fluid given by:

$$\psi = \phi_0 \cdot \exp\left[i \sum_{a=1}^{N} \chi(\mathbf{r}_a) \right] \tag{2.60}$$

where ϕ_0 is the ground state wavefunction and $\chi(\mathbf{r})$ is the velocity field potential:

$$\mathbf{v}(\mathbf{r}) = \frac{\hbar}{m} \nabla \chi(\mathbf{r}) \tag{2.61}$$

The velocity field potential corresponding to surface modes of the droplet is given by equation (1.15) on page 6 in the previous chapter.

J. Henderson and J. Lekner [20] proposed that the static structure function corresponding to the surface excitation can be reconstructed from the Feynman's expression for the energy spectrum (2.23) and the dispersion relation of the surface mode (2.58) and given by:

$$S_{\text{surf}}(q) = \frac{1}{2} \hbar \sqrt{\frac{n}{\sigma m}} q^{1/2} \tag{2.62}$$

where n is the density of the helium.

The contribution of the surface modes to dynamic structure function will be discussed in the next section.

2.4.3 Dynamic structure function $S(q, \omega)$ of helium droplets

Computer simulations also allows for the reconstruction of the dynamic structure function of helium clusters. The details of these calculation is beyond the current discussion. However the results will be discussed.

The 3D profiles of the dynamic structure function $S(q, \omega)$ calculated for the droplets containing $112, 240, 1000$ atoms is shown in figures 2.10(a)-(c). The solid lines shown

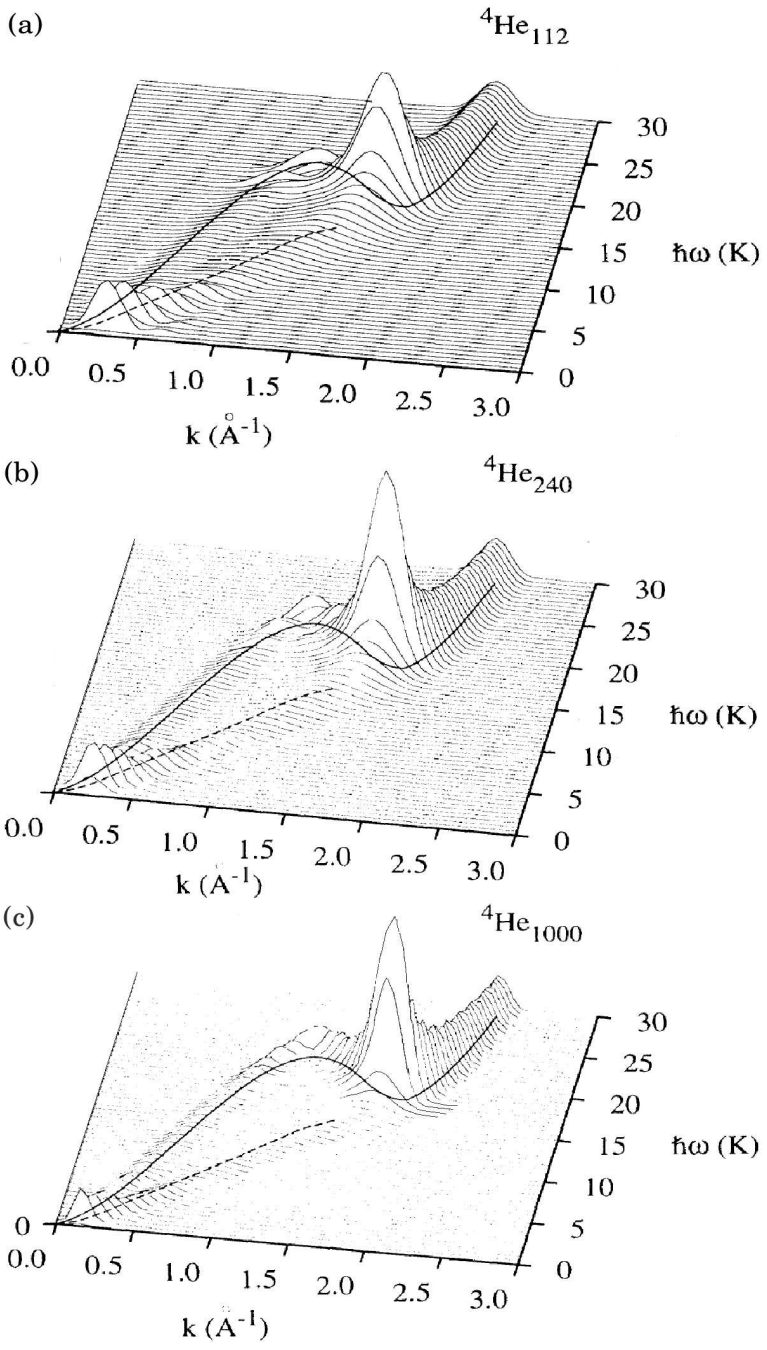

Figure 2.10: Dynamic structure functions of helium droplets containing N =112(a), 240(b) and 1000(c) helium atoms. [8] The solid line shows Feynman's energy spectrum for *bulk helium*. Dashed lines show ripplon dispersion curve.

in these figures represents Feynman's energy spectrum of *bulk helium*. As one can see the profile of $S(q,\omega)$ of every one of these clusters follow this curve rather faithfully. This fact adds support to our original assumption that it is possibe to extend the microscopic theory of bulk helium in the case of helium droplets. It also suggests that the Feynman approximation that assumes only a single particle is excited in during scattering adequately describe the situation in the case of helium droplets.

A series of well defined resonances in the maxon-roton region can be observed on the profile of the dynamic structure function of the clusters containing 112 and 240 atoms. These resonances do not appear on the profile of $S(q,\omega)$ of the 1000-atom cluster. Thus these resonances also called as "diffractive echoes" are the leftovers of the discrete excitation spectrum.

The most remarkable feature is the appearance of the ripplon branch on the profile of the dynamic structure of the clusters. The dashed lines in Fig. 2.10 represent the dispersion relation of the ripplons. This branch started at the origin and goes up to approximately the roton minimum. The ripplon branch can be observed on the dynamic structure function plots corresponded to all cluster sizes discussed here. Its intensity decreases slowly with the cluster size. However, even for the clusters containing 1000 atom the intensity of the ripplon branch is comparable to the intensity of the phonon branch in this region.

The consideration would not be complete if a discussion concerning the influence of an impurity on the dynamic structure function profile is excluded. The dynamic structure function of a cluster with 112 helium atoms containing SF_6 molecule is shown in figure 2.11.

The first thing noted is that the profile of the dynamic structure function is severely distorted. While the ripplon branch stays mostly unperturbed, the intensity of the

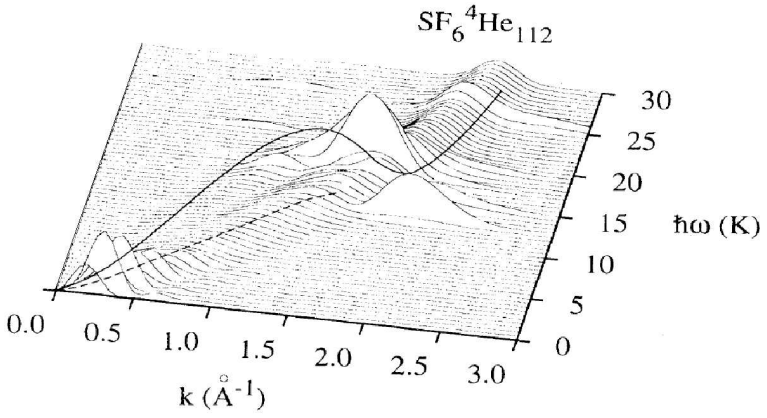

Figure 2.11: Dynamic structure functions of SF_6 doped helium droplet containing N =112 He atoms [8]. The solid line shows Feynman's energy spectrum for *bulk helium*. The dashed line shows ripplon dispersion curve.

phonon branch is substantially decreased. The overall dynamic structure function profile becomes fractioned. It may be a signature of the *quantum solidification* phenomenon.

Fluidity of helium has essentially quantum origin. It can be understood from the following example. Consider a classical crystal. Each atom of the crystal oscillates in the potential energy well formed by the surrounding atoms. At low temperature the amplitude of this oscillation is negligible compared to interatomic distance. One can say that the atom is located at certain position. However, the amplitude of the oscillation raises with temperature and eventually becomes comparable with the interatomic distance. The crystal melts and the classical fluid is formed.

The situation with quantum fluid, such as liquid helium, is different. The potential energy well resulting from interaction of a helium atom with its neighbors is shallow. The amplitude of the oscillation corresponded to the very first vibrational level, i.e. zero point oscillation, is comparable with the interatomic distance. Therefore, helium is liquid even at temperatures close to the absolute zero.

Interaction of the majority of atoms and molecules with helium is stronger than interaction between helium atoms. If a molecule is placed in superfluid helium environment the helium atoms in the close vicinity of the molecule find themselves being affected by a strong attractive potential imposed by the molecule. The amplitude of the zero-point oscillation decreases and become less than the interatomic distance. Thus, the helium near the molecule acquire classical properties. Having classical character, the helium tends to solidify.

This phenomenon was first observed by K. R. Atkins [4]. Measuring mobility of ions in superfluid helium he found that the effective mass in liquid helium of the ions is about 50 times the mass of the free ion. He suggested that the strong attractive potential of the ion causes formation of a small helium crystal around it leading to the effective mass increase.

The effect of distortion of the dynamic structure function of helium droplet doped with SF_6 molecule discussed here can possibly be explained in the same way. However, it must be noted that the helium droplet taken in this case is rather small, leading to an interesting question: would the increase of the droplet size lead to recovery of the dynamic structure function of the droplet?

2.5 Influence of helium environment on unimolecular reaction rate

In this section the influence of the helium environment on chemical reactions will be discussed. The discussion begins with noting that chemical reactions may proceed in helium and helium nanodroplets indeed. While the observation of elementary chemical reactions is obscured in bulk liquid helium because embedded impurities tend to coalesce, helium nanodroplets are the perfect reactors to study these kinds of reactions.

The *proof-of-principle* experiment has been done by A. F. Vilesov et.al who observed chemiluminescence resulting from the chemical reaction Ba + NO_2 = BaO + NO. [31]. An enhancement of the probability of this reaction has been observed due to the fact that reactants are collecting inside helium droplet and the cross section of this reaction becomes the geometrical cross section of helium droplet. Laser initiated unimolecular decomposition of CF_3I has been observed by M. Drabbels et. al. [5]

Interaction between solvent and reactants is very complex. One way the solvent may affect a reaction is by changing the chemical nature of the solutes. In this case the reaction proceeds between solvated complexes rather than original reactant molecules. It may lead to substantial decrease of the reaction activation energy. The good example is ionic reactions in polar solvents. [39]

It is not the case of helium. The polarizability of helium is low and the interaction between helium and impurity molecules is weak. In the next chapter the experiment on measuring absorption spectrum of NO_2 molecule will be dicussed. One important observation in this experiment is that the pattern of the spectrum is mostly preserved. Thus, the influence of the helium environment on the nature of the molecule is negligible.

Solvents may also affect chemical reactions by hindering mutual motion of reactant molecules preventing them from approaching each other, and inhibiting reaction, or vice versa, keeping them together and hence increasing the chemical reaction probability (caging effect). It is not clear if the quantum solidification of helium around impurities discussed in the previous section is able to prevent recombination reaction. Even a tiny barrier on the reaction pathway may preclude otherwise barrierless recombination reaction in conditions of low temperature and slow molecular motion. On the other hand attractive forces between reacting species are expected to be sufficient to cause helium rearrangement.

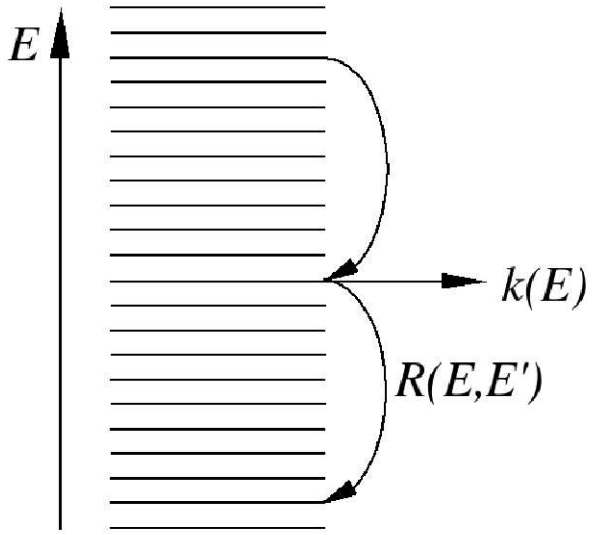

Figure 2.12: Linderman mechanism of chemical reaction in conditions of collisional energy transfer

The most apparent effect of the liquid helium environment on the embedded species is that the excitation energy of the reacting molecules can be efficiently transfered to helium environment. Simply speaking helium acts like an efficient heat sink. Absorption spectrum of NO_2 molecule in a helium droplet exhibit homogeneous line broadening due to the efficient relaxation as will be dicsussed in the next chapter. The lifetime of an excited state of the molecule calculated from the line width is of order of 0.7 ps. The efficient dissipation of the kinetic energy of reactant molecules approaching each other causes them to follow minimum energy pathway. Generally speaking, this pathway does not coincide with the reaction coordinate. Thus, reacting molecule approaching each other eventually end up in a local minimum of the potential in the geometry that precludes the reaction.

Consider a molecule that undergoes unimolecular decomposition in conditions of collisional energy transfer. Assume that the molecule has a manifold of states $|i\rangle$ with

energies E_i and unimolecular reaction rate k_i can be assigned to each of the states. The corresponding diagram is shown in figure 2.12 In the absence of collisional energy transfer the set of equations defining time dependence of the state populations $x_i(t)$ would be:

$$\frac{dx_i}{dt} = -k_i x_i$$

Collisional energy transfer causes redistribution of the state populations. It can be characterized by the rate R_{ji} of the transition from state $|i\rangle$ to state $|j\rangle$. Thus, beside the loss of the population x_i due to the unimolecular reaction there is an additional loss of the population of the state $|i\rangle$ due to transition from the state $|i\rangle$ to all other states and an additional gain of the population due to the transition from all other states to the state $|i\rangle$ as it is shown in figure 2.12. Thus, the state populations can be found from the set of differential equations:

$$\frac{dx_i}{dt} = -\sum_j R_{ji} x_i + \sum_j R_{ij} x_j - k_i x_i \tag{2.63}$$

If the unimolecular reaction rate, population of states, and collisional energy transfer rates can be defined as functions of energy, equations (2.63) can be recast in integral form:

$$k_{\text{uni}}^{\text{eff}}(E)x(E) = \int_0^\infty \left[R(E,E')x(E') - R(E',E)x(E)\right] dE' - k(E)x(E) \tag{2.64}$$

where $k_{\text{uni}}^{\text{eff}}(E)$ is effective unimolecular reaction rate and $R(E,E')$ is energy transfer rate defined as the probability of transition of the molecule having initial energy E' to

the states in the energy interval from E to $E + dE$ per unit time. The relation between the matrix $\mathbb{R}$ and the function $R(E, E')$ is given by:

$$R_{ij} = \frac{R(E_i, E_j)}{E_j - E_{j-1}} \tag{2.65}$$

The set of equations (2.63) can also be recast in matrix notation. If a matrix $\mathbb{J}$ is defined in the following way:

$$\begin{aligned} J_{ij} &= R_{ij} \quad \text{if } i \neq j \\ J_{ii} &= -k_i - \sum_{j \neq i} R_{ji} \end{aligned} \tag{2.66}$$

then the set of equations (2.63) can be rewritten as follows:

$$\frac{d\mathbf{x}}{dt} = \mathbb{J}\mathbf{x} \tag{2.67}$$

where $\mathbf{x}$ is population vector with elements x_i.

The formal solution of the equation (2.67) is given by:

$$\mathbf{x}(t) = \exp(\mathbb{J}t)\mathbf{x}_0 = (\mathbb{I} + \mathbb{J} + \frac{1}{2!}\mathbb{J}^2t^2 + \cdots)\mathbf{x}_0 \tag{2.68}$$

where $\mathbb{I}$ is a unit matrix and $\mathbf{x}_0 = \mathbf{x}(t)|_{t=0}$.

Generally speaking, the matrix $\mathbb{J}$ can be diagonalized to find its eigenvectors $\mathbf{g}_i$ and eigenvalues λ_i, so that:

$$\mathbb{J}\mathbf{g}_i = \lambda_i\mathbf{g}_i \tag{2.69}$$

The eigenvectors are written as:

$$\exp(\mathbb{J}t)\mathbf{g}_i = \exp(\lambda_i t)\mathbf{g}_i \tag{2.70}$$

Expanding the vector $\mathbf{x}_0$ in the basis set of the eigenvectors $\{\mathbf{g}_i\}$, the solution of the equation (2.68) can be rewritten as:

$$\frac{d\mathbf{x}(t)}{dt} = \sum_i (\mathbf{x}_0 \cdot \mathbf{g}_i) e^{\lambda_i t} \mathbf{g}_i \tag{2.71}$$

All eigenvalues given by equation (2.69) are negative. Otherwise populations of the states would grow exponentially. Assume that the eigenvalues and corresponded eigenvectors are enumerated so that $\lambda_0 > \lambda_1 > \lambda_2 \ldots$. Equation (2.71) suggests that the unimolecular reaction proceeds in the following way: after some induction period all the components corresponding to $\mathbf{g}_i$, other than $\mathbf{g}_0$, will decay and the stationary population distribution proportional to the vector $\mathbf{g}_0$, will be achieved. After that, the unimolecular reaction would proceed with reaction rate given by $k_{\text{uni}}^{\text{eff}} = -\lambda_0$ [16].

To apply the approach discussed above to the case of chemical reaction in liquid helium environment it is necessary to evaluate the corresponding energy transfer rate either as a matrix $\mathbb{R}$ from the equation set (2.63) or as function $R(E, E')$. The latter is prefered because it is less specific. It will be done in the next section.

2.6 Collisional energy transfer function for liquid helium environment

Consider a particle (an atom or a molecule) moving through liquid helium. Along its way it may experience collisions with helium atoms. As the result of this collisions, the kinetic energy of the particle will be transferred to helium environment. The dissipation of the kinetic energy of the particle is accompanied with creation of quasiparticles in liquid helium. There is a certain analogy between this process and inelastic scattering of neutrons discussed below. One of the important conclusions that follows from this

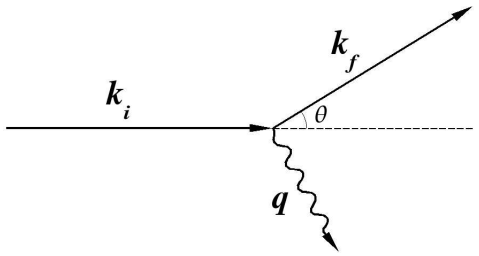

Figure 2.13: Vector diagram of the elementary scattering event. $\mathbf{k}_i$ and $\mathbf{k}_f$ initial and final wavevectors of the particle, q is the wavevector of the quasiparticle created in collision and θ is the scattering angle.

discussion is that in the spirit of Feynman's approximation one can assume that only a single particle is created in an elementary act of the kinetic energy dissipation. Thus, it is governed by the conservation laws:

$$\mathbf{k}_i = \mathbf{k}_f + \mathbf{q} \tag{2.72a}$$

$$\frac{\hbar^2 k_i^2}{2M} = \frac{\hbar^2 k_f^2}{2M} + \mathcal{E}(q) \tag{2.72b}$$

In the equations above, M is the mass of the particle, $\mathbf{k}_i$ and $\mathbf{k}_f$ are its initial and final wavevectors, and q is the wavevector of the quasiparticle created in collision. The vector diagram of the particle scattering process is shown in figure 2.13.

As is the case of neutron scattering, one can consider the elementary act of energy dissipation as the transition between continuum states and apply the Fermi's Golden Rule formula to obtain the probability of such an event per unit time.

$$dw_{fi} = \frac{2\pi}{\hbar}|U_{fi}|^2 \cdot \delta\left(\frac{\hbar^2 k_i^2}{2M} - \frac{\hbar^2 k_f^2}{2m_M} - \mathcal{E}(q)\right)\frac{d^3\mathbf{k}_f d^3\mathbf{r}}{(2\pi)^3} \tag{2.73}$$

here

$$\frac{d^3\mathbf{k}_f d^3\mathbf{r}}{(2\pi)^3}$$

is an elementary volume in the phase space of the final states of the particle.

Continuing to use the analogy of neutron scattering we may try to use the Fermi δ-potential given by the equation (2.32) can be used to describe the interaction between particle and liquid helium. However, the validity of using this potential to describe scattering of an atom or a molecule on liquid helium discussed herein is questionable and has to be justified. This potential is perfect for the purpose of calculation of the neutron inelastic scattering cross section, because neutrons does not interact with electrons and the scattering actually occurs on atomic nuclei [27]. Atoms or molecules would interact with helium atoms of the liquid via their electron shells. It must be taken into account that the potential of interaction between an atom (or a molecule) is not purely repulsive and generally speaking can be anisotropic. However, the matrix element of the Fermi potential can be evaluated easily. This matrix element will be used for the problem under consideration keeping in mind that the theory we will end up with will probably not be accountable for every effect that may take place and leaving the hope to employ it to obtain any *precise* numerical values.

Thus, the potential used here is given by:

$$U(\mathbf{r}) = \sqrt{\frac{\sigma}{4\pi}}\frac{2\pi\hbar^2}{\mu}\sum_{a=1}^{N}\delta(\mathbf{r}-\mathbf{r}_a) \tag{2.74}$$

where μ is the effective mass of the scattered particle and the scattering center and σ is mutual scattering cross section of the particle and helium atom. For the zeroth-order approximation its gas-kinetic value might be taken but assigning it some effective value may be considered as a first step toward improving the potential.

The matrix element of the scattering potential is than given by

$$|U_{fi}(q)|^2 = \frac{\pi\hbar^4\sigma}{V\mu^2} n_{\mathrm{He}} S(q); \tag{2.75}$$

where μ is the effective mass of the particle and helium atom, n_{He} is the number density of liquid helium, and V is the volume of the system.

$S(q)$ is the static structure function discussed above. This function is different for bulk helium, helium droplets, and other liquid helium systems such as helium films. For example, the shapes of the structure functions of liquid helium and helium droplets are similar except for the region of small q. Beside that, structure function for the helium droplet has an additional branch corresponding to ripplon excitations.

The right side of the equation (2.73) will then be integrated in order to evaluate the collisional energy transfer probability rather than scattering cross section. Hence we will integrate it over different set of variables.

The transition probability is given by:

$$w_{fi} = \frac{V}{\hbar(2\pi)^2} \int |U_{if}(q)|^2 \delta\left(\frac{\hbar^2 k_i^2}{2M} - \frac{\hbar^2 k_f^2}{2M} - \mathcal{E}(q)\right) d^3\mathbf{k}_f$$

to proceed further switch to spherical coordinates, choosing the z-axis to be directed along $\mathbf{k}_i$. As one can see from the diagram shown in figure 2.13, the absolute value of the momentum transfer is given by:

$$q = \sqrt{k_i^2 + k_f^2 - 2k_i k_f \cos\theta} \tag{2.76}$$

and the expression for the transition probability becomes:

$$w_{fi} = \frac{V}{2\pi\hbar} \int_0^{k_i} dk_f \int_0^{\pi} d\theta k_f^2 \sin\theta \left[|U_{if}(q)|^2 \delta\left(\frac{\hbar^2 k_i^2}{2M} - \frac{\hbar^2 k_f^2}{2M} - \mathcal{E}(q)\right)\right] \tag{2.77}$$

substitution $\{u = \cos\theta, du = -\sin\theta d\theta\}$ transforms this integral into

$$w_{fi} = \frac{-V}{2\pi\hbar}\int_0^{k_i} dk_f \int_0^1 du k_f^2 \left[|U_{if}(q)|^2 \delta\left(\frac{\hbar^2 k_i^2}{2M} - \frac{\hbar^2 k_f^2}{2M} - \mathcal{E}(q)\right)\right] \tag{2.78}$$

Switching to another set of coordinates:

$$q = \sqrt{k_i^2 + k_f^2 - 2k_i k_f u};$$
$$E_f = \frac{\hbar^2 k_f^2}{2M};$$

The Jacobian for this transformation is given by:

$$dk_f du = \frac{-q}{2k_i E_f} dq dE_f$$

And the transition probability now becomes:

$$w_{fi} = \frac{V}{2\pi\hbar}\frac{1}{2k_i}\frac{2M}{\hbar^2}\int_0^{E_i} dE \int_{k_i-k_f}^{k_i+k_f} dq q \left[|U_{if}(q)|^2 \delta\left(E_i - E_f - \mathcal{E}(q)\right)\right] \tag{2.79}$$

where $E_i \equiv \hbar^2 k_i^2/2M$ is initial kinetic energy of the scattering particle. After substituting the value of $|U_{fi}(q)|^2$ given by (2.75) into the expression above, it becomes:

$$w_{fi} = \frac{n_{\mathrm{He}}\sigma\hbar}{2k_i}\frac{M}{\mu^2}\int_0^{E_i} dE_f \int_{k_i-k_f}^{k_i+k_f} qS(q)\delta\left(E_i - E_f - \mathcal{E}(q)\right) dq \tag{2.80}$$

The right part of the equation above should not be integrated in over E_f. Then it yields the energy transfer function $R(E_f, E_i)$ as it is defined in the previous section. Thus, the expression for the the $R(E_f, E_i)$ is given by:

$$R(E_f, E_i) = \frac{n_{\mathrm{He}}\sigma\hbar}{2k_i}\frac{M}{\mu^2}\int_{k_i-k_f}^{k_i+k_f} qS(q)\delta\left(E_i - E_f - \mathcal{E}(q)\right) dq \tag{2.81}$$

Integrating it over q gives:

$$R(E_f, E_i) = \sum_n \begin{cases} \left(\frac{n_{\mathrm{He}}\sigma\hbar}{2k_i}\frac{M}{\mu^2}\right)\frac{q_n S(q_n)}{|\mathcal{E}'(q_n)|} & \text{if } k_i - k_f < q_n < k_i + k_f \\ 0 & \text{if } (k_i - k_f > q_n) \text{ or } (q_n > k_i + k_f) \end{cases} \tag{2.82}$$

where q_n's are all solutions of the equation

$$\mathcal{E}(q_n) = E_i - E_f = \Delta E \tag{2.83}$$

To understand the behavior of the energy transfer function $R(E_f, E_i) = R(\Delta E, E_i)$ given by the equation (2.82), divide ΔE scale into different regions corresponding to different part of the excitation spectrum of liquid helium. In these regions $\mathcal{E}(q)$ and $S(q)$ can be expressed analytically.

2.6.1 Phonon region

In the phonon part of the excitation spectrum $\mathcal{E}(q), \mathcal{E}'(q)$ and $S(q)$ are given by:

$$\mathcal{E}(q) = \hbar c q$$
$$\mathcal{E}'(q) = \hbar c$$
$$S(q) = \frac{\hbar q}{2mc}$$

Equation (2.83) has the only one solution

$$q_0 = \frac{\Delta E}{\hbar c}$$

Thus, the energy transfer function is:

$$R(\Delta E, E_i) = \left(\frac{n_{\mathrm{He}} \sigma \hbar}{2k_i} \frac{M}{\mu^2} \right) \frac{\Delta E^2}{2\hbar^2 c^4 m} \tag{2.84}$$

if q_0 satisfies the constrains $k_i - k_f < q_0 < k_i + k_f$. The latter can be expanded as follows:

$$\begin{aligned}
&k_i - k_f < q_0 < k_i + k_f \\
&k_i - k_f < \frac{\Delta E}{\hbar c} < k_i + k_f \\
&k_i - k_f < \frac{\hbar}{2Mc}(k_i - k_f)(k_i + k_f) < k_i + k_f
\end{aligned}$$

It can be transformed into:

$$\begin{aligned}
v_i - v_f &< 2c \\
v_i + v_f &> 2c
\end{aligned}$$

where v_i and v_f are initial and final velocities of the particle. The first of these inequalities says that the velocity of the particle cannot change on the value exceeding $2c$ in the phonon region. The second says that the momentum transfer does not occur if the velocity of the particle less than the speed of sound of liquid helium. The latter can be used as a definition of *microscopic superfluidity*.

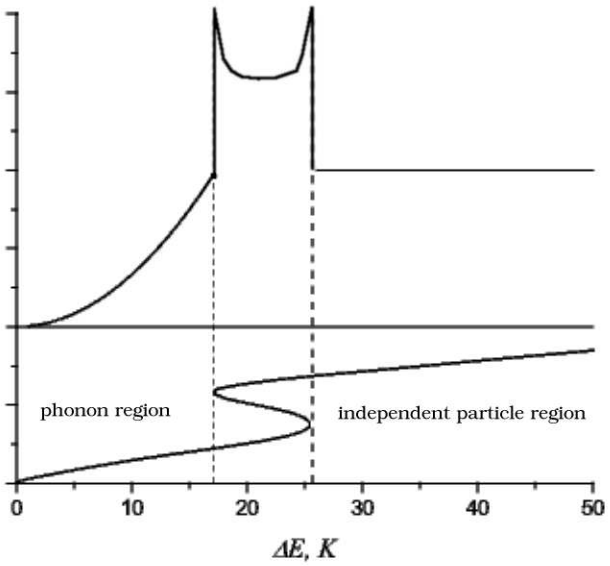

Figure 2.14: Sketch of the energy transfer function $R(\Delta E)$, $\Delta E = E_i - E_f$. The Feynman excitation spectrum curve is shown below. (Spikes at $\Delta E = E_{\text{roton}}$ and $\Delta E = E_{\text{roton}}$ are due to $\mathcal{E}'(q) = 0$ at these points.)

2.6.2 Independent particle region

In the independent particle region part of the excitation spectrum $\mathcal{E}(q)$, $\mathcal{E}'(q)$ and $S(q)$ are given by:

$$\mathcal{E}(q) = \frac{\hbar^2 q^2}{2m}$$
$$\mathcal{E}'(q) = \frac{\hbar^2 q}{m}$$
$$S(q) = 1$$

As in the case of phonon region the equation (2.83) has the only one solution

$$q_0 = \frac{\sqrt{2m\Delta E}}{\hbar}$$

Thus, the energy transfer rate is given by:

$$R(\Delta E, E_i) = \left(\frac{n_{\text{He}} \sigma \hbar}{2k_i} \frac{M}{\mu^2} \right) \frac{m}{\hbar} = \frac{n_{\text{He}} \sigma}{2k_i} \frac{Mm}{\mu^2} \tag{2.85}$$

As one can see the energy transfer rate does not depend on ΔE in the independent particle region. The constraints in the equation (2.82) require special consideration. Substituting q_0, defined above, into $k_i - k_f < q_0 < k_i + k_f$ gives:

$$k_i - k_f < \frac{\sqrt{2m\Delta E}}{\hbar} < k_i + k_f$$

All parts of these inequalities are positive because $k_i > k_f$. Therefore the squares of the parts obey the same inequalities. Expanding the ΔE, the expression above is recasted as:

$$(k_i - k_f)^2 < \frac{m}{M}(k_i - k_f)(k_i + k_f) < (k_i + k_f)^2$$

The expression above can be simplified as

$$k_i - k_f < \frac{m}{M}(k_i + k_f)$$
$$k_i - k_f < \frac{M}{m}(k_i + k_f)$$

Depending on the ratio $\frac{m}{M}$ one of these inequalities is more strict than the other one. Assume that $M > m$, because only few atoms are lighter than helium and hence this situation is often the case. Then the first of the inequalities includes the second one. It can be easily shown that it is equivalent to the inequality given by:

$$\frac{k_f}{k_i} = \frac{M - m}{M + m}$$

This means that the conservation laws restrict the amount of energy that can be transfered in a collision. The greater the mass difference of the helium atom and the particle the less amount of energy that can be transfered.

Finally, the energy transfer rate $R(\Delta E, E_i)$ in the independent particle region is given by:

$$R(\Delta E, E_i) = \begin{cases} \dfrac{n_{\text{He}}\sigma}{2k_i}\dfrac{Mm}{\mu^2} & \text{if } \Delta E < \dfrac{4mM}{(M+m)^2}E_i \\ 0 & \text{if } \Delta E > \dfrac{4mM}{(M+m)^2}E_i \end{cases} \tag{2.86}$$

The sketch of the energy transfer rate function is shown in figure 2.14. In the intermediate region $E_{\text{roton}} < \Delta E < E_{\text{maxon}}$, the equation (2.83) has three solutions. All these solutions contribute to the energy transfer rate. Thus the energy transfer rate function has local maximum in this region. Spikes at $\Delta E = E_{\text{roton}}$ and $\Delta E = E_{\text{roton}}$ are due to $\mathcal{E}'(q) = 0$ at these points.

Reference List

[1] Cowley R. A. and Woods A. D. Inelastic scattering of thermal neutrons from liquid helium. *Canadian Journal of Physics*, 49:177–200, 1971.

[2] Eugene K. Achter and Lothar Meyer. X-ray scattering from liquid helium. *Physical Review*, 188(1):291–300, 1969.

[3] J. F. Allen and A. D. Misener. Flow of liquid helium II. *Nature*, 141(3558):75, January 1938.

[4] K. R. Atkins. Ions in liquid helium. *Physical Review*, 116(6):1339–1343, December 1959.

[5] Andreas Braun and Marcel Drabbels. Imaging the translational dynamics of CF_3 in liquid helium droplets. *Physical Review Letters*, 93(25):253401, 2004.

[6] C. C. Chang and Michael Cohen. Microscopic theory of surface excitations in superfluid He^4. *Physical Review B (Solid State)*, 11(3):1059–1065, 1975.

[7] S. A. Chin and E. Krotscheck. Structure and collective excitations of [sup 4]he clusters. *Physical Review B (Condensed Matter)*, 45(2):852–874, 1992.

[8] S. A. Chin and E. Krotscheck. Systematics of pure and doped ^{4}He clusters. *Physical Review B (Condensed Matter)*, 52(14):10405–10428, 1995.

[9] B. E. Clements, H. Forbert, E. Krotscheck, H. J. Lauter, M. Saarela, and C. J. Tymczak. Dynamics of boson quantum films. *Physical Review B (Condensed Matter)*, 50(10):6958–6981, 1994.

[10] Michael Cohen and Richard P. Feynman. Theory of inelastic scattering of cold neutrons from liquid helium. *Physical Review*, 107(1):13–24, 1957.

[11] R. J. Donnelly, J. A. Donnelly, and R. N. Hills. Specific heat and dispersion curve for helium II. *Journal of Low Temperature Physics*, 44(5):471–504, 1981.

[12] R. Schiavilla D. S. Lewart V. R. Pandharipande Steven C. Pieper R. B. WiringaS. Fantoni. Structure functions and correlations in nuclei. *Nuclear Physics A*, 473(2):267–289, October 1987.

[13] Eugene Feenberg. *Theory of Quantum Fluids*, volume 31 of *Pure and Applied Physics*. Academic Press, New York and London, 1969.

[14] E. Fermi. *Ricerca, Sci.*, 7:13, 1936.

[15] R. P. Feynman. Atomic theory of the two-fluid model of liquid helium. *Physical Review*, 94(2):262–277, 1954.

[16] R. G. Gilbert and S. C. Smith. *Theory of Unimolecular and Recombination Reactions*. Physical Chemistry Texts. Blackwell Scientific Publications, Oxford, 1990.

[17] Henry R. Glyde. *Excitations in Liquid and Solid Helium*. Oxford Science Publications. Oxford University Press, Oxford University Press, Walton Street, Oxford, 1994.

[18] Keesom W. H. and Wolfke M. Two liquid states of helium. *Konink. Acad. Wetensch. Amsterdam Proc.*, 31(190b):90–94, 1928.

[19] Keesom W. H. and Keesom A. P. *Konink. Acad. Wetensch. Amsterdam Proc.*, 35:736, 1932.

[20] J. R. Henderson and J. Lekner. Theory of surface excitations of liquid helium four. *J. Phys. C:Solid State Phys.*, 10:4955–4963, 1977.

[21] Leon Van Hove. Correlations in space and time and born approximation scattering in systems of interacting particles. *Physical Review*, 95(1):249–262, 1954.

[22] P. Kapitza. Viscosity of liquid helium below the $\lambda-$point. *Nature*, 141(3558):74, January 1938.

[23] E. Krotscheck and M. Saarela. Theory of ^{3}He-^{4}He mixtures: energetics, structure, and stability. *Physics Reports*, 232(1):1–86, September 1993.

[24] L.D. Landau. The theory of superfluidity of helium II. *J.Phys.(U.S.S.R.)*, 5:71, 1941.

[25] L.D. Landau. On the theory of superfluidity of helium II. *J.Phys.(U.S.S.R.)*, 11:91, 1947.

[26] L.D. Landau and E. M. Lifshitz. *Statistical Physics, Part 2*, volume 9 of *Course of Theoretical Physics*. Butterworth-Heinemann, Oxford, 3rd edition, 1980.

[27] L.D. Landau and E. M. Lifshitz. *Quantum mechanics : non-relativistic theory*. Course of Theoretical Physics. Pergamon Press, Ney York, 3 edition, 1991.

[28] Landau L.D. On the theory of superfluidity. *Physical Review*, 75(5):884–885, 1949.

[29] F. London. The $\lambda-$phenomenon of liquid helium and the Bose-Einstein degeneracy. *Nature*, 141(3571):643–644, April 1938.

[30] F. London. On the bose-einstein condensation. *Physical Review*, 54(11):947–954, December 1938.

[31] Evgeni Lugovoj, J. Peter Toennies, and Andrey Vilesov. Manipulating and enhancing chemical reactions in helium droplets. *The Journal of Chemical Physics*, 112(19):8217–8220, 2000.

[32] B. Schilling M. Lewerenz and J. P. Toennies. A new scattering deflection method for determining and selecting the sizes of large liquid clusters of ^{4}He. *Chemical Physics Letters*, 206(1-4):381–387, April 1993.

[33] E. Manousakis and V. R. Pandharipande. Theoretical studies of the dynamic structure function of liquid ^{4}He. *Physical Review B (Condensed Matter)*, 33(1):150–161, 1986.

[34] Allen Miller, David Pines, and Philippe Nozieres. Elementary excitations in liquid helium. *Physical Review*, 127(5):1452–1464, 1962.

[35] Bogolubov N. On the theory of superfluidity. *J. Phys. (U.S.S.R.)*, 11:23, 1947.

[36] V. Peshkov. Determination of the velocity of propagation of the second sound in helium II. *J. Phys. (U.S.S.R.)*, 10:389, 1946.

[37] L. P. Pitaevskii. *Sov. Phys. JETP*, 9:830, 1959.

[38] E. C. Svensson, V. F. Sears, A. D. B. Woods, and P. Martel. Neutron-diffraction study of the static structure factor and pair correlations in liquid ^{4}He. *Physical Review B (Condensed Matter)*, 21(8):3638–3651, 1980.

[39] James T.Hynes. Chemical reaction dynamics in solutions. *Annual Review of Physical Chemistry*, 36:573–596, 1985.

[40] L. Tisza. Transport phenomena in helium II. *Nature*, 141:913, 1938.

[41] L. Tisza. *J. de phys. et rad.*, 1:164,350, 1940.

[42] K.B. Whaley. *Advances in Molecular Vibrations and Collosion Dynamics*, volume 3, chapter Spectroscopy and Microscopic Theory of Doped Helium Clusters, pages 397–451. Academic Press, Greenwich, 1998.

Chapter 3

Experimental methods and instrumentation

3.1 Mass depletion spectroscopy

Spectroscopy is an established tool to study molecular dynamics. Comparing a spectrum of a molecule embedded in helium droplet with the spectrum of the molecule in gas phase one can reveal the influence of the liquid helium environment on the molecular dynamics. In some situations, mostly limited to big organic molecules, the deactivation of the electronic excitation by liquid helium is slow and laser induced flourescence spectrum can be recorded [5]. In the case of small molecules such as NO_2 discussed below in detail, the deactivation is efficient and the flourescnce is quenched. The direct measurement of an absorption spectrum is not feasible due to the low concentration of

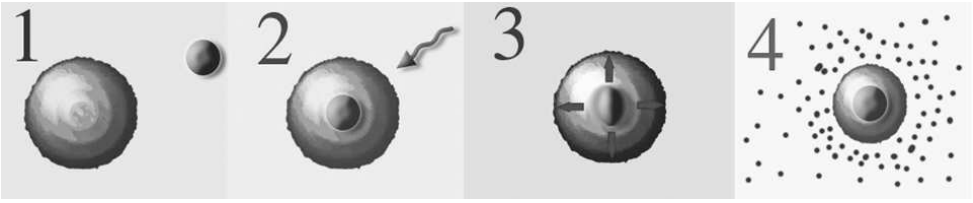

Figure 3.1: Schematic representation of the process the mass depletion spectroscopic technique is based on. Step (1) represents the doping of the helium droplet with the molecule. Step (2) showes the photon-induced excitation of the molecule. The excitation energy is transfered to the helium droplet (3) and causes evaporation of the helium (4) resulting in decrease of ionization cross section.

molecules in the doped helium droplet beam. The solution of this problem is given by mass depletion spectroscopic technique.

This spectroscopic technique is based on the rapid transfer of the photon-induced excitation of the molecule to the helium droplet. The process enables the use of mass depletion technique is shown schematically in figure 3.1. In this figure, the first step represents the doping of the helium droplet in pickup cell. The droplet beam is irradiated with laser light. When the wavelength of the laser radiation coincides with the resonance of the molecule, the excitation of the molecule occurs (figure 3.1(2)). The excited molecule interacts with the liquid helium environment. As a result of this interaction the excitation energy is transfered to the helium droplet (figure 3.1(3)). This causes evaporative cooling of the droplet. Every 5 cm^{-1} of the energy of the photon causes the evaporation of one helium atom. The evaporation of helium eventually leads to the decrease of the size of the droplet (figure 3.1(4)).

Quadrupole mass spectrometer can be used to detect the decrease of the droplet size. When a helium droplet arrives in the detection region of the mass spectrometer it is exposed to electron bombardment. It causes fragmentation and ionization of the droplet. The resulting mass spectrum is very rich [1]. It contains lines corresponding to helium droplet fragnments, He_n^+, with amplitudes decreasing with n, as well as lines corresponded to the doping molecule and its fragments. The cross section of the fragmentation and ionization due to the collisions with electrons is approximately proportional to the size of the droplet. Thus, the shrinkage of the droplet caused by evaporation resulting from the excitation energy transfer, eventually leads to the decrease of the mass spectrometer signal. If the molecule is not destroyed in the result of the excitation, the amplitudes of all lines of the mass spectrum are decreased by the approximately same amount. However, since not all of the droplets contain the doping molecule, it is wise to

tune the mass spectrometer on the ion mass corresponding to the molecule itself or one of its fragments.

Mass depletion spectroscopy can also be used to study unimolecular reactions in helium droplets. Lets for example consider a molecule AB embedded in helium droplet excited above its dissociation threshold. In the absence of the droplet it would undergo unimolecular reaction AB→A+B. The mass spectrometer monitors ion current at $m/z = 8$ amu correspondent to He_2^+ ion as well as ion currents corresponded to fragments A^+, B^+, and the ion current corresponding to the whole molecule AB^+. There are two competing processes that follow the excitation of the molecule: unimolecular reaction and deactivation of the molecule by the liquid helium environment. If the deactivation is more efficient the photon energy is transfered to the liquid helium. It causes evaporation of helium and result in high depletion signal at the all ion masses we monitor. The spectrum at these excitation energies is expected to be congested and there should be no variation in the depletion signal while tuning the excitation laser wavelength. The situation is not very different in the case when unimolecular reation actually occurs, but the recoiling fragments loose their kinetic energy before leaving the droplet, come back to each other, and recombine. Mass depletion measurements do not provide distinction between these two scenarios.

The situation is differnt if one of the fragments leaves the droplet. In this case, the photon energy is spent on breaking the bond, leaving almost no energy on evaporation of the cluster. Thus, there should be no depletion signal on the mass $m/z = 8$ amu, but the depletion signal corresponding to the mass of the fragment leaving the droplet, as well as the signal corresponding to the mass of the whole, molecule will be high due to the decrease of the transport of the molecule and the fragment leaving the droplet to the detection region.

Depletion signal	A^+	B^+	AB^+	He_2^+
unimolecular dissociation is suppressed	high	high	high	high
recombination occurs	high	high	high	high
A leaves the droplet	high	low	high	low
B leaves the droplet	low	high	high	low
A and B leave the droplet	high	high	high	low
van-der-Waals complex is formed	low	low	low	low

Table 3.1: The expected outcome of the mass depletion measurements for the molecule AB embedded in helium droplet excited above its dissociation threshold. The mass delpetion signal levels at masses correponded to ions A^+, B^+, AB^+ and He_2^+ are shown in the table. The left colomn contains description of possible scenario (refer to the text for the discussion).

Another possible scenario is that none of the fragments leaves the droplet, but when they come together they do not recombine but rather form metastable van der Waals complex. The photon energy in this situation goes mostly on the bond breaking. Little energy would be left for the helium evaporation. In this case, no considerable depletion signal should be observed at all masses monitored. Instead, the ion current signal corresponding to one of the fragnments can *increase* because the fragmentation and ionization process of the van-der-Waals complex proceeds in a different way than the fragmentation and ionization of the molecule.

The summary of the discussion above is represented in the table 3.1. The results of the experiment on mass depletion measurement of NO_2 in helium droplet excited above its dissociation threshold will be discussed in detail in the chapter 5

3.2 Experimental

The next two chapters discuss the results of the experiment on measuring mass depletion spectra of NO_2 in the regions below and above its gas phase dissociation threshold. These experiments address different aspects of molecular dynamics on NO_2 in the presence of the liquid helium environment. However, in both of these experiments, the

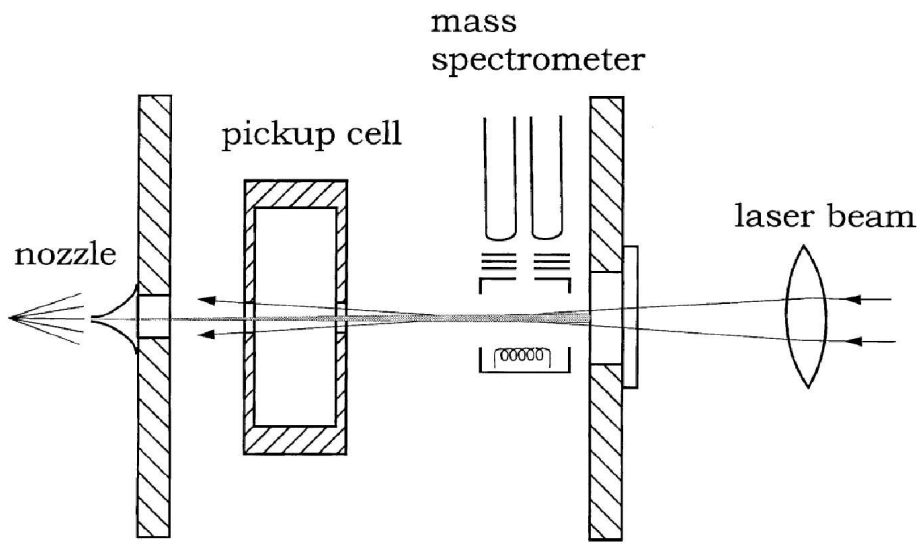

Figure 3.2: Experimental arrangement (not to scale). The source, pickup, and detection chambers are pumped separately. The nozzle is at 14.5 K, and the He pressure behind the nozzle is 40 bar. The laser beam is brought to a focus in the detection chamber to avoid damaging the nozzle.

experimental procedure followed and the experimental arrangement used are essentially the same and the second experiment can be considered as a continuation of the first one. The details of these experiments relevant for the further discussion is described below. Please refer to [4] for the detailed description of the experimental setup.

The experimental layout is shown schematically in Fig.3.2. There are three separately pumped chambers. In the first, He_n droplets are produced by expanding ultrapure helium (99.9999%, Spectra Gases) through a 5 μm diameter hole (National Aperture) that is cooled by using two closed-cycle helium refrigerators (CTI Cryogenics), one of which pre-cools the helium before it enters the nozzle assembly. In the experiments discussed here, the stagnation temperature was 14.5 K and the pressure was 40 bar. The mean size of the clusters produced under these conditions is $\langle n \rangle \sim$9000 [3].

Temperatures were measured with a Si diode sensor (Lakeshore $\pm$ 0.1 K). The source chamber operating pressure is 2×10^{-4} mbar.

After passing through a 400μm diameter skimmer, the droplet beam goes through a 3 cm long pickup cell containing NO_2 (Matheson, 99.5%, used without purification) that is 10 cm downstream from the nozzle.

The pickup process can be monitored, albeit with some uncertainty, by observing intensities of peaks in the mass spectra that correspond to NO_2^+, $(NO_2)_2^+$, etc. Despite the fact that N_2O_4 does not absorb in this wavelength region, it was found that the depletion signal increases with pickup cell pressure. This is consistent with the formation of metastable (i.e., van der Waals type) complexes that absorb in this region, e.g., NO_2-NO_2 instead of N_2O_4. In consideration of this, the pickup cell pressure was adjusted to achieve "optimal" conditions. Namely, when the number of droplets that contain a single NO_2 molecule is about 70% of its maximum value, only a few percent of the droplets contain more than one NO_2 molecule. The pressure in the pickup chamber was monitored with a "micro" ion gauge (Granville-Phillips); its reading under optimal conditions was 2.7×10^{-7} Torr.

The detection region is separated from the pickup chamber by a 5 mm diameter aperture that is 12 cm from the exit of the pickup cell. The background pressure in the detection chamber is $\sim 10^{-8}$mbar. The use of turbomolecular pumps in the second and third chambers minimizes problems that arise from contamination by impurities. A quadrupole mass spectrometer (Balzers) was used to monitor the depletion of signals arising from droplets containing NO_2.

The mass spectrometer was installed with its quadrupole axis perpendicular to the molecular beam axis so the laser beam could be overlapped with the molecular beam. The length of this interaction region is $\sim$75 cm, corresponding to a duration of the

depletion signal of $\sim$2.5 ms. The electron multiplier output of the mass spectrometer was connected directly to a 12-bit ADC computer board (Gage Applied Sciences, CS8012).

In the experiment discussed in the chapter 4 a dye laser (Continuum ND6000) pumped by the second harmonic of a Nd-YAG laser (Continuum, Powerlite 7020) was used. The explored spectral region of 546-565 nm is covered by Fluorescein 548 dye. High energy pulses (40 mJ) were used, because of the small NO_2 absorption cross-sections (i.e., $\sim 10^{-19}$ cm^2 for the corresponding gas phase transitions [2]).

The absorption of laser radiation results in the evaporation of He atoms from the droplets, each atom requiring $\sim$5 cm^{-1} for evaporation. Thus, $\sim$3600 He atoms are evaporated following the absorption of an 18 000 cm^{-1} photon. This shrinkage results in less efficient electron impact ionization of those clusters that have absorbed a photon, and consequently have a smaller cross-section. This is the basis of the mass spectrometer depletion spectrum. The largest depletions observed in the experiment discussed in chapter 4 are $\sim$7% (Fig. 4.1). The spectrum shown in Fig. 4.1 was obtained by monitoring m/e =30. No significant differences were observed when monitoring different m/e peaks, i.e., 46 (NO_2^+), 30 (NO^+), and 8 (He_2^+).

For the experinment discussed in the chapter 5 the laser system was modified to cover the wavelength region from 340 to 402 nm. On the short-wavelength side of this region, radiation was obtained by doubling the output of a dye laser (Continuum ND6000) pumped by the second harmonic of a Nd:YAG laser (Continuum Powerlite 9020). The region 340-365 nm was covered by using the dyes DCM, LDS 698, LDS 722, and LDS 750. Energies ranged from 5 to 19 mJ, with a mean of 12.5 mJ.

Radiation from 365 to 402 nm was obtained by mixing the dye laser output with the Nd:YAG fundamental. Injection-seeding (LightWave Technologies) of the Nd:YAG laser narrows its line width, thereby increasing conversion efficiency. The following

dyes were used in this region: R590; a mixture of R590 and R610; R610; a mixture of R610 and R640; R640; and DCM. The 365-402 nm energies varied from 8 to 22 mJ, with an average of 17 mJ.

As discussed in the previous section the difference of the depletion signal corresponded to different masses: 46 (NO_2^+), 30 (NO^+), and 8 (He_2^+) was expected to be observed. The results of the experiment is disscused in the chapter 5.

Reference List

[1] Berton E. Callicoatt, Kirk Forde, Lilian F. Jung, Thomas Ruchti, and Kenneth C. Janda. Fragmentation of ionized liquid helium droplets: A new interpretation. *The Journal of Chemical Physics*, 109(23):10195–10200, 1998.

[2] Davidson J.A. Cantrell C.A. McDaniel A.H. Shetter R.E. Madronich S. Calvert J.G. Visible-ultraviolet absorption cross sections for NO_2 as a function of temperature. *Journal of Geophysical Research*, 93(D6):7105–7112, 1988.

[3] B. Schilling M. Lewerenz and J. P. Toennies. A new scattering deflection method for determining and selecting the sizes of large liquid clusters of ^{4}He. *M. Lewerenz, B. Schilling and J. P. Toennies*, 206(1-4):381–387, April 1993.

[4] Elena Polyakova. *Multiphoton Ionization of Molecules Embedded in Superfluid Liquid Helium Droplets*. PhD thesis, University of Southern California, 2005.

[5] Frank Stienkemeier and Andrey F. Vilesov. Electronic spectroscopy in He droplets. *The Journal of Chemical Physics*, 115(22):10119–10137, 2001.

Chapter 4

Mass-depletion spectroscopy of NO_2 in helium droplets below its gas phase dissociation threshold

4.1 Introduction

Superfluid helium nanodroplets (hereafter referred to as He_n, where n is the number of He atoms) provide convenient environments for carrying out detailed studies of embedded molecules and aggregates under well-characterized, ultracold (0.37 K) conditions [32, 24, 26]. Research in this area has flourished following the seminal experiments of Vilesov, Toennies, and coworkers, in which molecular-level manifestations of He_n superfluidity were revealed in a series of elegant spectroscopic studies [15, 14, 13, 12], and several exciting directions have been identified [2, 31].

At this point in time, a significant number of fundamental and overtone vibrations of molecules and weakly bound complexes in their ground potential energy surfaces (PESs) have been examined [4, 5, 23]. In addition, molecular electronic spectra have revealed phonon wings, including a "roton gap," radiationless decay, and details of the dopant-He_n interactions [30, 17, 16, 11, 28]. These studies have been carried out mainly in the regime of regular nuclear dynamics, where the goodness of vibrational quantum numbers is high. On the other hand, vibrational congestion, which often goes hand-in-hand with complex dynamics, has been noted in electronic spectra of large molecules,

e.g., tetracene and pentacene [17, 16]. However, in systems of such high dimensionality (i.e., having 84 and 108 vibrational degrees of freedom, respectively), state-resolved studies in the regime of chaotic dynamics are not feasible.

In this chapter spectroscopic observations - *in a regime where the intramolecular dynamics are believed to be chaotic* - of a small molecule embedded in superfluid helium nanodroplets will be discussed. Chaotic and regular dynamical regimes differ qualitatively, and quantum-chaotic dynamics of the molecule under consideration (NO_2) has been implicated throughout the energy range of interest [6].

In the study reported here, the chaotic system is coupled weakly to an exceptionally well-characterized bath. The ultracold He_n host is used to *probe the dopant* by introducing two observables that are expected to provide signatures in and near the regime of quantum chaos: spectral shifts and widths.

It is advantageous that a great deal is known about NO_2. Strong mixing of the A^2B_2 and X^2A_1 states above the conical intersection of these potential energy surfaces, due to breakdown of the Born-Oppenheimer approximation, yields A_1 and B_2 vibronic species, whose only means of communication in collision-free environments is rotation [7, 20]. Each of these vibronic manifolds is believed to be quantum chaotic, e.g., for a given set of good quantum numbers (J and M_J) the nearest neighbor spacings follow a Wigner distribution [10]. Because NO_2 is small, its eigenstates are widely separated, i.e., they are $\sim$10 cm^{-1} apart on average for each vibronic manifold at $E \sim$18 000 cm^{-1}.

Thus, NO_2 is a good candidate for carrying out state-to-state studies of a chaotic molecular system embedded in He_n, inviting several questions: Will there be a correspondence between the respective line positions and intensities in the He_n and gas phase environments? What will be the shifts of the center frequencies relative to the gas phase values, and what is to be expected for the magnitudes and distributions of the

decay widths associated with deactivation by the helium? What are the implications for photochemical studies? And so on.

It will be shown below that absorption lines are readily identified and related to their gas phase counterparts. With the current, admittedly modest, signal-to-noise ratio (S/N), the spectra can be fitted surprisingly well by blue-shifting all of the gas phase R_0 line positions by 7 cm^{-1}, adding 7 cm^{-1} widths to all of the lines, and adjusting the peak intensities to fit the spectrum. Fits obtained by fine-tuning the individual shifts and widths indicate modest dispersions around the central values. It is suggested that the results can be understood by consideration of the couplings that arise from the He_n perturber acting on the states of NO_2.

4.2 Experimental results

Fig. 4.1a shows the experimental spectrum. The scan used a step size of 0.6 cm^{-1}, with a 0.08 cm^{-1} laser linewidth; 1000 points were recorded. This large step size was deemed appropriate after many scans over smaller frequency intervals, using smaller step sizes, revealed the large linewidths shown in Fig. 4.1a. Each point averages the results from 3000 laser pulses; approximately 50 h was required to record the spectrum. Fig. 4.1b shows the R_0 lines recorded by Georges et al. [10] by using LIF, and in Fig. 4.1c each of these lines has been assigned a 7 cm^{-1} width, the entire spectrum has been blue-shifted by 7 cm^{-1}, and the peak heights have been adjusted to fit the experimental spectrum. Fig. 4.1d shows an overlay of (a) and (c).

Varying all of the widths and center frequencies independently provides, of course, excellent fits. Though not unique, they indicate that the dispersions of the distributions of shifts and widths around their central values are modest. For example, 90% of the shifts and widths thus obtained lie within 2 cm^{-1} of the central values. More quantitative

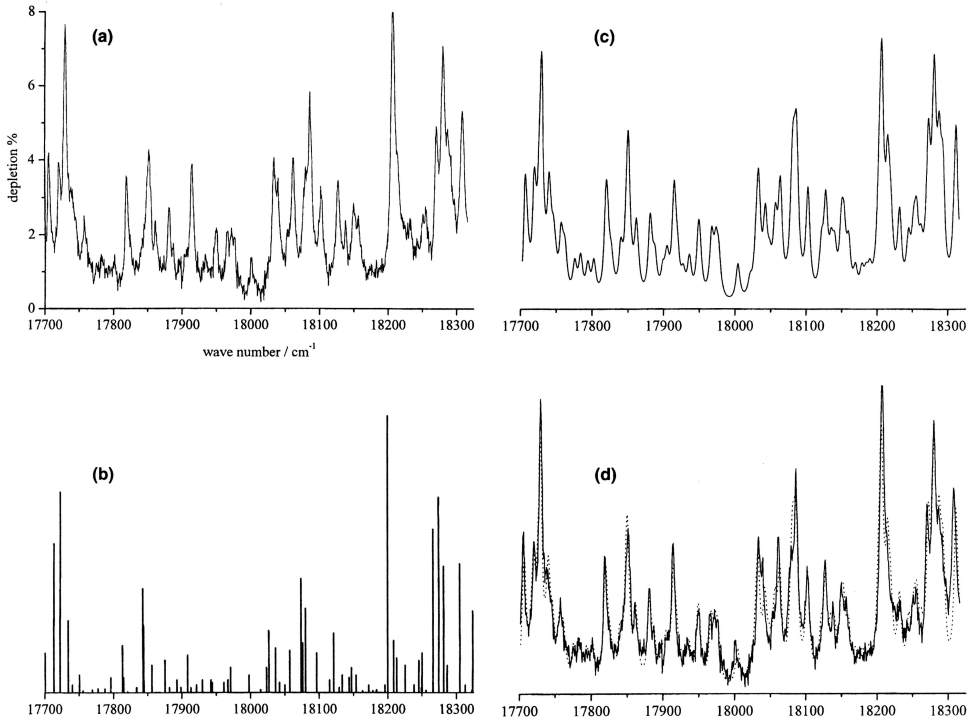

Figure 4.1: (a) Mass spectrometer depletion spectrum. (b) Frequencies and intensities of R_0 lines recorded by using LIF are taken from Georges et al. [10] (c) All of the lines in (b) have been assigned 7 cm^{-1} widths and blue-shifted by 7 cm^{-1}. The intensities are fitted to the experimental spectrum. (d) The experimental and simulated spectra are overlapped.

information about the dispersions will be forthcoming when higher quality spectra are available.

To our surprise, we were unable to find a literature report of a uv/visible spectrum of NO_2 recorded under matrix isolation conditions. Thus, an experiment was carried out in which Ne atoms were added to embedded NO_2. Even a single Ne atom obliterated the structure shown in Fig. 4.1, resulting in continuous absorption. This underscores the importance of the weak, homogeneous helium matrix.

4.3 Theoretical considerations

Hamiltonian of a quantum system composed of two weakly interacting subsystems A and B is given by:

$$\widehat{H}_{AB}(\mathbf{r}_A, \mathbf{r}_B) = \widehat{H}_A(\mathbf{r}_A) + \widehat{H}_B(\mathbf{r}_B) + \widehat{V}_{AB}(\mathbf{r}_A, \mathbf{r}_B) \tag{4.1}$$

where $\mathbf{r}_A$ and $\mathbf{r}_B$ are coordinates belonging to A and B; $\widehat{H}_A(\mathbf{r}_A)$, $\widehat{H}_B(\mathbf{r}_B)$ are the hamiltonians of the systems A and B in the absence of interaction, and $\widehat{V}_{AB}(\mathbf{r}_A, \mathbf{r}_B)$ is the operator describing the interaction. In some cases, $\widehat{V}_{AB}$ can be represented as a product of operators V_A and V_B acting in different spaces corresponded to the subsystems A and B:

$$\widehat{V}_{AB}(\mathbf{r}_A, \mathbf{r}_B) = V_0 \left(\widehat{V}_A(\mathbf{r}_A) \cdot \widehat{V}_B(\mathbf{r}_B) \right) \tag{4.2}$$

The matrix element of $\widehat{V}_{AB}(\mathbf{r}_A, \mathbf{r}_B)$ is then given by

$$V_{AB}^{(1,2)} = \langle \Psi_{AB}^{(1)} | \widehat{V}_{AB} | \Psi_{AB}^{(2)} \rangle = V_0 \langle \psi_A^{(1)} | \widehat{V}_A | \psi_A^{(2)} \rangle \langle \psi_B^{(1)} | \widehat{V}_B | \psi_B^{(2)} \rangle \tag{4.3}$$

In some situations, contribution of one of the subsystems (which will be called the primary subsystem) is more important. In this case the wavefunctions of the this primary subsystem appear explicitly in calculation of the matrix element while the contribution of the other subsystem is replaces with a constant or a smooth function of system parameters.

An example of such a situation is the interaction of an atom or a molecule with electromagnetic radiation. The probability of a transition between molecular states as a result of photoexcitation is given by the matrix element of the dipole momentum operator which is solely acting in space of molecular wavefunctions.

In the experiment described herein there are two experimental observables, the shifts and the broadenings of the spectral lines, that appears in result of interaction between the molecule and liquid helium. The shifts of the spectral lines reflect static properties of helium which are nearly the same for different excited states of the molecule. However, the properties of the molecular states are quite different. Thus, if we follow the philosophy described above is followed in consideration of the problem of the spectral line shifts, the primary subsystem in this case would be the molecule while the influence of the liquid helium is responsible for introducing some perturbation. The actual states of the helium subsystem are irrelevant.

The situation with spectral line broadening is quite different. It mostly reflects the dynamic properties of liquid helium environment. It will be discussed later in detail that the origin of the broadening is due to the shortening of the lifetime of an excited state due to deactivation of this state by liquid helium. This deactivation is accompanied with the excitation of a quasiparticle (or several of them) in the liquid helium. Apparently, the wavefunction corresponding to the excitation must explicitly appear in the equation for the broadening. At the same time, the molecular contribution to the transition matrix element should not change dramatically from state to state and in the first approximation can be represented as a smooth function of the initial and final energy of the molecule.

4.3.1 Spectral line shifts

Assume that the helium that surrounds embedded NO_2 acts as a perturbation to the gas phase molecule, and consider matrix elements that account for mixing, shifting, and deactivation of the NO_2 levels. Leaving aside rotation, which plays a secondary role,

each of the NO_2 vibronic levels can be expanded in a basis of the vibrational levels of the A^2B_2 excited and X^2A_1 ground PESs, with the αth wavefunction given by:

$$\psi^{\alpha}(\mathbf{r}_e, \mathbf{Q}) = \psi_e^A(\mathbf{r}_e) \sum_j C_j^{\alpha} \phi_j^A(\mathbf{Q}) + \psi_e^X(\mathbf{r}_e) \sum_k C_k^{\alpha} \phi_k^X(\mathbf{Q}) \tag{4.4}$$

where the summations, with indices j and k, are over the A^2B_2 and X^2A_1 vibrational levels, respectively; $\psi_e^A(\mathbf{r}_e)$ is the A^2B_2 electronic wave function; $\phi_j^A(\mathbf{Q})$ is the jth vibrational wavefunction of the A^2B_2 PES; and C_j^{α} is the expansion coefficient for the jth vibrational level of the A^2B_2 PES. Likewise, $\psi_e^X(\mathbf{r}_e)$ is the X^2A_1 electronic wavefunction, etc. The A^2B_2 part of ψ^{α} is much smaller than the X^2A_1 part, as is always the case for internal conversion [9].

Now consider perturbations of the NO_2 states, with explicit helium excitations suppressed; deactivation will be discussed below. The matrix elements of the perturbation brought about by the surrounding helium, V, is expressed as:

$$\begin{aligned} V_{\alpha\beta} = \Big\langle \sum_j C_j^{\alpha} \psi_e^A(\mathbf{r}_e) \phi_j^A(\mathbf{Q}) + \sum_k C_k^{\alpha} \psi_e^X(\mathbf{r}_e) \phi_k^X(\mathbf{Q}) | V | \\ \times \sum_{j'} C_{j'}^{\beta} \psi_e^A(\mathbf{r}_e) \phi_{j'}^A(\mathbf{Q}) + \sum_{k'} C_{k'}^{\beta} \psi_e^X(\mathbf{r}_e) \phi_{k'}^X(\mathbf{Q}) \Big\rangle \end{aligned} \tag{4.5}$$

The randomness of the expansion coefficients results in small off-diagonal matrix elements due to cancellation, upon summation, of terms with $\alpha \neq \beta$. The degree of cancellation depends on the extent to which the levels are thorough mixtures of a separable Hamiltonian basis [22]. For example, in the limit of complete cancellation, the surviving matrix elements are diagonal:

$$V_{\alpha\alpha} = \sum_j |C_j^{\alpha}|^2 V_{jj} + \sum_k |C_k^{\alpha}|^2 V_{kk} \tag{4.6}$$

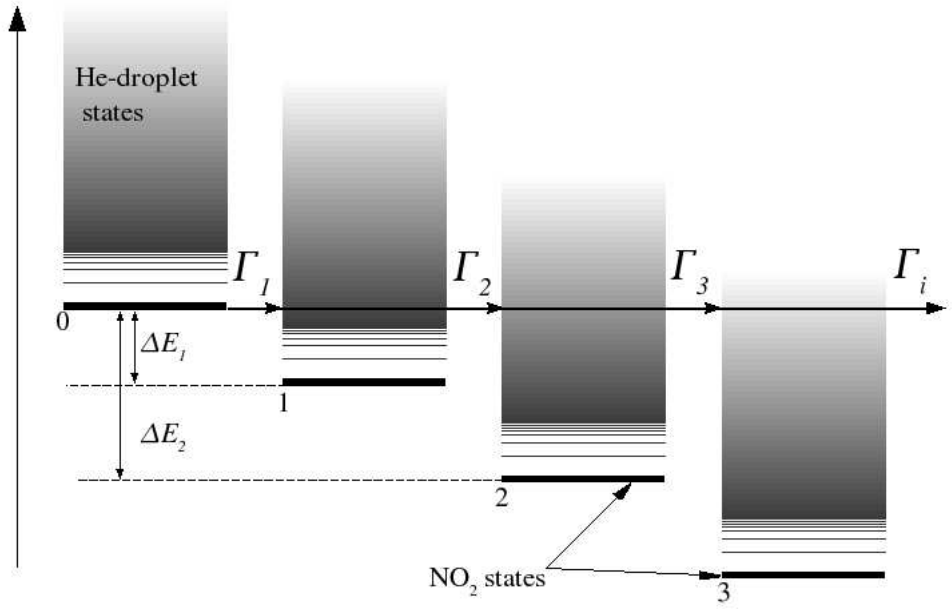

Figure 4.2: Collisional deactivation of NO_2 molecule by liquid helium environment

where $V_{jj} = \langle \phi_j^A | V | \phi_j^A \rangle$ and likewise for V_{kk}. It is assumed that V does not couple zeroth-order A^2B_2 and X^2A_1 levels. The V_{jj} and V_{kk} are the same for all of the ϕ^α; only the expansion coefficients change from one level to the next.

According to Eqs. (4.4), (4.5), and (4.6)) for a modest energy interval, such as the one studied here (17 700 - 18 300 cm^{-1}) the energy levels will all be shifted relative to their gas phase values by comparable amounts when the mixing is thorough. This differs from the regime of regular dynamics, where shifts are mode-specific. In other words, the chaotic nature of the ψ^α levels results in vibrational averaging that leads to modest dispersion about the mean of the distribution of shifts. A similar conclusion is reached with the widths: the randomness of the expansion coefficients results in the different ψ^α levels having comparable decay widths.

4.3.2 Spectral line widths

An excited NO_2 molecule being surrounded by liquid helium experiences collisions with helium atoms. In result of these collisions the excitation energy of the molecule is transfered to liquid helium. This leads to the shortening of the lifetime of the state originally excited and hence to the homogeneous broadening of spectral lines. As will be discussed in the next section, the shortening of the excited state lifetime due to its deactivation by liquid helium environment is the major origin of spectral line broadening in this case.

The deactivation scheme is shown in figure 4.2. Interaction between the molecule and the liquid helium environment causes the transition from the initially excited state to one of lower lying molecular state. This transition is accompanied by the excitation of the liquid helium around the molecule. Thus, the transition matrix element is given by:

$$V_{fi} = \langle \psi_i^{\mathrm{NO_2}}, \phi_0^{\mathrm{He}} | \widehat{V} | \psi_{\mathbf{q}}^{\mathrm{He}}, \psi_f^{\mathrm{NO_2}} \rangle \tag{4.7}$$

where $\psi_i^{\mathrm{NO_2}}$ and $\psi_f^{\mathrm{NO_2}}$ are wavefunctions of the initial states, prepared by photoexcitation, and the final states of the NO_2 molecule. ϕ_0^{He} and $\psi_{\mathbf{q}}^{\mathrm{He}}$ are wavefunctions of liquid helium before and after the deactivation event. Assume that before the deactivation of the molecule occurs, the liquid helium is in its ground state. Another assumption will be made make is that only one quasiparticle is excited in the transition.

In the spirit of the discussion in the beginning of this section, the molecular and helium contributions to the transition matrix element can be separated:

$$V_{fi} = V_0 \langle \psi_i^{\mathrm{NO_2}} | \widehat{V}_{\mathrm{NO_2}} | \psi_f^{\mathrm{NO_2}} \rangle \cdot \langle \phi_0^{\mathrm{He}} | \widehat{V}_{\mathrm{He}} | \psi_{\mathbf{q}}^{\mathrm{He}} \rangle \tag{4.8}$$

Assume that the major contribution is given by the helium part of the matrix element, while the molecular part can be represented as a smooth function of molecular energy.

To describe the process of deactivation the collisional energy transfer model discussed in the chapter 2 can be employed. According to the equation (2.63) the decay of the population of the initially excited state x_0 is given by:

$$\frac{dx_0(t)}{dt} = x_0(t) \sum_j R_{j0} = x_0(t) \int_0^{E_0} R(E, E_0) dE \tag{4.9}$$

Here all of the unimolecular reaction rate will be set to zero because only the stationary states of the molecule are considered. Another assumption is that the energy transfer proceeds only in one direction: from the upper states to the lower ones. Thus there is no gain of population of the initially excited state due to collisional energy transfer. The R_{j0} is the rate of the transition from the state $|0\rangle$ to the state $|j\rangle$. $R(E, E_0)$ is the energy tranfer rate of NO_2 molecule in liquid helium environment.

Previously, the shape of the energy transfer rate function $R(E_f, E_0)$ for the case of a particle moving through liquid helium was discussed. Deactivation of a molecule by liquid helium is a more complicated problem than the slowing of a moving particle and requires special consideration. However, it follows from this discussion that as long as the major contribution to the transition matrix element is given by transition between states of liquid helium, the energy transfer rate function $R(E_f, E_0)$ corresponding to the molecule and the function corresponding to a free particle discussed in the chapter 2 are proportional to each other with a factor given by a smooth function of energy. This factor would includes the ratio of density of states of NO_2 molecule equal to δE^{-1}, and the translational energy of states given by [1]:

$$\rho(E) = \frac{4}{h^3} \pi m^{3/2} (2E)^{1/2} V \tag{4.10}$$

This suggests that the energy transfer function for the molecule deactivation has the same major features:(i) it is equal to 0 at $\Delta E = E_i - E_f = 0$; (ii) it is reaching its

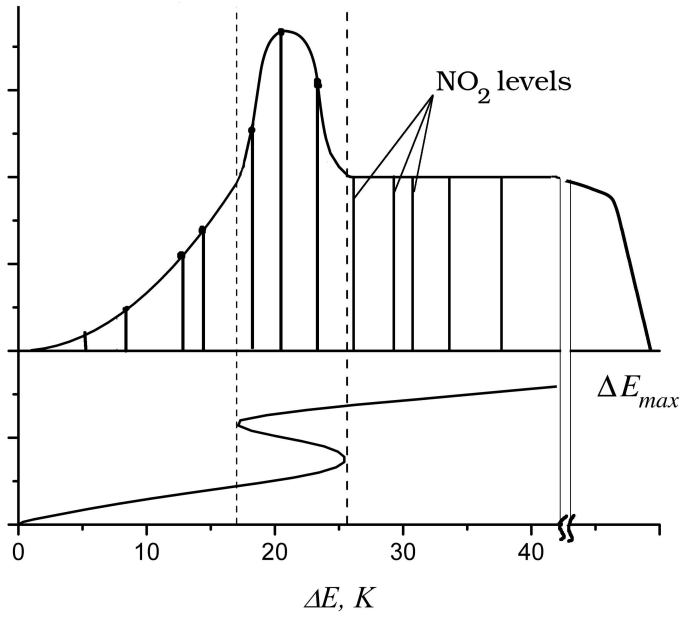

Figure 4.3: Calculation of the homogeneous spectral line broadening. The sketch of the energy transfer function for the molecule deactivation is shown in the upper part of the plot. Vertical lines represent NO_2 levels starting from the one that was initially excited. The spectral line width is given by the sum of the function values at the positions corresponded to NO_2 levels. The lower part of the plot shows the Feynman excitation spectrum of liquid helium.

maximum in the region $E_{\text{roton}} < \Delta E < E_{\text{maxon}}$; (iii) it is changing slowly with ΔE in the "independent particle" region of liquid helium; (iv) it is equal to zero for the $\Delta E \geqslant E_{\text{max}}$ and E_{max} is a function of masses of the atoms in the molecule. The sketch of such a function is shown in the figure 4.3. The solid line in the lower part of the plot represents the Feynman energy spectrum of liquid helium. Vertical lines show the position of NO_2 levels starting from the initially excited level.

The spectral line broadening is proportional to the sum of the energy transfer rate function at positions corresponding to the position of NO_2 states. To calculate the line

broadening of the adjacent line, we have to shift all the states by one. Apparantly, it does not change the result of summation. This provides an explanation for the experimental observation where all of the spectral lines observed have the same width.

The spectrum discussed herein is taken in the region from 565 nm to 545 nm. However, NO_2 exhibit an absorption spectrum over the entire visible region. It is interesting to see how the line broadening change with wavelength over a wider region. The line broadening is proportional to the density of states of the molecule. It is known that the density of states grows with excitation energy [10]. This suggests that the spectal line width would grow as the excitation wavelength becomes shorter.

The energy level separation at the excitation enegy range explored in the experiment described herein is about 10 cm^{-1}. This value is slightly greater than that required to map the feature of the energy transfer rate function corresponded to the maxon-roton region of the liquid helium excitation spectrum. In the spectrum taken at shorter wavelengths the energy separation becomes smaller, and the liquid helium excitations in the maxon-roton region should be able to participate in the deactivaction process. This would lead to some increase of the line broadening that would be noticable on the graph of the broadening as a function of excitation energy.

It is noteworthy, that the presence of ^3He atoms in the liquid helium would add a quadratic branch to the structure function and also change the energy transfer rate function. It would leadr to the further broadening of spectral lines. Thus, measuring a depletion spectrum of NO_2 embedded in liqud helium droplet doped with ^3He atoms could also be considered as an interesting experiment.

4.4 Discussion

A noteworthy aspect of the spectrum presented here is that the shifts and widths do not differ significantly from line to line. Namely, the region 17 700-18 300 cm^{-1} can be fitted reasonably well by using the gas phase line positions and a 7 cm^{-1} blue-shift and a 7 cm^{-1} width. Because intramolecular coupling in NO_2 is strong, whereas the coupling of NO_2 to the helium is relatively weak, the shifts and widths can be understood on the basis of the model described by Eqs. (4.4),(4.5) and (4.6). In this section, we: (i) argue against effects other than relaxation as the main origin of the widths; (ii) point out an important earlier paper that is germane to the work discussed here; and (iii) comment on the mechanism and model.

4.4.1 Origin of the widths

The saturation of allowed electric dipole transitions of gaseous molecular absorbers is encountered frequently in experiments that use pulsed laser radiation [7]. Because of the large laser energies used here (i.e., 40 mJ), effects that might accompany efficient optical excitation must be considered. Specifically, can they account for widths of $\sim$7 cm^{-1}?

A useful figure-of-merit is the product $\sigma_{\rm abs}\Phi$, where $\sigma_{\rm abs}$ is the photon absorption cross section and is the fluence Saturation occurs when $\sigma_{\rm abs}\Phi$ is comparable to or exceeds unity. For example, with $\sigma_{\rm abs} \sim 10^{-19}{\rm cm}^2$, which is characteristic of gas phase NO_2 transitions $\Phi \sim 10^{19}$ photons$cdot$cm^{-1} will result in saturation. Absorption cross-sections of gaseous species are usually reported as empirical parameters that are valid for a given instrumental resolution, often with a measurement linewidth that exceeds the linewidth of the absorber. The estimate of $\sigma_{\rm abs} \sim 10^{-19}{\rm cm}^2$ is conservative in light of the fact that our 0.08 cm^{-1} laser linewidth is significantly larger than the

widths due to spontaneous emission and Doppler broadening. Because the pulses used in our experiment contain approximately 10^{17} photons, saturation should be considered for laser beam diameters comparable to, and smaller than, $\sim$1 mm, which occurs in the focal region (Fig. 1).

Saturation broadening of NO_2 transitions cannot, by itself, be responsible for the linewidths, because this would require abs values of $\sim 10^4$ [8] which is unreasonably large. For example, for a $\sigma_{\mathrm{abs}}\Phi$ value of $\sim 10^{-19}\mathrm{cm}^2$, would have to be $\sim 10^{23}$ photons$\cdot$ cm^{-2}, and beam diameters smaller than $\sim$10 m would be required. Even then, saturation would occur only over a small fraction of the region where the laser and molecular beams overlap, i.e., near the focal region indicated in Fig. 1.

Photoexcitation followed by relaxation heats the cluster, resulting in evaporation, with the cluster temperature in excess of 0.37 K for the remainder of the laser pulse, as demonstrated by Vilesov and co-workers [17]. For large clusters, the mass spectrometer ionization cross-section is proportional to the geometric cross-section [21] which varies as $n^{2/3}$. In this regime, the one-photon depletion signal for a given cluster size is given by:

$$I_{\mathrm{depl}} = 1 - \left[1 - \frac{3600}{n}\right]^{2/3}, n < 3600 \tag{4.11a}$$

$$= 1, n \leqslant 3600 \tag{4.11b}$$

where it is assumed that the absorption of an 18 000 cm^{-1} photon results in the evaporation of 3600 He atoms. Eqs. ((4.11a) and (4.11b)) must be averaged over the distribution of n values, corrected for the fraction of the molecular beam that is overlapped by the laser beam (including its radial intensity dependence), and multiplied by the fraction of the embedded NO_2 molecules that absorb a photon. Note that absorption of the second,

third, etc. photons takes place with a higher He_n temperature and the NO_2 not necessarily in its ground state, and results in the evaporation of most of the helium. The resulting lineshapes may differ from those of one-photon excitation, i.e., they are expected to be slightly narrower than for the one-photon case.

Two additional observations argue against $\mathrm{A}^2\mathrm{B}_2 \leftarrow \mathrm{X}^2\mathrm{A}_1$ saturation playing an important role. First, saturated transitions would yield comparable intensities for all lines. This is not what is observed; there is an order of magnitude difference between the strong and weak lines in the spectrum shown in Fig. 4.1. Second, we have recorded a linear fluence dependence of the depletion signal, as shown in Fig. 4.4. Thus, it is concluded that the large widths are not the result of $\mathrm{A}^2\mathrm{B}_2 \leftarrow \mathrm{X}^2\mathrm{A}_1$ saturation. Broadening due to excited state absorption has been reported for gas phase NO_2 [3]. Again, we argue that the large observed widths cannot be attributed solely to this effect, because $\sigma_{\mathrm{abs}}\Phi$ values of $\sim 10^4$ would be required.

Transitions originating from the lowest few rotational levels are contained in a narrow band of frequencies for each vibronic transition. For example, the rotational widths for a number of molecules embedded in He_n (SF_6, OCS, NCCCH, propyne, trifluoropropyne, tert-butyl-acetylene, etc.) are < 1 cm^{-1} [15, 13, 4, 19]. Only $\Delta K = \pm 1$ transitions with large A rotational constants display large widths [25] Thus, we believe that rotations do not account for the large widths reported here. Finally, we note that inhomogeneous broadening is insignificant for the cluster sizes and widths reported here.

4.4.2 The He-NO_2 binary complex

In 1976, Smalley et al. [29] recorded spectra of the He-NO_2 binary complex, and noted that the frequencies were blue-shifted by approximately 1.5 cm^{-1} relative to those of

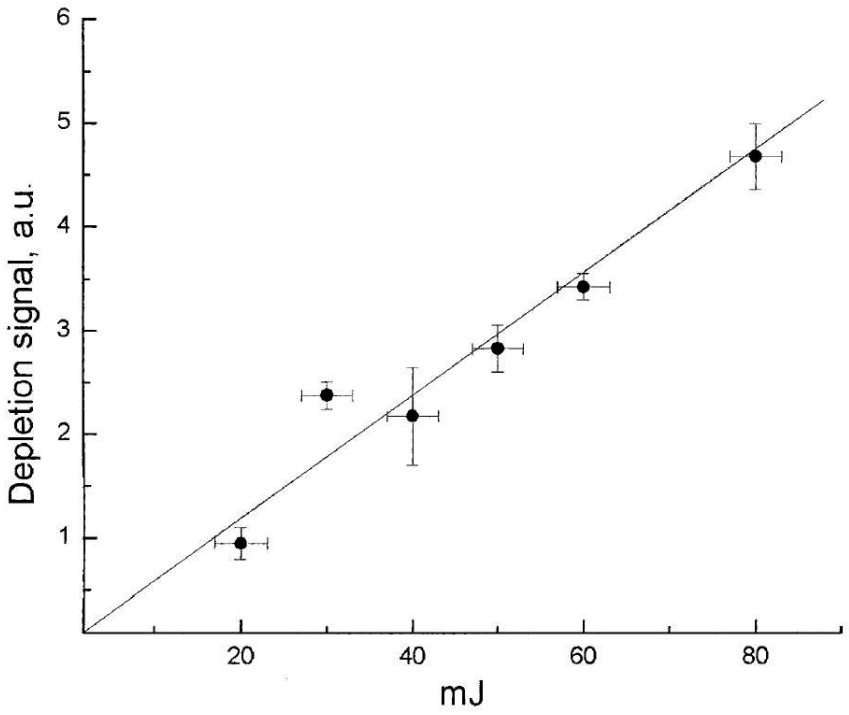

Figure 4.4: The depletion signal versus laser fluence can be fitted with a straight line.

uncomplexed NO_2 for all of the vibronic bands examined. In addition, widths of approximately 0.8 cm^{-1} (due to dissociation of the complex) were noted for all of the He-NO_2 bands examined.

The origin of these constancies can now be understood as being due to the quantum chaotic nature of the vibronic eigenstates. The number of helium atoms attached to the NO_2 chromophore does not affect this conclusion. It is reasonable to assume that the first shell of He atoms around the NO_2 increases the shifts and widths, and in this sense our results are in accord with this earlier work, though the two sets of experiments were carried out under quite different conditions.

4.4.3 Mechanism and model

The vibrational relaxation of polyatomic molecules in the regime of regular intramolecular dynamics is known to be mode-specific. Likewise, the predissociation of weakly bound complexes is also known to be mode-specific. The work presented here deals with vibronic levels that each contain numerous combinations of vibrational modes. The fact that the widths and shifts do not vary significantly from one level to the next is consistent with the levels having little mode specific character. Though the origin of this propensity is conceptually straightforward, we cannot yet predict the magnitudes of the widths and shifts, nor their distributions, i.e., dispersions about their mean values.

In bulk liquid helium at 0.37 K, the superfluid fraction is $\rho_s/[\rho_n+\rho_s] = 0.99995$ [27]. Likewise, in 0.37 K He_n droplets having $\langle n \rangle = 9000$, there will be little normal fluid. With an embedded dopant, there is a boundary between the helium atoms adjacent to the dopant and the surrounding superfluid. The relaxation of NO_2 vibronic levels on a picosecond timescale involves mainly the helium atoms adjacent to the NO_2. This follows from the fact that picosecond relaxation times are too short for an excitation to appear in the superfluid. Namely, the NO_2-superfluid distance is $\sim 5\mathring{A}$, which is too large to be accessed in a picosecond, given that the speed of sound in helium is 200 m/s. Thus, relaxation creates particle-like excitations of the helium atoms that lie immediately adjacent to the NO_2. This is akin to predissociation of a van der Waals complex. The number of lower NO_2 levels thus created, as well as the overall relaxation mechanism as the NO_2 returns to its ground state, are unknown, but will hopefully be figured out in due course.

The proposed model enables some predictions to be made: (i) Photoinitiated unimolecular reactions will be quenched near their gas phase thresholds, because reaction rates must be at least comparable to deactivation rates if there is to be appreciable reaction. (ii) With NO_2, spectra will show (congested) structure at energies up to 25 000

cm^{-1} (for gas phase NO_2, $D_0 = 25128.5\mathrm{cm}^{-1}$ [18]). (iii) Unlike the gas phase, as D_0 is approached from below, the molecular phase space will not increase along the NO_2 reaction coordinate, because a "helium blockade" will deny access to the large-r region of the molecular phase space.

Reference List

[1] Tomas Baer and William L. Hase. *Unimolecular Reaction Dynamics: Theory and Experiments*. Oxford University Press, New York, 1996.

[2] A. Bartelt, J. D. Close, F. Federmann, N. Quaas, and J. P. Toennies. Cold metal clusters: Helium droplets as a nanoscale cryostat. *Physical Review Letters*, 77(17):3525–3528, 1996.

[3] Laurence Bigio and Edward R. Grant. Intramolecular dynamics and multiresonant absorption spectroscopy. I reduced non-franck-condon intensity in the high-power two-photon absorption spectrum of NO_2. *The Journal of Chemical Physics*, 83(11):5361–5368, 1985.

[4] C. Callegari, A. Conjusteau, I. Reinhard, K. K. Lehmann, and G. Scoles. First overtone helium nanodroplet isolation spectroscopy of molecules bearing the acetylenic CH chromophore. *The Journal of Chemical Physics*, 113(23):10535–10550, 2000.

[5] Carlo Callegari, Kevin K. Lehmann, Roman Schmied, and Giacinto Scoles. Helium nanodroplet isolation rovibrational spectroscopy: Methods and recent results. *The Journal of Chemical Physics*, 115(22):10090–10110, 2001.

[6] A. Delon, R. Jost, and M. Lombardi. NO_2 jet cooled visible excitation spectrum: Vibronic chaos induced by the $\widetilde{X}^2A_1 - \widetilde{A}^2B_2$ interaction. *The Journal of Chemical Physics*, 95(8):5701–5718, 1991.

[7] Antoine Delon, Remy Jost, and Marcel Jacon. Laser induced dispersed fluorescence spectroscopy of 107 vibronic levels of NO_2 ranging from 12 000 to 17 600 cm^{-1}. *The Journal of Chemical Physics*, 114(1):331–344, 2001.

[8] Demtröder. *Laser Spectroscopy*. Springer, Berlin, 1998.

[9] V. I. Osherov E. S. Medvedev. *Radiationless Transitions in Polyatomic Molecules*. Springer, Berlin, 1995.

[10] Robert Georges, Antoine Delon, and Remy Jost. The visible excitation spectrum of jet cooled NO_2: The chaotic behavior of a set of $^2B_2$ vibronic levels. *The Journal of Chemical Physics*, 103(5):1732–1747, 1995.

[11] S. Grebenev, M. Havenith, F. Madeja, J. P. Toennies, and A. F. Vilesov. Microwave-infrared double resonance spectroscopy of an OCS molecule inside a ^{4}He droplet. *The Journal of Chemical Physics*, 113(20):9060–9066, 2000.

[12] Slava Grebenev, Matthias Hartmann, Martina Havenith, Boris Sartakov, J. Peter Toennies, and Andrei F. Vilesov. The rotational spectrum of single OCS molecules in liquid ^{4}He droplets. *The Journal of Chemical Physics*, 112(10):4485–4495, 2000.

[13] Slava Grebenev, J. Peter Toennies, and Andrei F. Vilesov. Superfluidity Within a Small Helium-4 Cluster: The Microscopic Andronikashvili Experiment. *Science*, 279(5359):2083–2086, 1998.

[14] M. Hartmann, F. Mielke, J. P. Toennies, A. F. Vilesov, and G. Benedek. Direct spectroscopic observation of elementary excitations in superfluid He droplets. *Physical Review Letters*, 76(24):4560–4563, 1996.

[15] M. Hartmann, R. E. Miller, J. P. Toennies, and A. Vilesov. Rotationally resolved spectroscopy of SF_6 in liquid helium clusters: A molecular probe of cluster temperature. *Physical Review Letters*, 75(8):1566–1569, 1995.

[16] Toennies J.P. Hartmann M., Lindinger A. and Vilesov A.F. Laser-induced fluorescence spectroscopy of van der waals complexes of tetracene-Ar_N ($N \leqslant 5$) and pentacene-Ar within ultracold liquid He droplets. *Chemical Physics*, 239(1-3):139–149, December 1998.

[17] Toennies J.P. Hartmann M., Lindinger A. and Vilesov A.F. Hole-burning studies of the splitting in the ground and excited vibronic states of tetracene in helium droplets. *Journal of Physical Chemistry*, 105(26):6369–6377, 2001.

[18] Remy Jost, Jesper Nygrd, Adam Pasinski, and Antoine Delon. The photodissociation threshold of NO_2: Precise determination of its energy and density of states. *The Journal of Chemical Physics*, 105(3):1287–1290, 1996.

[19] D. T. Moore K. Nauta and R. E. Miller. Molecular orientation in superfluid liquid helium droplets: high resolution infrared spectroscopy as a probe of solvent-solute interactions. *Faraday Discuss*, 113:261 – 278, 1999.

[20] Bernd Kirmse, Antoine Delon, and Remy Jost. The NO_2 vibronic levels near the $X^2A_1 - A^2B_2$ conical intersection observed by laser induced dispersed fluorescence. *The Journal of Chemical Physics*, 108(16):6638–6651, 1998.

[21] B. Schilling M. Lewerenz and J. P. Toennies. A new scattering deflection method for determining and selecting the sizes of large liquid clusters of ^{4}He. *M. Lewerenz, B. Schilling and J. P. Toennies*, 206(1-4):381–387, April 1993.

[22] Madan Lal Mehta. *Random matrices*. Academic Press Inc., Boston, MA, second edition, 1991.

[23] K. Nauta and R. E. Miller. Solvent mediated vibrational relaxation: Superfluid helium droplet spectroscopy of HCN dimer. *The Journal of Chemical Physics*, 111(8):3426–3433, 1999.

[24] K. Nauta and R. E. Miller. Stark spectroscopy of polar molecules solvated in liquid helium droplets. *Physical Review Letters*, 82(22):4480–4483, 1999.

[25] K. Nauta and R. E. Miller. The hydrogen fluoride dimer in liquid helium: A prototype system for studying solvent effects on hydrogen bonding. *The Journal of Chemical Physics*, 113(22):10158–10168, 2000.

[26] J. H. Reho, J. Higgins, M. Nooijen, K. K. Lehmann, G. Scoles, and M. Gutowski. Photoinduced nonadiabatic dynamics in quartet Na_3 and K_3 formed using helium nanodroplet isolation. *The Journal of Chemical Physics*, 115(22):10265–10274, 2001.

[27] Steven W. Van Sciver. *Helium Cryogenics*. International Cryogenics Monograph Series. Plenum Press, 1986.

[28] Alkwin Slenczka, Bernhard Dick, Matthias Hartmann, and J. Peter Toennies. Inhomogeneous broadening of the zero phonon line of phthalocyanine in superfluid helium droplets. *The Journal of Chemical Physics*, 115(22):10199–10205, 2001.

[29] R. E. Smalley, L. Wharton, and D. H. Levy. The fluorescence excitation spectrum of the $HeNO_2$ van der waals complex. *The Journal of Chemical Physics*, 66(6):2750–2751, 1977.

[30] Frank Stienkemeier and Andrey F. Vilesov. Electronic spectroscopy in He droplets. *The Journal of Chemical Physics*, 115(22):10119–10137, 2001.

[31] J. Peter Toennies, Andrej F. Vilesov, and K. Birgitta Whaley. Superfluid helium droplets: An ultracold nanolaboratory. *Physics Today*, 54(2):31–37, 2001.

[32] Vilesov Andrei F. Toennies J. Peter. Spectroscopy of atoms and molecules in liquid helium. *Annual Review of Physical Chemistry*, 49(1):1–41, 1998.

Chapter 5

Mass-depletion spectroscopy of NO_2 in helium droplets above its gas phase dissociation threshold

5.1 Introduction

The photophysics and photochemistry of molecules and clusters embedded in/on superfluid helium nanodroplets continues to receive a great deal of attention. These droplets, hereafter denoted He_n, where n is the number of helium atoms in the droplet, are said to provide ideal matrixes for isolating molecules and small aggregates and studying a broad range of fundamental interactions [18, 19, 10, 7, 14].The interactions can be intramolecular within a single dopant molecule, intermolecular between dopant species (e.g., molecule-molecule, molecule-atom), between one or more dopant species and the helium host, or combinations of the above.

The He_n droplets act as benign matrixes in many respects. They are composed of a 0.4 K superfluid quantum liquid that resides in essentially its ground state. For doped clusters in their native states, the dopant-host interactions are among the weakest in nature. Thus, for many purposes, there can be no better-characterized matrix host than superfluid helium droplets.

Photoexcitation of the dopant can alter dramatically this tranquil situation by introducing strong interactions. For example, the electrophobic nature of helium wreaks

havoc with excitations that transfer electron density toward the outer reaches of the chromophore, in effect expanding its size and leading to large blue shifts in ultraviolet absorption spectra [18].Moreover, vigorous and complex intramolecular vibrational dynamics and their associated dopant-host interactions do not perceive of the host as being merely a quiescent fluid. Rather, in this case, the helium responds as an ensemble of particles, akin to a dense gas, and average line widths of $\sim$ 7 cm^{-1} fwhm have been recorded in absorption spectra of NO_2 embedded in He_n as we discussed it in the previous chapter.

In the quantum liquid, these line widths are homogeneous, so they correspond to subpicosecond deactivation times, which is hardly a small effect. These studies were carried out in the energy range 17700-18300 cm^{-1}, where it is known that strong nonadiabatic interaction via conical intersection of the and $\widetilde{A}$ adiabats yields manifolds of A_1 and B_2 vibronic symmetries, each of which can be said to be quantum chaotic [6, 5]. This spectrum is shown in the figure 4.1

It is not difficult to appreciate that vibrational relaxation in the regime of quantum chaos can be efficient. Sensitivity to initial conditions and the associated divergence of nearby trajectories-a signature effect in chaotic classical systems-suggests a sensitivity to perturbation that is manifest as efficient relaxation of resolved levels of quantum-chaotic manifolds. This scenario differs qualitatively from that of low-lying vibrational levels, such as one or two quanta of a normal or local mode. These cases are usually characterized by relatively slow vibrational relaxation, as evidenced, for example, by narrow spectral line widths. [3]

Referring to figure 4.1, though the broad line widths indicate efficient relaxation, the average amounts of energy lost by each of the levels is unknown. We believe that there is no mode specificity. In the regime of quantum chaos, the levels can be described

as random mixtures of any vibrational basis that is derived from a separable Hamiltonian, and perturbation by the helium transfers excitation among such levels with good efficiency, in accord with the sensitivity to perturbation in the regime of quantum chaos.

It is not surprising that the spectrum shown in figure 4.1 can be fit reasonably well by using a width of 7 cm^{-1} for each of the levels, as well as a shift to higher energies of 7 cm^{-1} for each of the levels. Namely, the randomness mentioned above results in each of the widths having roughly the same value, and likewise for the shifts. As the energy is increased from $\sim$18 000 cm^{-1} to the gas-phase photodissociation threshold, $D_0 = 25128.5\ cm^{-1}$, [9]the density of states increases and the intramolecular dynamics become more vigorous. Thus, spectral congestion is inevitable.

The general scientific issue of photoinitiated unimolecular decomposition in He_n nanodroplets remains open. The physical content of this dissociation mechanism differs qualitatively from that of direct photodissociation. With direct photodissociation, fragments are thrust apart forcefully on a short time scale (typically $<$100 fs), and a high percentage of the available energy appears as interfragment exit channel repulsion along the reaction coordinate. This has been examined recently for CH_3I in He_n by Drabbels. [2] He reports that both CH_3 and $I(^2P_{3/2})$ enter the gas phase following the photodissociation of CH_3I embedded in He_n, with the iodine atom being caged more effectively than the CH_3. Along similar lines, Kanaev et al. have excited H_2O in He_n at short wavelengths (40-140 nm). [11] They report fluorescence from several electronically excited dissociation products, and they note that ionization is suppressed relative to dissociation, which is not surprising, given that the electron must be ejected through a sea of helium.

In contrast to direct photodissociation, in the case of unimolecular decomposition, the molecule's intramolecular vibrational dynamics ensue prior to dissociation, and this

excitation can be coupled strongly to the host medium. This presents an obvious question: given the competition between vibrational relaxation and unimolecular decomposition, what are their respective efficacies, and how does dissociation, if it occurs at all, vary with energy?

In the experiments described below, we have examined the photoexcitation, in He_n droplets, of an embedded molecule that is known to undergo photoinitiated unimolecular decomposition in the gas phase over a broad range of photon energies, namely, NO_2. The NO_2 molecule is an especially attractive candidate for such a study because it places at our disposal a wealth of knowledge about its gas-phase photochemistry, as well as its relaxation in He_n in the regime of vibronic chaos. [1]

In addition, it provides access to the largest possible gas-phase reaction rate coefficients that are consistent with a unimolecular decomposition mechanism, i.e., $k_{\rm uni}$ values as high as $\sim 5 \times 10^{12}{\rm s}^{-1}$. [8] With larger rate coefficients, it is unreasonable to assume that intramolecular vibrational redistribution (IVR) proceeds much more rapidly than reaction-an assumption that is a basic tenet of the theory of unimolecular decomposition. With rate coefficients as large as$\sim 5 \times 10^{12}{\rm s}^{-1}$, if unimolecular decomposition cannot win the competition against vibrational relaxation, it never will.

The He_n droplets are sufficiently small (i.e., $\langle n \rangle \sim 10000$) [13] that we must consider the possibility that one (or even both) of the fragments exits its droplet, because the momentum it receives via dissociation has not been fully dissipated when it reaches the surface. For this to happen with droplets that consist of several thousand helium atoms, the fragment must, on average, make its way past at least half a dozen helium atoms to get to the surface, and then pass from there into the gas phase. This is not easy. After its formation, the fragment will knock about in the helium, progressively losing memory of its original momentum direction. If it fails to reach the surface with translational energy in excess of its solvation energy, it is trapped, never to leave the droplet.

This leads us to the central issue addressed in the work reported here. Do fragments, in fact, leave their droplets, and if so, to what extent and retaining how much internal excitation and in which forms? Photoexcitation is carried out by using photon energies that range from the gas-phase dissociation threshold, D_0, to approximately $D_0 + 4300$ cm^{-1} (where $k_{\rm uni}$ is $\sim 5 \times 10^{12}$s^{-1} for gas-phase NO_2). D_0 is chosen as a reference energy, even though we know that dissociation will not occur for photon energies at, or just above, D_0 when NO_2 is embedded in He_n.

Photoinitiated unimolecular decomposition is, notwithstanding a few details, a well-understood phenomenon for gas-phase molecules. When molecules embedded in He_n are considered, however, it becomes complex. In contrast to direct photodissociation, which occurs rapidly and with considerable interfragment repulsion, the dissociation mechanism itself, even the issue of what constitutes dissociation, is intimately related to interactions of the molecular system with its helium environment. The most obvious example is the competition between vibrational relaxation and unimolecular decomposition, and even here the matter is subtle.

When there is no barrier along the reaction coordinate for the gas-phase counterpart, it is hard to define the point at which reaction has taken place in He_n [17].For example, with NO_2, if the O-NO distance reaches, e.g., 6 Å, does that mean that reaction has occurred? In the gas phase, the answer is, except barely above threshold, where the interfragment de Broglie wavelength is huge, an unequivocal yes. At 6 Å, the system has evolved to the product side of the transition state.

In He_n, however, the fragments may never get further apart than 6 Å, e.g., if the attractive interaction between them at 6 Å exceeds the amount of translational energy that remains after they have been slowed by their helium environment. In fact, if the fragments do not exit their cluster, it is inevitable that they will recombine, forming

ground-state NO_2 or, conceivably, a metastable form that corresponds to a local minimum on the potential surface. They have no alternative; their mutual attraction, though small at large distances, overcomes their solvation energies in the liquid. Moreover, in many cases the "fragments" will not even get sufficiently far apart before their momentum is dissipated to justify calling them fragments. In consideration of the above, we believe that there can be no well-defined reaction threshold for a system whose gas-phase counterpart is unimolecular decomposition via a loose transition state.

On the other hand, a system having a significant exit channel barrier (in addition to the reaction exoergicity) will behave differently. In this case, the transition state lies near the exit barrier and it is relatively well-defined. Past this barrier, products are accelerated and they encounter the helium with momentum gained past the barrier, which can be significant. This increases the probability of products escaping from the cluster. Most importantly, they cannot recombine except to form weakly bound van der Waals species, so even if they fail to enter the gas phase, there can be a drop in the mass spectrometer depletion signal. Ultimately, it will be interesting to compare these two kinds of unimolecular reaction. Here, we examine the He_n analogue of the barrierless gas-phase reaction.

5.2 Results and Discussion

The data presented in Figure 5.1a for $m/z = 8$ (i.e., monitoring He_2^+) indicate that there is no significant change in the depletion of the $m/z = 8$ signal as the photon energy is varied throughout its tuning range. The He_2^+ ion arises from electron impact ionization of clusters, regardless of the nature of the embedded species they contain. For clusters that contain NO_2, photoexcitation of the embedded NO_2 yields depletion signals, as discussed in the previous section. The size of the depletion signal (i.e., $\sim$7% throughout

the tuning range, see Figure 5.1a) is consistent with the degree of doping (∼26% of the He_n clusters contain a single NO_2 molecule) and efficient photoexcitation, which is achieved by using high-energy laser pulses. A photon energy of 25 000 cm^{-1} is sufficient to evaporate approximately 5000 helium atoms. For $h\nu < D_0$, the photoexcited molecules relax to the ground state, and therefore the full photon energy is available for the evaporation of helium atoms.

When a large fraction of the photon energy is needed to break a bond, there is relatively little energy left for the evaporation of helium atoms. However, even if fragments are produced within a droplet, if they recombine, there is no net reaction. Consequently, the full photon energy goes into heat, and the amount of evaporation is large, i.e., it is essentially identical to that which would occur without fragmentation.

The situation is quite different if one (or both) of the photofragments leaves the cluster. In this case, the depletion signal will be relatively small because most of the photon energy is used to break the bond, which remains broken. Thus, the constancy of the percent depletion throughout the range 24900-29400 cm^{-1} indicates that there is little, if any, net reaction over this energy range. The photon energy goes into the evaporation of helium, and it brings about no chemical change.

Let us now consider the case of $m/z = 46$ (i.e., monitoring NO_2^+) shown in Figure 5.1b. The percent depletion is larger than that obtained by monitoring $m/z = 8$ (i.e., ∼18% versus ∼7%, as shown in Figure 5.1b,a, respectively), in large part because the mass spectrometer signals at $m/z = 8$ contain significant contributions from clusters that contain no NO_2, and which therefore cannot contribute to the depletion signal. For cases in which dissociation results in one or both fragments leaving the droplet, the NO_2^+ mass spectrometer signal vanishes, yielding the largest possible depletion signal. If neither fragment leaves the droplet, the NO_2^+ mass spectrometer signal diminishes significantly-but it does not vanish-because all of the photon energy contributes to

shrinkage of the droplet. For a cluster containing 10000 helium atoms, the number of helium atoms that evaporate for photon energies in the range 24900-29400 is roughly 5000-6000, and the cross sectional area is reduced to ∼60% of its original value. Thus, the data shown in Figure 5.1b-namely, the fact that there is no discernible change over the photon energy tuning range-indicate that fragments do not leave their cluster to any significant degree. This is consistent with the data shown in Figure 5.1a.

Figure 5.1c shows the variation of the mass spectrometer depletion signal obtained at $m/z = 30$ (i.e., monitoring NO^+). If dissociation causes an oxygen atom to leave the cluster, with NO remaining in the cluster, the depletion signal will diminish but only slightly. If, on the other hand, NO leaves the cluster, either by itself or with a modest number of helium atoms attached, the amount of depletion will be significant. Because the oxygen atom receives 65% of the center-of-mass translational energy, and because it is smaller than NO, it will have an easier time exiting the cluster than would NO. Consequently, the $m/z = 30$ signal will increase, because shrinkage of the cluster is modest, whereas NO^+ is now a primary ion, rather than a daughter ion that derives from NO_2. The constancy observed in Figure 5.1c therefore is consistent with there being no net reaction, in accord with the other data. The signal at $m/z = 30$ contains contributions from the wings of the strong peaks at $m/z = 28$ (N_2^+) and $m/z = 32$ (O_2^+); this is why depletion at $m/z = 30$ is less than that at $m/z = 46$.

The data presented in the previous section show that, to within the experimental uncertainty, there is no net photoinitiated reaction over the 4300 cm^{-1} energy range that extends upward from D_0. The experiments do not provide direct information about the intracluster dynamics of photoexcited NO_2 interacting with its environment. They do, however, show that fragments do not, to any significant extent, leave the He_n clusters and pass into the gas phase. Nor do the fragments reunite to an appreciable extent in the

form of metastable species-akin to the phenomenon that occurs with molecules such as HCN, which forms linear chains in preference to lower energy structures [15].

The failure of this system to react in the energy region just above D_0 has been reported by Lehmann and co-workers, [12] who examined energies as high as several hundred cm^{-1} above D_0. At these energies, $k_{\rm uni}$ values are $5 \times 10^{11}{\rm s}^{-1}$ [8, 4].On the basis of the broad line widths seen in Figure **??** (which were not available at the time of the measurements of Lehmann and co-workers), it is clear that reaction in this energy regime is unlikely, as $k_{\rm uni}$ is at least several times smaller than the deactivation rates. Even if the average energy that is lost upon the deactivation of a given level is modest, $k_{\rm uni}$ drops from $4 \times 10^{11}{\rm s}^{-1}$ at $E - D_0 = 200$ cm^{-1} to $< 10^{11}{\rm s}^{-1}$ just above D_0, making reaction progressively less likely as E decreases.

Most importantly, at these small energies in excess of D_0, fragments cannot escape the immediate confines afforded by the surrounding helium, and net reaction is out of the question. The fact that the formation of a metastable NO-O species does not occur to an appreciable extent is consistent with our understanding of NO_2 intramolecular dynamics near D_0, because the long-range potential supports NO rotation relative to the oxygen atom, as evidenced by the efficient production of low NO rotational levels just above D_0, in accord with statistical theory [17, 16].

In the current study, the energy in excess of D_0 has been varied from zero to 4300 cm^{-1}. At the upper end of this range, $k_{\rm uni}$ is $\sim 5 \times 10^{12}$ s^{-1}, which is as large a rate coefficient as is possible for a system that reacts via a unimolecular decomposition mechanism. Consequently, NO_2 serves as a benchmark example of the photoexcitation of an embedded small polyatomic whose gas-phase counterpart undergoes a barrierless reaction. Its rate coefficient can be increased easily to the maximum value possible, and relaxation in the regime of quantum chaos has been measured for resolved levels, due to the modest density of vibronic levels.

For the largest $k_{\rm uni}$ values ($\sim 5 \times 10^{12}$ s^{-1}), it is likely that in He$_n$ the O-NO distance increases beyond the loose transition-state region for the corresponding gas-phase reaction; i.e., the molecule comes apart. This conjecture is based on the fact that $k_{\rm uni}$ is at least as large as, and probably larger than, the rate of deactivation. The system then recombines, as it must as long as it remains within the droplet, whose liquidity guarantees recombination. Were the photoexcited moiety in a solid matrix, products could be isolated.

The fact that net reaction has not been observed in this system leads us to the conclusion that no photoexcited polyatomic molecule will undergo barrierless unimolecular decomposition in He$_n$ droplets of sizes similar to the ones used here, with two possible exceptions. First, a product with a positive chemical potential inside the droplet will be expelled, as with alkali atoms. Second, a small cross section for collision of a product with a helium atom, as with atomic hydrogen, enhances the escape probability.

Finally, we note that reaction is assured with small droplets. For example, 4300 cm^{-1} is sufficient to evaporate $\sim 10^3$ atoms. Thus, with $\langle n \rangle \sim 10^3$, a significant fraction of the clustered helium will evaporate completely, leaving gas-phase NO_2 with $E > D_0$.

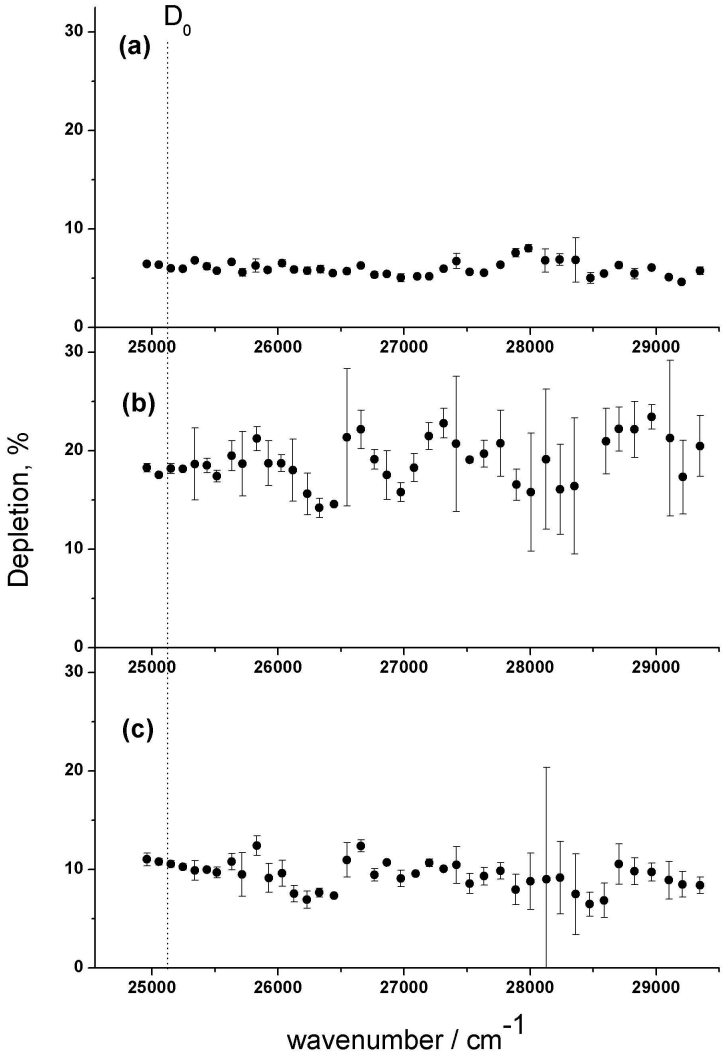

Figure 5.1: Mass spectrometer depletion spectra for m/z values of: (a) 8 (He_2^+); (b) 46 (NO_2^+); (c) 30 (NO^+). When error bars are not visible, they are smaller than the points.

Reference List

[1] Intramolecular quantum chaos in doped helium nanodroplets. *Chemical Physics Letters*, 375(3-4):253–260, 2003.

[2] Andreas Braun and Marcel Drabbels. Imaging the translational dynamics of CF_3 in liquid helium droplets. *Physical Review Letters*, 93(25):253401, 2004.

[3] Carlo Callegari, Kevin K. Lehmann, Roman Schmied, and Giacinto Scoles. Helium nanodroplet isolation rovibrational spectroscopy: Methods and recent results. *The Journal of Chemical Physics*, 115(22):10090–10110, 2001.

[4] I. Bezel D. Stolyarov, E. Polyakova and C. Wittig. Rate coefficients for photoinitiated NO_2 unimolecular decomposition: energy dependence in the threshold regime. *Chemical Physics Letters*, 2002.

[5] A. Delon, R. Jost, and M. Lombardi. NO_2 jet cooled visible excitation spectrum: Vibronic chaos induced by the $\widetilde{X}^2a_1 - \widetilde{A}^2b_2$ interaction. *The Journal of Chemical Physics*, 95(8):5701–5718, 1991.

[6] Robert Georges, Antoine Delon, and Remy Jost. The visible excitation spectrum of jet cooled NO_2: The chaotic behavior of a set of $^2b_2$ vibronic levels. *The Journal of Chemical Physics*, 103(5):1732–1747, 1995.

[7] M. Hartmann, F. Mielke, J. P. Toennies, A. F. Vilesov, and G. Benedek. Direct spectroscopic observation of elementary excitations in superfluid He droplets. *Physical Review Letters*, 76(24):4560–4563, 1996.

[8] S. I. Ionov, G. A. Brucker, C. Jaques, Y. Chen, and C. Wittig. Probing the $NO_2 \longrightarrow$NO+O transition state via time resolved unimolecular decomposition. *The Journal of Chemical Physics*, 99(5):3420–3435, 1993.

[9] R. Jost, J. Nygård, A. Pasinski, and A. Delon. Magnetic field control of the NO_2 photodissociation threshold. *Physical Review Letters*, 78(16):3093–3096, 1997.

[10] D. T. Moore K. Nauta and R. E. Miller. Molecular orientation in superfluid liquid helium droplets: high resolution infrared spectroscopy as a probe of solvent-solute interactions. *Faraday Discuss.*, 113:261–278, 1999.

[11] A. V. Kanaev, L. Museur, T. Laarmann, S. Monticone, M. C. Castex, K. von Haeften, and T. Moller. Dissociation and suppressed ionization of H_2O molecules embedded in He clusters: The role of the cluster as a cage. *The Journal of Chemical Physics*, 115(22):10248–10253, 2001.

[12] K Lehmann. *Faraday Discuss. Chem. Soc*, 2001.

[13] M. Lewerenz, B. Schilling, and J. P. Toennies. Successive capture and coagulation of atoms and molecules to small clusters in large liquid helium clusters. *The Journal of Chemical Physics*, 102(20):8191–8207, 1995.

[14] Evgeni Lugovoj, J. Peter Toennies, and Andrey Vilesov. Manipulating and enhancing chemical reactions in helium droplets. *The Journal of Chemical Physics*, 112(19):8217–8220, 2000.

[15] K. Nauta and R. E. Miller. Nonequilibrium Self-Assembly of Long Chains of Polar Molecules in Superfluid Helium. *Science*, 283(5409):1895–1897, 1999.

[16] S. A. Reid, J. T. Brandon, M. Hunter, and H. Reisler. Fluctuations in state-selected unimolecular decomposition: Double-resonance infrared visible photofragment yield spectroscopy of NO_2. *The Journal of Chemical Physics*, 99(6):4860–4863, 1993.

[17] Scott A. Reid and Hanna Reisler. Unimolecular reaction of NO_2: Overlapping resonances, fluctuations, and the transition state. *Journal of Physical Chemistry*, 1996.

[18] Frank Stienkemeier and Andrey F. Vilesov. Electronic spectroscopy in He droplets. *The Journal of Chemical Physics*, 115(22):10119–10137, 2001.

[19] Vilesov A.F. Toennies J. Peter. Spectroscopy of atoms and molecules in liquid helium. *Annual Review of Physical Chemistry*, 49(1):1–41, 1998.